RESEARCH REPORT

Attic Ventilation and Moisture Appendix

Canada

CMHC SCHL
HOME TO CANADIANS

CMHC—HOME TO CANADIANS

Canada Mortgage and Housing Corporation (CMHC) has been Canada's national housing agency for more than 60 years.

Together with other housing stakeholders, we help ensure that Canada maintains one of the best housing systems in the world. We are committed to helping Canadians access a wide choice of quality, affordable homes, while making vibrant, healthy communities and cities a reality across the country.

For more information, visit our website at **www.cmhc.ca**

You can also reach us by phone at 1-800-668-2642 or by fax at 1-800-245-9274.

Outside Canada call 613-748-2003 or fax to 613-748-2016.

Canada Mortgage and Housing Corporation supports the Government of Canada policy on access to information for people with disabilities. If you wish to obtain this publication in alternative formats, call 1-800-668-2642.

ATTIC VENTILATION AND MOISTURE

APPENDIX

APPENDIX

ATTIC VENTILATION AND MOISTURE

T.W. Forest and I.S. Walker

Department of Mechanical Engineering
University of Alberta
Edmonton, Alberta, CANADA, T6G 2G8

March, 1993

Appendix to Final Report prepared for
Canada Mortgage and Housing Corporation

TABLE OF CONTENTS

SECTION ONE

ATTIC VENTILATION AND MOISTURE

Ventilation of houses and attics with outdoor air is the most common method of controlling moisture in a building envelope during cold weather. This is necessary since moisture in the building envelope can lead to decay of structural members, loss of insulating properties, and a potential for the growth of micro-organisms. In many regions of Canada, the attic is one part of the envelope that is particularly prone to moisture damage because of high levels of ceiling insulation that result in large daily temperature variations during winter.

The traditional approach to controlling attic moisture has been to ventilate the attic. This has been recognized in the National Building Code with the requirement that total attic vent area be 1/300th of the attic floor area. As a result, most new attics have some type of soffit venting together with roof vents that satisfy the code. In fact there has been a tendency in recent years to add more vent area resulting in higher ventilation rates; this tendency is probably based on the notion that if some ventilation is good then more ventilation should be better. Unfortunately, there are very few comprehensive field measurements of attic ventilation rates that indicate how much ventilation is provided by the code requirement under a wide range of ambient conditions. Furthermore, there is very little information on how attic ventilation affects moisture deposition and removal and if there is some optimum ventilation rate. Intuitively, one may expect that, on the one hand, at very low ventilation rates, the attic air temperature will be higher than outdoors with a resulting ability to convey moisture away from the attic; however, this is offset by the low ventilation rates. On the other hand, at very high ventilation rates, attic air temperatures tend to be very close to the outdoor value; when temperatures are low, the air has a low moisture bearing capacity making large ventilation rates less effective at removing moisture.

1.1 Scope of the Study

The present study was undertaken to determine how attic ventilation rates are related to ambient conditions and attic leakage configuration and how attic ventilation affects moisture accumulation in an attic. The study was carried out in three phases:

- A large database of attic ventilation rates, temperatures, and moisture contents was collected in two test attics located at the Alberta Home Heating Test facility.
- Separate models were developed for predicting the ventilation rate (including passive and mechanical ventilation), temperature distribution, and moisture distribution within an attic and then these three models integrated. Measured values were used to verify the models.
- The combined model was used to simulate the performance of an attic in a number of different climatic zones to identify which ventilation strategies are effective in controlling moisture.

1.2 Review of Attic Ventilation and Moisture Studies

The field of moisture studies in the building envelope including attics is a very active area where much work has been done ranging from detailed mathematical modelling to field surveys of moisture damage in houses. The intent in this section is to provide some background information on work applied specifically to attic ventilation and moisture. What will become apparent is that there has been more work done on the measurement and modelling of moisture transport in attics than on measurement and modelling of attic ventilation rates although the two are inextricably connected.

The need for ventilation in attics has been recognized for quite some time and field tests carried out in the late 40's in the United States led to the introduction of the so-called "1:300" rule for attics with ceiling vapour barriers where it is recommended that the free vent area be 1/300th the attic floor area (an interesting discussion of the origin of the "1:300" rule is presented in Energy Design Update, 1993 based on some archival research of Rose, 1992). It seems that for these early field tests, the 1:300 vent area ratio was chosen, more or less arbitrarily but was subsequently adopted for code requirements since the ventilation provided by this free vent area seemed to prevent moisture problems. There certainly was no attempt to determine whether different vent area ratios might be more effective.

Interest in moisture problems in attics increased in the late 70's when it was noticed that the high levels of ceiling insulation, which were being recommended as a means of reducing house energy demand, were leading to increased moisture problems. Up until the oil crisis of the early 70's, there was a minimal amount of ceiling insulation (typically, batt or loose-fill insulation at about 2 RSI or R12) which kept the attic relatively warm; the much higher levels of ceiling insulation inevitably led to colder attics which developed moisture problems despite being properly ventilated according to the building code. A field survey of general moisture problems in Canadian housing was carried out in the early 80's by CMHC (1983) where it was noted that attic moisture problems occurred in two distinct climates; coastal climates which had prolonged periods of cold weather combined with high outdoor relative humidity and a minimum of sunshine and far northern climates with prolonged periods of cold weather (see also CMHC, 1984 for attic moisture problems in northern housing). Generally, it was observed that the problem houses had high indoor relative humidity and poor attic ventilation due to blocked soffits, etc. In many instances, it was noted that a large moisture load was imposed on the attic by air leakage from indoors to the attic. This had been recognized as an important means of transporting moisture by other studies, such as those by Hutcheon (1963) and later by Orr (1974).

In this same period, a number of studies were undertaken to model the moisture dynamics occurring in attics. One of the earliest works along these lines was that by Burch and Luna (1980) who formulated a steady state model of the thermal and moisture balance in an attic and posed the question "What is the minimum ventilation rate required to prevent moisture accumulation on the roof sheathing?" Their basic assumption was that no net daily moisture accumulation would occur if the daily-averaged temperature of the roof sheathing was greater than the daily-averaged dew point of the attic air. In this case, the model was used to calculate a specific ventilation rate which satisfied the above criterion. Ford (1982) developed a combined thermal and moisture model to predict moisture distribution within an attic. The thermal model first calculated the temperature distribution in the attic (including transient effects) which was then used in a simplified moisture model. This was based on the transient mass balances of the indoor air and the attic air with and without condensation on the inner surface of the roof sheathing; the roof sheathing was therefore, either at the saturation vapour pressure or at zero vapour pressure. In this model, the attic ventilation and indoor-attic exchange rates had to be specified although Ford did make some field measurements of these quantities. Ford's model was able to model condensation on the roof sheathing but was unable to include the effect of moisture storage in the wood sheathing. Cleary (1985) noted that wood in the attic absorbed and desorbed moisture from the air which had a considerable effect of attic air moisture content. This

realization helped considerably to make sense of the complex dynamics of moisture movement within a cold attic. Burch et al.(1984) extended his previous attic model to include moisture absorption and desorption from the roof sheathing and this was further refined by Gorman (1987) who separated the north and south-facing roof sheathing into separate nodes to account for the large difference in solar gains on these two roof faces. In field measurements of the seasonal wood moisture contents in attics, Harrje et al.(1985) noted that the south-facing sheathing had a mid-winter moisture content of 11% MC compared with 20% for the north sheathing. Both the steady state models of Burch and Gorman required that the ventilation and indoor-attic exchange rates be specified; as such, these models can only be used for parametric analysis where these flow rates are specified inputs. In comparison to the work on moisture modelling, the key question of how ventilation rates are dependent on ambient conditions has received less attention.

Several studies have been carried out to quantify the relationship between attic ventilation rates and moisture accumulation. Hinrichs (1962) performed some measurements for a company that manufactured attic vents, on the ventilation effectiveness of various types of fixed vents and provided information on vent flow rates as a function of wind speed. These results were summarized in a recommendation for a ventilation flow of 0.8 cfm per square foot of ceiling area. It is believed (by the authors) that this work formed the basis for a subsequent report (available form Alcoa Building Products, Sydney, Ohio - undated) which recommends 1.5 cfm per square foot of ceiling area at a wind speed of 7.5 mph. This work provides little or no information on how ventilation rates are affected by the ambient conditions, particularly wind speed, wind direction, and shelter from nearby obstacles. Saunders (1982) reported some measurements of attic ventilation and indoor-attic exchange rates for tests conducted the UK. Attic ventilation rates varied between 0.5 and 12 ac/h (air changes per hour) and increased roughly linearly with wind speed; indoor-attic exchange rates (quoted as a volume flow rate) showed no correlation with wind speed. These results are interesting but of little use as the size and type of attic and size of vent area were not given. Other than the limited measurements of attic ventilation and indoor-attic exchange rates (noted above), there has been little activity in this area until the more recent work by CMHC (1989a and 1991). The attics in a number of houses in eastern and central Canada were monitored to provide some background information on ventilation and moisture. The air tightness of each attic was measured by a dual blower technique (CMHC, 1989b), occasional measurements of attic ventilation rates were carried out using a constant injection rate tracer gas method, and the seasonal wood moisture content variation was measured throughout one complete year, commencing in early November. Unfortunately, with regard to measured ventilation rates, there was no correlation between

ambient conditions (notably wind speed) or attic envelope leakage area and this was attributed to varying ambient conditions (results presented in this study will show that the large variation in attic ventilation rate is mainly due to varying wind direction). Wood moisture content measurements indicated that, in general, roof sheathing moisture contents reached higher levels than the joists and trusses in the attic; occasionally, the sheathing moisture contents were well above fibre saturation (~30% MC), although this may have indicated the presence of surface condensation only. This work provides useful information but no firm conclusions or recommendations can be made about attic ventilation and resulting wood moisture contents. Rose (1992) has reported on measurements over the past several years, of temperatures and wood moisture contents in a number of differently configured attics (both flat ceiling and cathedral). Although ventilation rates were not measured directly in each attic, the effect of high and low ventilation rates was obtained by comparing wood moisture contents in a vented and non-vented attic. He observed that unvented attic was generally drier than the vented attic except on very cold days when moisture accumulated in the unvented attic. Future plans are to carry out some modelling in order to extend these results to other climatic zones and attic configurations.

From this brief review, it is obvious that more work needs to be carried out on modelling ventilation rates in attics as a function of ambient conditions and attic configuration. This is central to the needs of the moisture modelling which has proceeded quite a bit farther. If a useable ventilation model can be developed and integrated with the moisture models that now exist then a unique tool will be available to investigate how attics with different configurations behave in various climatic zones.

SECTION TWO

TWO ZONE VENTILATION MODEL

The two zone ventilation model is an extension of a mass balance approach that was developed by Wilson and Walker (1991) in a study of indoor passive ventilation of houses. The model allows the user to specify the size and location of particular leakage sites such as, open windows, flues, and passive vents. For given ambient conditions, the interior pressure is determined by equating the infiltrating air mass flow rates with the exfiltrating flow. Indoor infiltration rates are then determined from the predicted indoor-outdoor pressure difference. Attic ventilation rates were predicted using a similar approach, except that the model was extended to include two well-mixed zones (house interior and attic) which were coupled together through the ceiling leakage. This was an important extension to the previous model since the predictions for attic ventilation rate and indoor-attic exchange rate were both required. Since the modelling procedure for the two zones is essentially the same, details will only be presented for the attic zone in the following section.

2.1 TWO ZONE VENTILATION MODEL

Development of the ventilation model for the interior and attic space is essentially identical. Therefore, this section concentrates on the attic ventilation model. Prediction of attic ventilation rates is based on an air flow mass balance of the enclosed attic volume. The key assumptions of the model are that the attic air is well mixed implying no significant temperature gradients in the air, background leakage (excluding site-specific vent openings) can be uniformly distributed over a surface, and the air flow through the attic is quasi-steady. Since the ventilation rate predictions are to be compared with hourly-averaged measurements, the last assumption is justified.

Consider some leakage site located on the outer envelope of an enclosed attic space, as

shown in Fig.2-1. The pressure difference across this leakage site is a combination of the stack and wind-induced pressure differences and can be expressed as

$$\Delta P_i = \Delta P_{ref} - \Delta P_T H_i + \Delta P_W C_{p_i} S_{wi}^2 \qquad (2\text{-}1)$$

where ΔP_i is the outdoor-attic pressure difference (defined to be positive when outdoor pressure is greater than attic pressure), H_i is the height of a leakage site above grade, C_{pi} is the exterior wind pressure coefficient for a leakage site (referenced to the wind speed at the eave height), and S_{wi} the shelter factor for a leakage site. The shelter factor is a dimensionless ratio that multiplies the wind speed at the height of the eaves to account for shelter due to neighbouring obstacles; the magnitude of S_{wi} is between 0 and 1, with 0 referring to complete shelter ie. no wind pressures on the attic and 1 referring to no shelter. The two factors ΔP_T and ΔP_w are defined as

$$\Delta P_T \equiv \rho_\infty g \frac{T_A - T_\infty}{T_A} \quad ; \quad \Delta P_w \equiv \rho_\infty \frac{U^2}{2}$$

where ρ_∞ is the ambient air density, g is the gravitational constant, U is wind speed at the eave height (the reference wind speed), T_A is attic air temperature, and T_∞ is ambient air temperature.

The term ΔP_{ref} in Eqn.2-1 is the unknown reference outdoor-attic pressure difference at zero height (at grade level) which must be calculated from the mass flow rate balance. It should be noted that the stack and wind-induced pressures are <u>not</u> additive but interact through this unknown reference pressure difference.

2.1.1 Wind Pressure Coefficients

Since the principle driving force for attic ventilation is wind induced pressure on the attic, it is important that the wind pressure coefficients, C_p be determined as accurately as possible. For the gable-end attic tested, shown in Fig.2-1, pressure coefficients on the two sloped sections of the roof, gable ends, and soffits were determined from the measurements made by Wiren (1985) and those reported by Liddament (1986). For wind directions normal to the roof ridge, the pressure coefficients on the upwind and downwind sloped roof sections, $C_p(1)$ and $C_p(2)$ (labelled as surfaces 1 and 2, respectively in Fig.2-1) are given in Table 2-1. For low sloped roofs, the pressure coefficients have negative values which implies that the entire roof surface is within a separated flow region. For higher sloped roofs, air flow is attached to the upwind section giving positive pressure coefficients while flow separation occurs at the roof ridge. When the wind direction changes by 90° so that flow is parallel to the roof ridge, the pressure coefficients on the sloped sections depend on whether the house is isolated

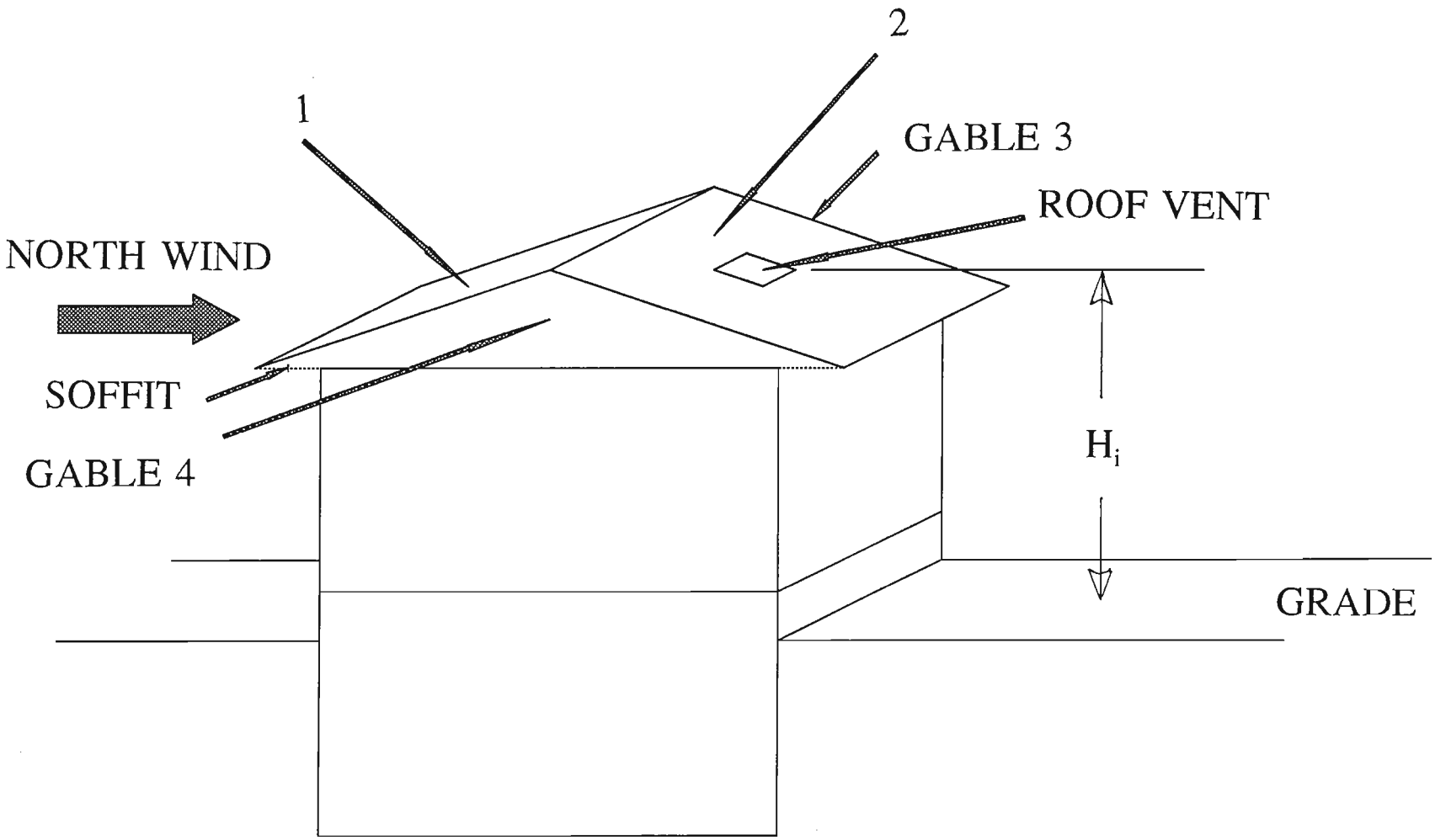

Figure 2-1. Gable-end attic showing numbered surfaces with respect to the north direction.

or is part of a row of houses. In this attic model, it is assumed that for wind directions parallel to the roof ridge, the sloped roof pressure coefficients behave in the same way as the vertical walls of the house. For the two vertical sections of a house parallel to the flow (labelled as surfaces 3 and 4 in Fig.2-1), Akins et al. (1979) measured a pressure coefficient

Table 2.1
Wind Pressure Coefficients on the Upwind and Downwind Sections of Sloped Roofs

Roof Pitch α	Pressure Coefficients	
	Upwind, $C_p(1)$	Downwind, $C_p(2)$
< 10°	-0.8	-0.4
10° to 30°	-0.4	-0.4
> 30°	0.3	-0.5

of -0.65 for an isolated house; for row houses, -0.2 is used as these surfaces are in the wake of upstream houses (Wiren 1984). From these limiting values for C_p, an harmonic trigonometric interpolation function was developed to obtain C_p values for varying wind directions;

$$C_p(\theta) = \frac{1}{2}[(C_p(1)+C_p(2))\cos^2\theta + (C_p(1)-C_p(2))F + (C_p(3)+C_p(4))\sin^2\theta + (C_p(3)-C_p(4))\sin\theta] \quad (2\text{-}2)$$

where θ is the angle between the roof section line and the normal to the wind direction measured in a clockwise direction. The effect of roof pitch, α, is contained in the factor, F, and is defined as

$$F = \frac{1-|(\cos\theta)^5|}{2}\left[\left|\frac{28^\circ - \alpha}{28^\circ}\right|\right]^{0.01} + \frac{1+|(\cos\theta)^5|}{2}.$$

The factor, F is close to 1 for roof pitch between 0 and 28°; at larger roof pitch, F behaves approximately as $\cos\theta$. Figure 2-2 shows the trigonometric interpolation function when the roof pitch is in the range of 10° to 30°; the measured ventilation rates, reported in the following section were taken in attics with a roof pitch of 18.4°. It should be emphasized that these data are for the sloped roof sections of the attic envelope. The pressure coefficients on

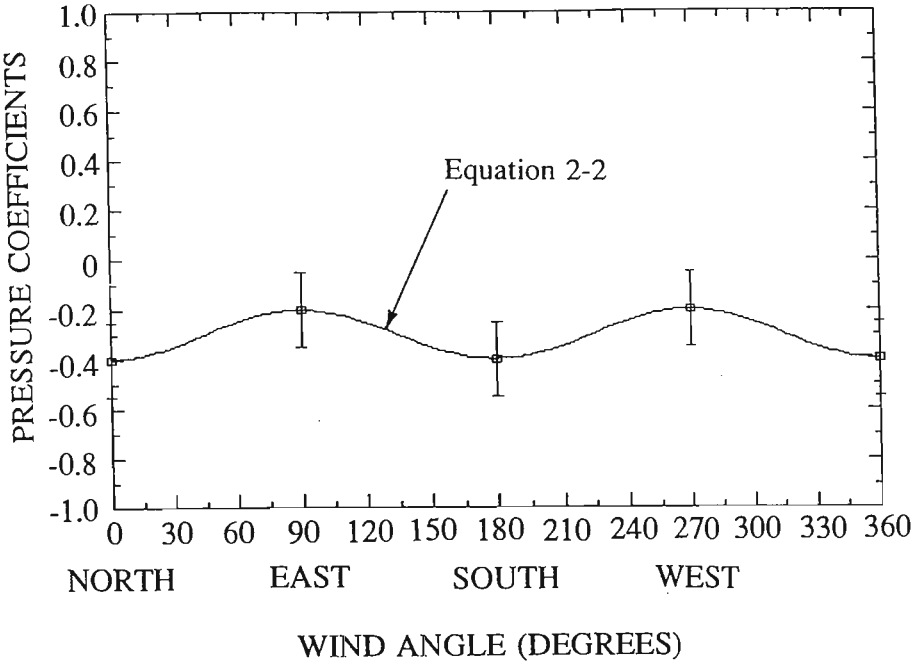

Figure 2-2 Wind angle dependence of measured (Wiren, 1985) and interpolated pressure coefficients on a 20° sloped roof surface for houses in a row.

the gable ends were assumed to be the same as the pressure coefficients on the vertical walls of the house, since the gables are simply an extension of the walls. A similar trigonometric interpolation approach was used to fit the pressure coefficient data of Akins et al. (1979) for vertical walls of houses. Finally, the pressure coefficients on the eaves (where soffit vents can be located), were assumed to be the same as that on the vertical wall beneath the eaves. In the absence of any detailed measurements of these pressure coefficients, this was the most reasonable assumption. In applying these pressure coefficients in the ventilation model, it was assumed that the pressure coefficient on each section of the attic envelope was a constant over that entire section. Again lack of detailed information on pressure coefficient distributions on a particular section, precludes incorporation of this effect in the model. Also, such detail would make the ventilation model more complex than it needs to be at this time.

2.1.2 Wind Shelter

Obstacles surrounding the attic produce a reduction in wind speed at the building due to the obstacle's wake. This effect can be expressed as a wind reduction factor or shelter factor, S_w which varies between 0 (complete shelter) and 1 (unsheltered). The method used to generate the shelter factors is based on a new wind-shadow technique and will only be briefly outlined in this section. The theory and complete development of this technique will be the subject of a forth-coming publication by Wilson and Walker. In this model, upwind obstacles create a wake of mean velocity defect. The shelter factor is obtained by projecting the wind "shadow" of an upwind obstruction on a particular surface of a building and calculating the wind reduction at that surface. The model also takes into account the effect of fluctuating wind directions due to turbulence by assuming a Gaussian distribution for wind direction. An example of the wind shelter function is shown in Fig.2-3 for the north wall of one of the test houses used in the field study (see Section 3). The attic ventilation model assumes that the shelter factor for the sloped roof sections are the same as the wall section beneath it. In each of the figures, the shelter factors decrease significantly for wind directions where the neighbouring houses in the east-west row, provide shelter.

2.2 CALCULATION OF VENTILATION FLOW RATES

Attic ventilation rates are calculated by balancing the mass flow rate of air into and out of the attic. The output of this calculation is the unknown value of ΔP_{ref} which balances the inflows and outflows. The mass flow rate of air through leakage site i, $\dot{m}_i$, is expressed as

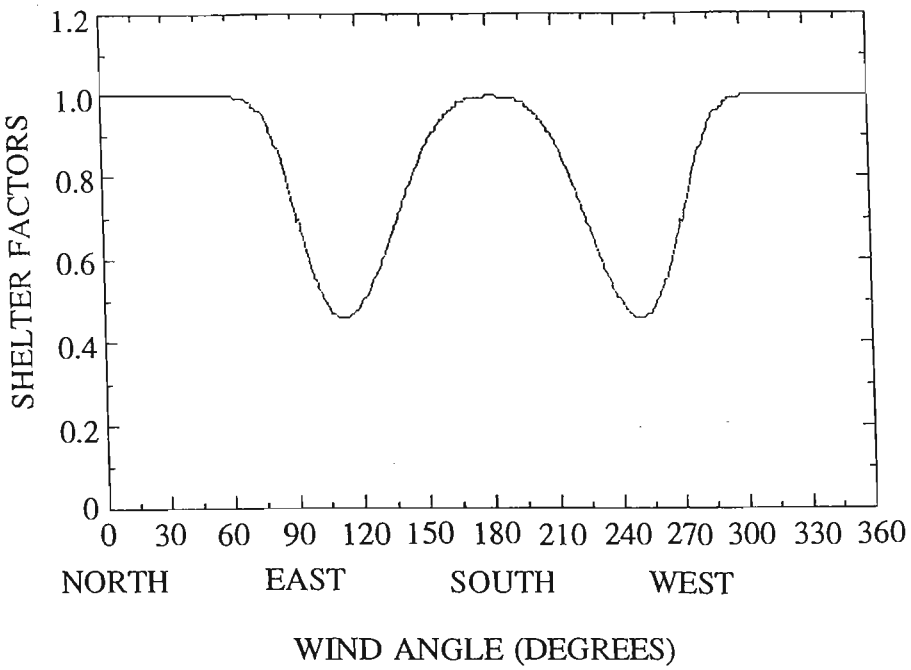

Figure 2-3 Wind angle dependence of shelter factor, S_w for the north wall of a house at AHHRF, calculated from the data of Wiren (1985).

$$\dot{m}_i = \rho_i C_i \Delta P_i^{n_i} \tag{2-3}$$

where ρ_i is the density of ambient air (ρ_∞ for in flow or ρ_A for out flow), C_i is the flow coefficient of each leak, and n_i is the corresponding flow exponent. A positive mass flow rate is defined as flow into the attic when $\Delta P_i > 0$ and vice versa when $\Delta P_i < 0$. The leakage sites on the attic envelope can be separated into a) unintentional leaks, such as tiny cracks and holes, which are assumed to be uniformly distributed over the attic envelope, b) intentional openings, such as roof vents, soffits, and c) mechanical ventilators, such as roof mounted fans. Expressions for the mass flow rate of air through each of these leaks is presented in the following sections.

2.2.1 Distributed Leakage

The unintentional leakage is assumed to be distributed uniformly over the roof surfaces and the flow through each surface is found by integrating the pressure difference over the height of that surface. Since different densities are applied to in flows and out flows, these must be calculated separately. The boundary between in flows and out flows is the height at which the attic pressure and outdoor pressure are equal. The height of this boundary above grade is the neutral height, H_{NL} and can be expressed as

$$H_{NL} = \frac{(\Delta P_{ref} + \Delta P_w C_p S_w^2)}{\Delta P_T}. \tag{2-4}$$

Note that the pressure coefficient and shelter factor are constant over the entire surface under consideration and the neutral height must be calculated separately for each surface of the attic envelope. Several cases exist depending on the attic-outdoor temperature difference and the neutral height. In the following development, the particular surface of the attic envelope under consideration is designated by the subscript, j where j assumes the values 1 through 4 corresponding to the surfaces labelled in Fig.2-1.

Attic-Outdoor Temperature Difference Zero. In the limit when there is no attic-outdoor temperature difference, ΔP_T is zero and the neutral height is undefined. In this case, there is no variation in pressure with height and the flow on the particular roof surface will be in or out depending on the wind pressures. For a constant pressure difference on the jth surface, ΔP_j, given by Eqn.2-1, the mass flow rates are

$$\dot{m}_{out,\,j} = \rho_A C_{r,\,j} \Delta P_j^{\,n} \qquad \Delta P_j < 0 \tag{2-5a}$$

$$\dot{m}_{in,\,j} = \rho_\infty C_{r,\,j}\Delta P_j^{\,n} \qquad \Delta P_j > 0 \tag{2-5b}$$

where $C_{r,j}$ refers to the flow coefficient of the particular surface of the roof,j being considered.

Attic-Outdoor Temperature Difference Not Zero. In this case, the pressure varies with height, h (measured relative to grade), which implies that the air flow varies over the surface of interest. The incremental mass flow rate, $d\dot{m}_j$ over height, dh of the surface is

$$d\dot{m}_j(h) = \rho\Delta P_j^{\,n}(h)dC_{r,\,j} \tag{2-6}$$

where ΔP_j is calculated using Eqn.2-1 with H_i set equal to h. The incremental flow coefficient of the roof surface, $dC_{r,j}$ can be expressed as

$$dC_{r,\,j} = \frac{C_{r,\,j}}{H_p - H_e}dh \tag{2-7}$$

where H_p is the roof peak height above grade, H_e is the eave height above grade. The expression for $dC_{r,j}$ follows from the assumption of uniform distribution of leakage area over the roof surface. The mass flow rate for a particular roof surface is found by integrating Eqn.2-6. However, the limits of integration depend on the neutral height. The first case is when the attic temperature is greater than the outdoor temperature. If the neutral height lies between H_p and H_e, the mass flows in and out are

$$\dot{m}_{in,\,j} = \frac{\rho_\infty C_{r,\,j}\Delta P_{2,\,j}^{\,n+1}}{(H_p - H_e)\Delta P_T\,(n+1)} \tag{2-8a}$$

$$\dot{m}_{out,\,j} = \frac{\rho_A C_{r,\,j}\Delta P_{1,\,j}^{\,n+1}}{(H_p - H_e)\Delta P_T\,(n+1)} \tag{2-8b}$$

where $\Delta P_{1,j}$ and $\Delta P_{2,j}$ are calculated using Eqn.2-1 with H_i set equal to H_p and H_e for the particular roof surface, j; if the entire roof surface is above the neutral height then mass flow out across the surface is

$$\dot{m}_{out,\,j} = \frac{\rho_A C_{r,\,j}(\Delta P_{1,\,j}^{\,n+1} - \Delta P_{2,\,j}^{\,n+1})}{(H_p - H_e)\Delta P_T\,(n+1)}; \tag{2-9a}$$

if the entire roof surface is below the neutral height the mass flow in across the surface is

$$\dot{m}_{in,\,j} = \frac{\rho_\infty C_{r,\,j}(\Delta P_{1,\,j}^{n+1} - \Delta P_{2,\,j}^{n+1})}{(H_p - H_e)\Delta P_T\ (n+1)}. \qquad (2\text{-}9b)$$

The second case is when the attic temperature is less than the outdoor temperature. If the neutral height lies between H_p and H_e then $\Delta P_{2,j}$ is replaced by $-\Delta P_{1,j}$ in Eqn.2-8a and $\Delta P_{1,j}$ is replaced by $-\Delta P_{2,j}$ in Eqn.2-8b; if the entire surface is above the neutral level, the mass flow of air into the attic is given by Eqn.2-9b with the pressure difference term $\Delta P_{1,j}^{n+1} - \Delta P_{2,j}^{n+1}$ multiplied by -1; if the entire roof surface is below the neutral level, the mass flow of air out of the attic is given by Eqn.2-9a with the same pressure difference term multiplied by -1.

The flow coefficients for each roof surface, $C_{r,j}$ are estimated from the total distributed leakage flow coefficient for the attic envelope, C_{attic}. This latter value has been measured using fan pressurization tests on the two attics that were monitored during the test period (this is discussed in Section 3). In this study, the distributed attic envelope leakage included the leakage in the roof surfaces and the soffits, but excluded any intentional openings, such as roof vents. When conducting attic pressurization tests, it is easy to block off roof vents but difficult to do the same for soffits. Thus, the soffit and roof flow coefficients, $C_{s,j}$ and $C_{r,j}$ are related to the measured flow coefficient, C_{attic} by

$$C_{attic} = \sum_{j=1}^{4} \left(C_{s,\,j} + C_{r,\,j} \right) \qquad (2\text{-}10)$$

This relation is valid only if it is assumed that the flow exponents, n for all roof surfaces are identical to the measured flow exponent. The individual values of soffit and roof flow coefficients for surface, j must be estimated from the fraction of the total leakage attributed to each surface. The leakage distribution that was assumed for this study will be discussed in Section 3. Finally, it should be noted that C_{attic} and n are usually measured during summer when air temperatures are near 20°C. In order to account for the small density and viscosity changes that occur with temperature, C_{attic} must be multiplied by $(T_{ref} / T)^{3n-2}$ where T_{ref} is assumed to be 293 K and T is the ambient or attic air temperature depending on whether the flow is into or out of the attic.

Once these flow coefficients are determined, the mass flow rate of air through each roof surface can be calculated using Eqns.2-5, 2-8, or 2-9, depending on the conditions in the attic. The mass flow rates through the soffits are calculated using Eqn.2-3 where the flow

coefficient is $C_{s,j}$ (suitably corrected for temperature), the flow exponent, n is the same as that obtained from fan pressurization tests, and ΔP_j is the pressure difference acting across the soffit. This pressure difference is obtained using Eqn.2-1 where the soffit height is H_e and the wind pressure coefficient and shelter factors are assumed to be the same as the vertical wall directly beneath them.

2.2.2 Intentional Leakage

For intentional openings, such as roof vents whose height above grade, H_i is known, the pressure difference is given by Eqn.2-1 and the mass flow of air through these leakage sites is calculated from Eqn.2-3. The coefficient, C_i and corresponding exponent, n_i are the leakage characteristics of the vent. The flow through vents can usually be assumed to behave as orifice flow with a flow exponent of 0.5; the corresponding flow coefficient, C_i can thus be estimated from the net vent area multiplied by a discharge coefficient (~ 0.6). The net area takes into account any blockage, such as insect screens. The pressure coefficient and shelter factor for each vent are assumed to be the same as for the attic surface on which they are located.

2.2.3 Ventilation Fans

If mechanical ventilation is installed in an attic, the mass flow rate of air through the fan is a significant fraction of the ventilation rate. It is therefore, important to model this flow as accurately as possible. In this model, the fan performance curve is incorporated to allow the flow rate through the fan to vary depending on the ambient conditions. This is a significant improvement over other studies (for example, Gorman (1987)) which assumed that the presence of a fan dominates resulting in a ventilation rate that is equal to the rated fan flow. As with attic vents, the pressure difference across the fan, ΔP_{fan} is given by Eqn.2-1 where the wind pressure coefficient and shelter factor are the same as the roof surface on which the fan is located and the height of the fan location above grade, H_{fan} is known. The mass flow rate through the fan corresponding to ΔP_{fan} is given by

$$\dot{m}_{fan} = \rho Q_{rated} \left(\frac{\Delta P_{rated} - \Delta P_{fan}}{\Delta P_{rated}} \right)^{0.3} \qquad (2\text{-}11)$$

where ρ is evaluated at the ambient or attic temperature depending on the flow direction, Q_{rated} is the maximum volume flow rate through the fan at zero pressure difference (usually

quoted by the manufacturer), and ΔP_{rated} is the maximum pressure difference at zero flow (the "shut-off" head). The exponent value of 0.3 is an approximation for centrifugal fans that are commonly used for mechanical ventilation. If the constant speed fan characteristics have been measured or supplied by the fan manufacturer than this can be used in the ventilation model.

2.3 THE HOUSE VENTILATION MODEL

A similar calculation procedure to that outlined above for the attic zone, was implemented for the interior, conditioned zone of the house. Inputs to this calculation procedure were the C and n for individual leakage sites such as open flues and fresh air vents and C and n for the background, distributed envelope leakage. These latter values were obtained from fan pressurization tests that were carried out on the interior zone of the test houses (see Section 3). For the interior zone, the pressure difference, $\Delta P_{I,i}$ across each leakage site, i was expressed as

$$\Delta P_{I,\,i} = \Delta P_{I,\,ref} - \Delta P_{T\,I}\, H_i + \Delta P_w C_{pi}\, S_{wi}^2 \qquad (2\text{-}11)$$

where $\Delta P_{I,ref}$ is the unknown reference outdoor-indoor pressure difference at zero height (at grade level); ΔP_{TI} is defined as

$$\Delta P_{T\,I} = \rho_\infty g\, \frac{T_I - T_\infty}{T_I}$$

where T_I is the interior zone temperature which is usually set at a constant value (~20°C).

2.3.1 Wind Pressure Coefficients for the Interior Zone

The most comprehensive wind tunnel tests to date that cover many different wind directions have been presented by Akins, Peterka and Cermak (1979). They measured surface pressures on a cube rather than a model house but their values of Cp are within the range of values presented elsewhere (ASHRAE (1991) in Chap.14, Liddament (1986) and Wiren (1985)) for isolated buildings. Akins, Peterka and Cermak also covered the most comprehensive set of wind directions and thus their data is most useful in developing correlations of Cp with wind angle. The only adjustment to these pressure coefficients in this model is a change of side wall Cp. For an isolated building the side wall is about Cp = -0.65 based on Akins, Peterka and Cermak's measurements. For houses in a row with the wind along the row the upwind houses change the flow pattern around the building so that large flow separations do not occur on the sidewalls. This requires a reduction in magnitude of the

side wall pressure coefficient to about Cp = -0.2 as found by Wiren in tests of row house shelter, and suggested by model errors in passive ventilation studies performed by Wilson and Walker (1991). Analysis of Wiren's data by Walker (1992) has shown that for a house to be considered to be in a row only one upwind house is necessary because the closest obstacle dominates the wind flow pattern. Table 2-2 contains wall-averaged wind pressure coefficients used for the house by the ventilation model for wind perpendicular to the upwind wall.

When the wind is not normal to the upwind wall these pressure coefficients do not apply. An harmonic trigonometric function similar to that for the attic envelope, was developed to interpolate between these normal values to fit the variation shown by Akins, Peterka, and Cermak and Wiren. For each wall of the building the harmonic function for Cp is given by

$$Cp(\theta)=\frac{1}{2}[(Cp(1)+Cp(2))(\cos^2\theta)^{\frac{1}{4}}+(Cp(1)-Cp(2))(\cos\theta)^{\frac{3}{4}} \\ +(Cp(3)+Cp(4))\sin^2\theta+(Cp(3)-Cp(4))\sin\theta] \qquad (2\text{-}12)$$

where Cp(1) is the Cp when the wind is at 0^o (+0.60)
Cp(2) is the Cp when the wind is at 180^o (-0.3)
Cp(3) is the Cp when the wind is at 90^o (-0.65 or -0.2)
Cp(4) is the Cp when the wind is at 270^o (-0.65 or -0.2)
and θ is the wind angle measured clockwise from the normal to the wall.

Table 2-2.
Wall Averaged Wind Pressure Coefficients for a Rectangular Building with the Wind Normal to Upwind Wall from Akins, Peterka and Cermak (1979) and Wiren (1985).

Shelter Configuration	Cp, Wind Pressure Coefficient		
	Upwind Wall	Side Walls	Downwind Wall
Isolated House	+0.60	-0.65	-0.3
In-Line Closely-Spaced Row	+0.60	-0.2	-0.3

This function is shown in Fig.2-4 together with data from Akins et al. for a cube. The error bars on the data points in Fig.2-4 represent the uncertainty in reading the measured values from the figures in Akins, Peterka and Cermak. Equation 2-12 fits the measured data within about Cp = ±0.02 except at about 150° and 210° (which are the same by symmetry) where the equation overpredicts the Cp by about 0.1. The function in Eqn.2-12 was chosen to have the above form so that if a different data set were to be fitted, for example from a rectangular building, then only the values for when the wind is normal to one wall are required and the function will estimate the intermediate values for different wind directions. This function also collapses to give the values in Table 2-2 when the wind is perpendicular to each wall, as shown in Fig.2-4. Equation 2-12 is shown in Fig.2-5 for the row Cp's where the sidewall Cp = -0.2. There are no intermediate measured values but this figure shows that Eqn.2-12 produces reasonable Cp's for this case.

2.3.2 Wind Shelter

Wind shelter factors, S_w for the interior zone of the house were calculated using the same procedure as discussed in Section 2.1.2. The wind shadow technique resulted in shelter factors that were the same for a particular vertical wall and the roof section immediately above it. Thus, the results shown in Fig.2-3 are applied to the north wall and roof section of one of the test houses.

2.4 CALCULATION PROCEDURE FOR THE TWO ZONE MODEL

Although the attic and interior zones of a house are separated by the ceiling, they are coupled together through the ceiling leakage. Depending on the amount of ceiling leakage, calculation of the ventilation rates for the two zones will involve some interaction between zones and will hence, require some iteration. The following solution procedure was used to calculate the ventilation rates in the two zones:

1. The ventilation rate was first estimated for the interior zone of the house. For given ambient temperature, wind speed and direction, the mass flow rates through each surface of the interior zone envelope were formulated according to the procedures described above. For this initial calculation, the pressure in the attic (which determines the ceiling mass flow rate) was estimated by assuming an area-weighted average pressure coefficient over the attic envelope. It was also assumed that the ceiling leakage had the same flow

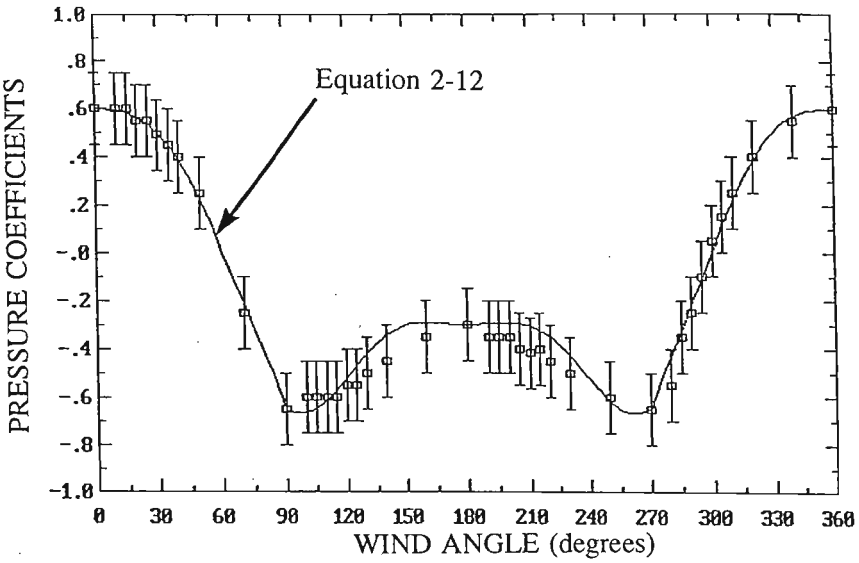

Figure 2-4 Wind angle dependence of measured (Akins et al., 1979) and interpolated wall pressure coefficients for isolated houses.

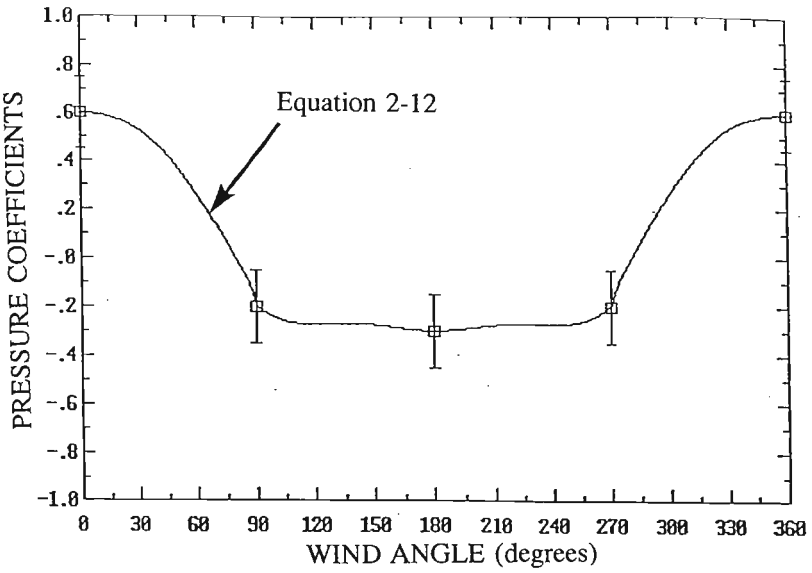

Figure 2-5 Wind angle dependence of measured (Wiren, 1985) and interpolated wall pressure coefficients for houses in a row.

exponent, n as that of the interior zone and a flow coefficient, C corresponding to the measured ceiling leakage area. Thus, the only unknown in the mass flow rate balance was $\Delta P_{I,ref}$ of the interior zone. An iterative procedure was used to solve for this pressure difference by initially assigning a value of zero. Mass flow rates for all surfaces of the house envelope were calculated; if the sum of the in flows was not equal the sum of the out flows then a new value was selected; $P_{I,ref}$ was chosen to be +1000 Pa if total in flow exceeded total outflow and -1000 Pa if out flow exceeded in flow. These large initial pressures were sufficient to encompass the range of pressure differences that are likely to be encountered in houses including the effects of mechanical ventilation. Succeeding iterations used the method of bisection in which $P_{I,ref}$ for the next iteration was reduced by half the difference between the last two iterations; thus the third iteration changed $P_{I,ref}$ by ±500 Pa. The sign of the pressure change was positive if inflow exceeded outflow and negative if outflow exceeded inflow. The limit of solution was determined by the number of iterations. Generally, it was found that after 17 iterations the change in $P_{I,ref}$ was < 0.01 Pa, which gave mass flow imbalances on the order of 0.001 kg/s (or 4 kg/hour). This procedure gave an initial estimate for $\Delta P_{I,ref}$ for the interior zone.

2. The calculation then moved to the attic zone, where the mass flow rates through the various leakage sites on the attic envelope were expressed according to the equations outlined in Sec.2.3. The pressure difference across the ceiling used the interior zone reference pressure, $\Delta P_{I,ref}$ that was calculated in step 1. The reference pressure, ΔP_{ref} for the attic was then calculated from the mass flow rate balance using the same iterative procedure outlined in step 1.

3. The new estimate for attic pressure was then used in step 1 to obtain a new value of the interior zone $\Delta P_{I,ref}$. The calculation procedure was repeated in both zones until the change in mass flow rate through the ceiling from iteration to iteration was less than 0.00001 kg/sec; this value is typically less than 0.1 % of the indoor ventilation rate. The ventilation rate in both zones was then calculated by summing all the inflows (which is equal to the sum of outflows) for each zone. In addition, the indoor-attic exchange rate (ceiling flow rate) was calculated from the final value of the indoor-attic pressure difference.

The equations given above for attic mass flow rates involve the attic temperature, T_A which is not known a priori; thus, an iterative procedure would have to be employed between the attic

ventilation model and an attic thermal model such as those developed by Wilkes (1983, 1989), Abrantes (1985), and Ford (1982). Since attic ventilation rates are not sensitive to the attic temperature (air density varies with the absolute temperature), one or two iterations would suffice for calculating attic ventilation rate. In the following section where measured and predicted attic ventilation rates are compared, the measured attic air temperature is used. This two zone ventilation model was verified with ventilation measurements that were taken in two separate attics located at field test site over the past two years. Section 3 describes the facility and test procedure and concludes with a comparison of measured and predicted ventilation rates.

SECTION THREE

THE ATTIC THERMAL MODEL

In this section, a model for the dynamic thermal balance in an attic is developed. The calculations of temperatures within the attic are essential for moisture calculations since the vapour pressures within the attic are the "driving forces" for mass transfer and vapour pressure depends strongly on moisture content (of either the wood or air) and the corresponding temperature. In addition, the thermal model interacts with the ventilation model mainly through the attic air temperature. As mentioned in the previous section, the attic air temperature determines the air density within the attic which is required when carrying out the mass flow balance for calculation of attic ventilation rate. Since ventilation rates affect the attic air temperature, there is an interaction between the thermal and ventilation models that requires iteration. Fortunately, this coupling of the ventilation and thermal models is weak because attic ventilation rates are not a strong function of attic air temperature, as will be shown by the measurements (see Section 5).

Some previous authors (Gorman, 1987 and Burch and Luna, 1980) used simple steady-state energy balances in the attic that included the attic air, attic floor and the sheathing. These steady-state approaches do not capture the strong diurnal changes in attic temperature due to daytime solar gains or rapid changes in temperatures due to changing ventilation rates. As will be shown later by the attic simulations, these effects cannot be ignored if wood moisture content and condensed mass accumulation are to be predicted. Another approach taken by Peavy (1979) and Wilkes (1989) is to use response factors that include the effect of previous temperatures and heat fluxes to calculate a time dependent response for the attic temperatures. Neither Peavy or Wilkes separated the sheathing surfaces into north and south parts that receive different solar radiation gains or included conduction heat transfer losses through gable end walls. The most comprehensive model to date is that of Ford (1982) who separated the attic into discrete masses (or nodes) and used a first order lumped heat capacity analysis where the change in energy at each mass was equal to the sum of the heat fluxes. Ford also separated the north and south

sheathing so that they may have different daytime solar gains and included heat losses through gable ends. Because Ford's model is the most thorough it will be used as the basis of the heat transfer model for this study. A few refinements and simplifications to Ford's attic heat transfer model will be made as listed below:

- an additional node is used to account for the mass of wood in joists and trusses in the attic
- attic ventilation and ceiling flow rates are calculated instead of being a required input
- forced convection heat transfer coefficients are used inside the attic as opposed to free convection coefficients estimated by Ford
- radiation heat transfer inside the attic is simplified to three nodes: the attic floor and the two pitched roof surfaces as these surfaces have the largest view factors

The energy balance for the attic is based on Ford's lumped heat capacity analysis using the nodes shown in Fig.3-1. The pitched roof sheathing is labelled north and south so that the differences in solar radiation between north and south facing surfaces may be included. The test houses used in this study were in an east-west row so that they have north and south facing sheathing surfaces. The roof sheathing, gable end walls, and ceiling are divided in half so that the two nodes are separated by one-half the element thickness; for the outer sheathing (nodes 3 and 5), the mass associated with these nodes are doubled to account for the additional mass associated with the shingles. The attic joists and trusses (node 6) are modelled with a single node whose temperature is uniform. The energy balances at each node together with the energy inputs are summarised in Section 3.1.

3.1 NODE ENERGY BALANCES

In a lumped capacity analysis, the time rate of change of energy at a node is equated to the sum of all heat fluxes into and out of the node. Thus, the energy balance at node i can be expressed as

$$\rho_i V_i C_{sh,i} \frac{dT_i}{dt} = \Sigma q \qquad (3\text{-}1)$$

where ρ_i is the density, V_i is the volume, $C_{sh,i}$ is the specific heat, T_i is temperature and q are the heat fluxes due to conduction, convection, and radiation. In order to preserve mathematical

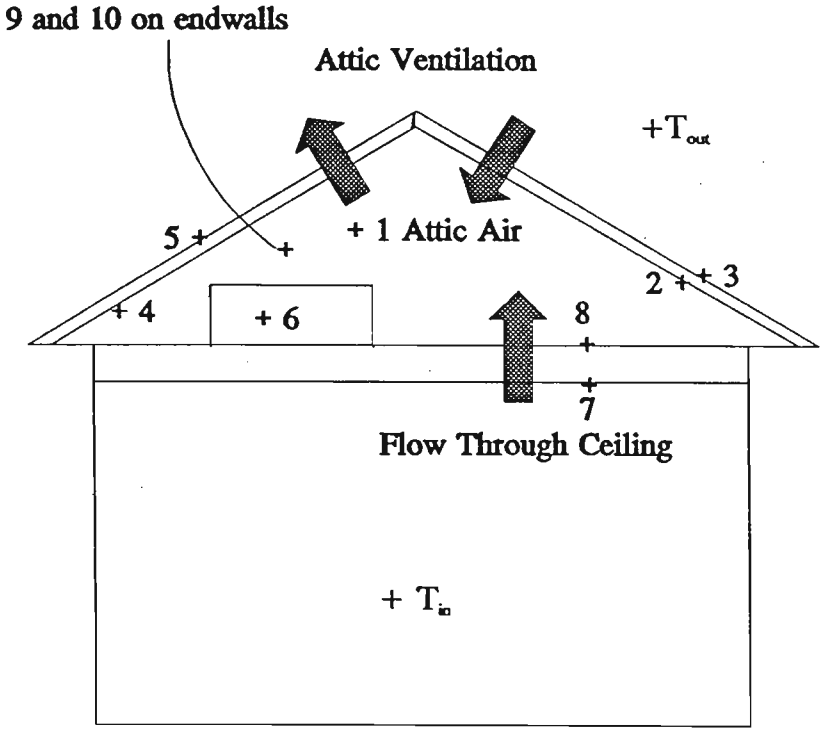

Figure 3-1 Node locations for attic thermal model.

1 is the attic air
2 is the inner north sheathing
3 is the outer north sheathing
4 is the inner south sheathing
5 is the outer south sheathing
6 is the joists and trusses
7 is the interior ceiling
8 is the attic side of ceiling
9 is the inner gable wall
10 is the outer gable wall

simplicity in the model (ie eliminate the complexity of solving a coupled set of first order differential equations), the time derivative is approximated with a backwards finite difference as

$$\rho_i V_i C_{sh,i} \frac{T_i^{\,j} - T_i^{\,j-1}}{\tau} = \Sigma q \tag{3-2}$$

were j refers to the current timestep and j-1 the previous timestep and τ is the length of the time step. The largest error in dT/dt that this approximation introduces is estimated to be 25% for south roof sheathing on a clear spring day when the measured rates were 7 C°/hr. However, these conditions occur for very few hours during the day and only for those nodes that have large solar gains; over 24 hours, the mean absolute error (where positive and negative errors do not cancel) is estimated to be 0.6 C°/hr. In the present study, τ is equal to one hour because this is the time interval between measured data points. The energy balance is performed at each hour j with the previous hour's temperature used in the expression for the rate of change of energy at each node.

The validity of using a lumped capacity approach is based on the assumption that for a mass exchanging heat with the surroundings, the convective resistance at the surface is larger than the internal conduction resistance. This criterion is expressed in terms of the Biot number as (Holman, 1981, pg.113)

$$Bi = \frac{h_U \left(\frac{V}{A}\right)}{k} < 0.1 \tag{3-3}$$

where h_U is the surface heat transfer coefficient, A is the surface area, V is the volume, and k is the thermal conductivity. For the same h_U and k the node with the largest V/A ratio is least likely to meet the restriction of Eqn.3-3. Node 6, representing the joists and trusses in the attic is the most critical. For 5 cm x 10 cm lumber, V/A is equal to 0.017 m. The convective heat transfer coefficient is estimated to be 3 W/m^2 K (see discussion below) and taking wood thermal conductivity, k_w to be 0.1 W/mK yields a Bi number of 0.5. These results show that in the worst case, the lumped capacity analysis will result in some error; however, for the other elements of the attic, these are divided into two nodes which reduces the V/A ratio resulting in smaller Biot numbers and a more accurate prediction of component temperatures.

The only other approximation that is made in the thermal model is the heat released by moisture absorbing in the wood and condensing on the attic surfaces does not affect the component temperatures. This assumption will be examined in Section 4.

3.1.1 Attic Air (node 1)

The heat fluxes for the attic air (node 1) include convective heat flux from all surfaces enclosing the attic (nodes 2, 4, 6, 8, and 9) as well as forced convective flow of air from outdoors (ventilation flow) and from the interior of the house (ceiling flow). For this lumped capacity analysis, the attic air is assumed to be well stirred so that the air temperature is uniform. For hour j, the energy balance is expressed as

$$\rho_a V_a C_{sh,\alpha} \frac{(T_1^j - T_1^{j-1})}{\tau} = h_{U,8}\, A_8 (T_8^j - T_1^j) + h_{U,4}\, A_4 (T_4^j - T_1^j) + h_{U,2}\, A_2 (T_2^j - T_1^j) + A_9 h_{U,9} (T_9^j - T_1^j) + M_c C_{sh,\alpha} (T_{in}^j - T_1^j) + M_a C_{sh,\alpha} (T_{out}^j - T_1^j) + h_{U,6}\, A_6 (T_6^j - T_1^j) \quad (3\text{-}4)$$

where ρ_a is the attic air density, V_a is the volume of the attic, $C_{sh,\alpha}$ is the specific heat of air, $h_{U,i}$ is the convective heat transfer coefficient for node i, A_i is the surface area of node i (for node 9, the end walls of the attic are identical and A_9 is therefore, the total end wall area), M_c is the mass flow rate through the ceiling from the two zone ventilation model, and M_a is the mass flow rate through the attic.

The convective heat transfer coefficients were estimated from experimental results for forced flow over flat plates. The heat transfer coefficients depend on the mean velocity, U_U within the attic and this value was estimated as

$$U_U = \frac{M_a}{\rho_a \frac{A_{L4}}{2}} \frac{1}{4} \quad (3\text{-}5)$$

where M_a is the attic ventilation rate and A_{L4} is the 4 Pa leakage area. The leakage area is divided by 2 in Eqn.3-4 as an estimate of the inflow area and 1/4 is an arbitrary velocity reduction factor which simply accounts for some reduction in velocity due to the expansion of the flow as it enters the attic. An estimate of U_U using Eqn.3-4 can be made using measured leakage area and ventilation rate; for A_{L4} of 1500 cm^2 and ventilation rate of 5 ac/h (based on an attic volume of 61 m^3 for the test attics), U_U was estimated to be 0.3 m/s. For these conditions, it can be shown that forced convection dominates over free convection (free convection occurs during those periods of large surface-air temperature difference and low

ventilation rates). By comparing convective heat transfer coefficients for turbulent flow over a flat plate with measured data of Burch (1980) and McAdams (1954), Ford found the length scale required in the heat transfer correlations for flat plates to be 0.5 m. Using this value, the flat plate correlations (given in Holman, 1981a) gave heat transfer coefficients for air in the following form

$$h_U=(18.192-0.0378T_\varepsilon)U_U^{\frac{4}{5}} \tag{3-6}$$

where T_ε is the average of the temperature of node i and the air temperature expressed in °C.

3.1.2 Inner North Sheathing (node 2)

The inside of the sheathing exchanges heat with the attic air by convection and with the outside of the sheathing by conduction. In addition there is radiant exchange with the attic floor and the inside of the south sheathing. The energy balance at the j^{th} hour is

$$\rho_W V_2 C_{sh,W}\frac{(T_2^{\,i}-T_2^{\,i-1})}{\tau}=h_{U,2}\ A_2(T_1^{\,i}-T_2^{\,i})+\frac{A_2}{R_2}(T_3^{\,i}-T_2^{\,i}) \\ +h_{R,2-8}\ A_2(T_8^{\,i}-T_2^{\,i})+h_{R,2-4}\ A_2(T_4^{\,i}-T_2^{\,i}) \tag{3-7}$$

where ρ_W is the density of wood, approximately 400 kg/m^3, V_2 is half the north sheathing volume, A_2 is the surface area of the north sloped roof surface, R_2 is the sheathing thermal resistance, $h_{R,2-8}$ is the radiation heat transfer coefficient between nodes 2 and 8, and $h_{R,2-4}$ is the radiation heat transfer coefficient between nodes 2 and 4. The radiation heat transfer coefficients, h_R are used to calculate the radiation heat flux in linearized form as h_R times the temperature difference between the two surfaces exchanging thermal radiation. Assuming that all surfaces behave as grey bodies, the net radiation flux between two surfaces i and k is expressed as (Holman, 1981, pg.330)

$$q_{i-k}=\frac{\sigma(T_i^{\,4}-T_k^{\,4})}{\frac{1-\varepsilon_i}{\varepsilon_i A_i}+\frac{1}{A_i F_{i-k}}+\frac{1-\varepsilon_k}{\varepsilon_k A_k}} \tag{3-8}$$

where σ is the Stefan-Boltzmann constant (5.669x10^{-8} W/m^2/K^4), ε is the surface emissivity,

and F_{i-k} is the view factor or the fraction of energy leaving i and reaching k. When the temperature difference in Eqn.3-7 is expressed as (T_i-T_k) (T_i+T_k) $(T_i^2+T_k^2)$, the radiation heat transfer coefficient becomes

$$h_{R,i-k}=\frac{\sigma(T_i+T_k)(T_i^{\,2}+T_k^{\,2})}{\frac{1-\varepsilon_i}{\varepsilon_i}+\frac{1}{F_{i-k}}+\frac{(1-\varepsilon_k)A_i}{\varepsilon_k A_k}} \qquad (3\text{-}9)$$

When calculating h_R in the thermal model using Eqn.3-8 at hour j, the temperatures from hour j-1 are used. From temperature measurements taken in the test attics during periods when sheathing temperatures are changing rapidly, the maximum error Eqn.3-8 produces is 9% although errors are more typically 1 to 2%. For the test attics, the emissivities of the plywood roof sheathing was estimated to be 0.90 (ASHRAE, 1989, Chap.37) while the attic floor with glass fibre batt insulation was assumed to be a rough surface with an emissivity of 0.94.

The view factors in Eqn.3-8 were based on the calculations made by Ford (1982 pg.85). Ford calculated view factors for an attic split into seven sections: floor, two gable end walls, two pitched roof surfaces and two eave overhangs (soffits). From Ford's analysis for a gable end attic the view factors were estimated to be as follows:

- from the attic floor and the pitched roof sheathing surfaces to the gable ends, view factors are about 0.03
- from the pitched roof surfaces to the eaves, view factors are about 0.11 for the eave directly below each pitched roof surface and about 0.003 for the eave across the attic from each pitched roof surface
- from the pitched roof surfaces to the floor, view factors are about 0.76 and from the floor to each pitched roof surface, about 0.47.

Since the pitched roof surfaces and the floor have the largest surface areas of the attic nodes, these three nodes dominate the internal radiation heat transfer in the attic. For simplicity the model developed for this study neglects the eave overhangs and the gable ends because they have a relatively small areas and corresponding view factors. This reduces the internal attic radiation heat transfer to a simple three surface problem involving the attic floor (node 8), the inner north sheathing (node 2), and the inner south sheathing (node 4). For these calculations, the attic floor area was assumed to be 51.1 m^2 (including some of the eave area), while the north and south sheathing areas were each 30.3 m^2. Based on these areas,

the view factors were estimated to be

$$F_{4-8}=F_{2-8}=0.84 \tag{3-10}$$

$$F_{4-2}=F_{2-4}=0.16 \tag{3-11}$$

3.1.3 Outer North Sheathing (node 3)

The outer sheathing surface experiences radiation fluxes from the surroundings with large solar gains during the day and large radiation losses during clear nights. Modelling of these external fluxes is important in order to accurately predict sheathing temperatures and consequent moisture adsorption and desorption. The energy balance for hour j is

$$\rho_W V_3 C_{sh,W}\frac{(T_3^j-T_3^{j-1})}{\tau}=h_{U,3}\ A_3(T_{out}^j-T_3^j)+\frac{A_3}{R_3}(T_2^j-T_3^j) \\ +A_3G_3\lambda_3+h_{R,3-sky}\ A_3(T_{sky}^j-T_3^j)+h_{R,3-g}\ A_3(T_{out}^j-T_3^j) \tag{3-12}$$

where V_3 is the total north sheathing volume, A_3 is the sheathing area of 30.3 m^2, R_3 is the sheathing thermal resistance, $h_{U,3}$ is the exterior forced convective heat transfer coefficient, λ_3 is solar absorptivity of shingles which was taken to be 0.9 for the test attics, G_3 is the total solar radiation on north sheathing, $h_{R,3\text{-}sky}$ is the radiation heat transfer coefficient from roof to sky, and $h_{R,3\text{-}g}$ is radiation heat transfer coefficient from roof to ground and clouds. The forced convective heat transfer coefficient, $h_{U,3}$ was calculated using Eqn.3-5 with air velocity set equal to the eave-height wind speed used in the ventilation model.

The daytime solar radiation, G includes both direct and diffuse radiation and is one of the ambient inputs to the thermal model. For this study, values were measured continuously at the test site and showed peak values during winter of 550 W/m^2 on the south roof and only 60 W/m^2 on the north roof; in summer, the peak solar radiation was 1050 W/m^2 on the south roof. The roof surface also exchanges long wave radiation with its surroundings which include the background sky, the ground, and clouds. In this model, it is assumed that the ground and clouds are at the same temperature as the ambient air. However, the sky temperature, T_{sky} is generally quite different from the air temperature. Parmelee and Aubele (1952) developed the following empirical fit to measured data to estimate T_{sky} for horizontal

surfaces exposed to a clear sky

$$T_{sky}=T_{out}\left(0.55+5.68*10^{-3}\sqrt{P_v}\right)^{0.25} \tag{3-13}$$

where P_v is in Pa and the temperatures are in K. Because Equation 3-12 is for horizontal surfaces fully exposed to a clear sky, Ford (1982 pg.96) developed the view factors $F_{i\text{-}sky}$ and $F_{i\text{-}g}$ to account for the amount of cloud in the sky and the slope of the pitched roof surfaces. The view factor from a horizontal surface, $F_{h\text{-}sky}$, to the sky that accounts for cloud cover is given by

$$F_{h-sky}=(1-S_C) \tag{3-14}$$

where S_C is the fraction of sky covered by cloud that must be estimated as an input to the model. The value of S_C varies from 0 (clear sky) to 1 (complete cloud cover). The fraction of the sky seen by an inclined surface, $F_{i\text{-}sky}$, is directly proportional to the angle of inclination from the horizontal, β such that

$$F_{i-sky}=\frac{180-\beta}{180} \tag{3-15}$$

Combining Equation 3-13 with 3-14 gives the view factor, $F_{i\text{-}sky}$, from an inclined roof to a cloudy sky at T_{sky}

$$F_{i-sky}=\frac{(1-S_C)(180-\beta)}{180} \tag{3-16}$$

The pitched roof surface sees either the clouds and ground or the sky and so the two view factors must add up to unity. Assuming that the ground, cloud and air temperatures are the same then a view factor to the ground and clouds, $F_{i\text{-}g}$, can be defined as

$$F_{i-g}=1-F_{i-sky} \tag{3-17}$$

With these view factors defined, the long wave radiation exchange between the roof and surroundings (which can be treated as a three surface problem in the same fashion as the interior of the attic) can be expressed in a linearized form as

$$q_{R,i}=A_i h_{R,i-g}(T_i-T_{out})+A_i h_{R,i-sky}(T_i-T_{sky}) \tag{3-18}$$

where $h_{R,i-g}$ is the radiation heat transfer coefficient from roof surface i to the ground and clouds and is given by

$$h_{R,i-g}=\frac{\sigma(T_i+T_{out})(T_i^{\,2}+T_{out}^{\,2})}{\frac{1-\varepsilon_i}{\varepsilon_i}+\frac{1}{F_{i-g}}} \tag{3-19}$$

and $h_{R,i-sky}$ is the radiation heat transfer coefficient from roof surface to the clear sky and is given by

$$h_{R,i-sky}=\frac{\sigma(T_i+T_{sky})(T_i^{\,2}+T_{sky}^{\,2})}{\frac{1-\varepsilon_i}{\varepsilon_i}+\frac{1}{F_{i-sky}}} \tag{3-20}$$

The long wave emissivity, ε_i of the roof shingles is assumed to be 0.90 for this study.

3.1.4 Inner South Sheathing (node 4)

The energy balance for the inside of the south sheathing has the same form as the inside north sheathing. For hour j,

$$\rho_W V_4 C_{sh,W}\frac{(T_4^{\,j}-T_4^{\,j-1})}{\tau}=h_{U,4}\,A_4(T_1^{\,j}-T_4^{\,j})+\frac{A_4}{R_4}(T_5^{\,j}-T_4^{\,j}) \\ +h_{R,4-8}\,A_4(T_8^{\,j}-T_4^{\,j})+h_{R,4-2}\,A_4(T_2^{\,j}-T_4^{\,j}) \tag{3-21}$$

where V_4 is half the sheathing volume, A_4 is the sheathing area, and R_4 is the thermal resistance of the roof.

3.1.5 Outer South Sheathing (node 5)

The energy balance for the inside of the south sheathing has the same form as the inside north sheathing. For hour j,

$$\rho_W V_5 C_{sh,W}\frac{(T_5^j - T_5^{j-1})}{\tau} = h_{U,5}\ A_5(T_{out}^j - T_5^j) + \frac{A_5}{R_5}(T_4^j - T_5^j) + A_5 G_5 \lambda_5 + h_{R,5-sky}\ A_5(T_{sky}^j - T_5^j) + h_{R,5-g}\ A_5(T_{out}^j - T_5^j) \quad (3\text{-}22)$$

where V_5 is the total sheathing volume, A_5 is the sheathing area, R_5 is the roof thermal resistance, $h_{U,5}$ is the exterior forced convective heat transfer coefficient, G_5 is the solar radiation on the south sheathing, λ_5 is the solar absorptivity for shingles, $h_{R,5\text{-}sky}$ is the radiation heat transfer coefficient from roof to sky, and $h_{R,5\text{-}g}$ is the radiation heat transfer coefficient from roof to ground and clouds.

3.1.6 Attic Joists and Trusses (node 6)

The joists and trusses are assumed to be a single node and only exchange heat with the attic air by convection. This node essentially adds thermal mass to the attic with a small time delay. For hour j

$$\rho_W V_6 C_{sh,W}\frac{(T_6^j - T_6^{j-1})}{\tau} = h_{U,6}\ A_6(T_1^j - T_6^j) \quad (3\text{-}23)$$

where V_6 is the volume of joists and trusses, and A_6 is the exposed surface area of the joists and trusses.

3.1.7 Ceiling Inside the House (node 7)

The underside of the ceiling has radiant exchange with the inside surfaces of the house that are assumed to be at the same temperature as the air in the house, T_{in} as well as convection with the air and conduction through the ceiling. For hour j

$$\rho_7 V_7 C_{sh,7}\frac{(T_7^j - T_7^{j-1})}{\tau} = h_{U,7}\ A_7(T_{in}^j - T_7^j) + h_{R,7-in}\ A_7(T_{in}^j - T_7^j) + \frac{A_7}{R_7}(T_8^j - T_7^j) \quad (3\text{-}24)$$

where ρ_7 is the average density of the ceiling drywall, joist and insulation, V_7 is half the volume of ceiling drywall, joist and insulation A_7 is the ceiling area which is 49 m^2, $C_{sh,7}$ is

the mean specific heat of the drywall, joists and insulation (1100 J/kg-K), $h_{U,7}$ is the convective heat transfer coefficient, $h_{R,7\text{-}in}$ is the radiation heat transfer coefficient between node 7 and the interior of the house, and R_7 is the ceiling thermal resistance. The thermal resistance of the ceiling was modelled as joist and insulation resistances in parallel with drywall resistance in series. For the test attics, the joist spacing is 61 cm with 10 cm glass fibre batt insulation depth yielding an overall resistance of 2.3 m^2K/W (RSI).

The heat transfer correlations of Fuji and Imura (1972) for a free convection from a cooled horizontal plate facing downwards were used to estimate the internal heat transfer coefficient. The heat transfer coefficient for air reduced to

$$h_{U,7} = 3.2\ \Delta T^{\frac{1}{3}} \tag{3-25}$$

where the temperature difference between node 7 and the interior temperature was evaluated at the previous hour.

The radiant exchange between the ceiling and the interior is modelled as a two body enclosed system with the interior surfaces assumed to be all at the same temperature as the inside air, T_{in}. The radiant heat transfer is linearized as discussed previously with the radiant heat transfer coefficient, $h_{R,7\text{-}in}$ given by

$$h_{R,7-in} = \frac{\sigma(T_7+T_{in})(T_7^{\,2}+T_{in}^{\,2})}{\frac{1-\varepsilon}{\varepsilon}+\frac{1}{F_{7-in}}+\frac{(1-\varepsilon)A_7}{\varepsilon A_{in}}} \tag{3-26}$$

where A_7 is the ceiling area, A_{in} is the internal house surface area (estimated to be 116 m^2), ε is the emissivity of the interior surfaces (0.9), $F_{7\text{-}in}$ is the view factor and equal to 1 because all the surfaces are enclosed.

3.1.8 Attic Floor (node 8)

The attic floor exchanges heat by radiation to the pitched roof surfaces, forced convection with the attic air and by conduction through the ceiling form the house below. For hour j

$$\rho_8 V_8 C_{sh,8} \frac{(T_8^j - T_8^{j-1})}{\tau} = h_{U,8}\ A_8(T_1^j - T_8^j) + \frac{A_8}{R_8}(T_3^j - T_8^j) + h_{R,8-4}\ A_8(T_4^j - T_8^j) + h_{R,8-2}\ A_8(T_2^j - T_8^j) \quad (3\text{-}27)$$

where ρ_8 is the mean density of the ceiling as for node 7, V_8 is half the ceiling volume, A_8 is the ceiling area, R_8 is the ceiling thermal resistance, $C_{sh,8}$ is the mean specific heat as for node 7, $h_{R,8-4}$ is the radiation heat transfer coefficient from node 8 to 4, and $h_{R,8-2}$ is the radiation heat transfer coefficient from node 8 to 2.

3.1.9 End Wall Inner Surface (node 9)

Both the endwalls (east and west) are assumed to be identical and are lumped together. The inside of the endwalls exchanges heat with the attic air by forced convection and with the outside of the endwalls by conduction. No radiant exchange occurs since these view factors are small. For hour j

$$\rho_W V_9 C_{sh,W}(T_9^j - T_9^{j-1}) = h_{U,9}\ A_9(T_1^j - T_9^j) + \frac{A_9}{R_9}(T_{10}^j - T_9^j) \quad (3\text{-}28)$$

where V_9 is half the total end wall volume, and R_9 is the thermal resistance based on the sheathing thickness.

3.1.10 End Wall Outer Surface (node 10)

The outside of the endwalls exchanges heat with the outside air by forced convection and with the inside of the endwalls by conduction. The external forced convection heat transfer coefficient, $h_{U,10}$, uses the same outside wind speed as the pitched roof surfaces. For hour j

$$\rho_{wood} V_{10} C_{shwood}(T_{10}^j - T_{10}^{j-1}) = h_{conv,10} A_{10}(T_{out}^j - T_{10}^j) + \frac{A_{10}}{R_{10}}(T_9^j - T_{10}^j) \quad (3\text{-}29)$$

where V_{10} is half the total end wall volume, R_{10} is the thermal resistance based on the sheathing thickness, and $h_{U,10}$ is the exterior forced convection heat transfer coefficient using the wind speed, U.

3.2 SOLUTION OF THE HEAT TRANSFER EQUATIONS

The above set of equations that are linear in temperature must be solved simultaneously. This simultaneous solution is found using gaussian elimination. When the temperatures have been calculated the attic air temperature (node 1) is returned to the attic ventilation model so that a new attic ventilation rate can be calculated. This new ventilation rate is then used in the thermal model at the attic air node to calculate temperatures. This iterative process is continued until the attic air temperature changes by less than 0.1°C. Because the attic ventilation rates are relatively insensitive to the attic air temperature usually fewer than five iterations between thermal and ventilation models are required.

SECTION FOUR

THE ATTIC MOISTURE MODEL

The ventilation of residential attics with outdoor air has been the standard method for controlling excessive temperatures and wood moisture contents during summer and winter. However, the exac2t nature in which ventilation has affected moisture has not been fully understood and that has limited building designers from specifying an appropriate level of ventilation for a given climatic zone. More specifically, is there an optimum level of attic ventilation for moisture control or are there ways in which attic construction could be altered to reduce moisture problems? Apart from carrying out many long term field tests, these questions can only be answered by developing suitable models for predicting moisture dynamics within an attic for given weather conditions. In this section, a simple moisture model is developed which is integrated with the ventilation and thermal models developed in Section 2 and 3.

The moisture model is based on separating the components of the attic (air, sheathing, and trusses) into lumped masses which exchange moisture with the surroundings by diffusion, surface convective mass transfer, and by the transport of moisture with air moving into and out of the attic. This latter "bulk" convective mass transfer produces by far, the largest mass fluxes within the attic and the two most important sources of moisture input to the attic are those associated with the ceiling flow and the ventilation flow of outdoor air. Even during winter when outdoor air humidity ratios are relatively small, the mass flux of moisture can still be large for high ventilation rates and can lead to condensation (or sublimation) of moisture inside the attic. In the complete model, these convective air flows are calculated by the two zone ventilation model, described in Section 2 as a function of the attic leakage configuration and the given weather conditions. It should be noted that there are other sources of moisture for an attic such as, rain or snow infiltration through attic vents or water penetration through shingles when ice damming occurs. These additional mechanisms are not specifically included in this model.

Previous attic moisture transport models have been developed, notably those of Ford (1982), Cleary (1985) and Gorman (1987). Ford's model is the simplest because wood moisture contents were not calculated. When conditions in the attic were such that no condensation or evaporation occurred, the moisture mass balance of the attic air did not include the wood surfaces. On the other hand, when condensation or evaporation occurred, the wood was included in the moisture balance and assumed to be at saturated conditions. Thus, all moisture that was transported to the sheathing condensed but did not change the wood moisture content. The amount of moisture transferred from the air to the wood surfaces was calculated from the vapour pressure of the attic air and the saturation pressure of the wood surface which is a function of its temperature only. The temperatures for Ford's model were calculated using an attic heat balance similar to that used in this study and given in Section 3. The ventilation rates for the attic and the flow rate through the ceiling in Ford's model were not calculated and had to be specified as a user input.

Cleary's model assumed a steady-state solution to the mass balance of moisture between the indoor air, attic air, and wood surfaces. The wood moisture content from the previous hour was used to find the humidity ratio of the wood surface using a empirical relationship (developed by Cleary) between wood moisture content, temperature, and humidity ratio. Knowing the humidity ratio of the outside air and the attic ventilation rate, the humidity ratio of the attic air was calculated. The change in moisture content of the attic wood was then obtained by calculating the mass of moisture transferred to the wood surface based on the new attic humidity ratio and the wood humidity ratio from the previous hour. This new moisture content was used to find the wood humidity ratio for use in the next hour's mass balance. Cleary's model did not include moisture transferred through the ceiling which can be a significant moisture load on the attic. Both the temperature of the attic wood and attic ventilation rate had to be specified as inputs to Cleary's model.

Gorman's model was based on Cleary's model and the work carried out by Burch et al. (1985) and included additional nodes for the north and south roof sheathing surfaces that may be at different temperatures. In addition, the flow of moisture into the attic through the ceiling was included in the attic air moisture balance. Gorman made Cleary's model more sophisticated by separating the wood into a surface node that exchanged moisture with the attic air and an inner node that exchanged moisture by diffusion with the surface node. This allowed for a more rapid change of surface wood moisture content rather than distributing the moisture throughout the wood. This is an important feature for moisture exchange with the wood because the wood surface comes to equilibrium faster than if the moisture is distributed throughout the bulk of the

wood; the wood surface then exchanges less moisture with the attic air. Gorman also separated condensed mass from water bound within the wood. In Gorman's model, a wood surface that is above it's fibre saturation point experiences condensation rather than a change in moisture content. Since the fibre saturation point is the moisture content at which the cell walls of wood have absorbed all of the water they can hold, any further moisture accumulation appears as free water within the cells. The temperatures of the wood and attic air were calculated by Gorman using an attic heat balance similar to that described in Section 3. As with the other attic moisture models, the ventilation and ceiling flow rates had to be specified as an input to the model.

The major differences between the current moisture transport model and those discussed above are summarised as follows:

- **Mass Balance:** The model developed for this study carries out a simultaneous moisture balance for all the nodes representing the attic components (see Section 4.1 for node locations). The model allows any node to reach saturation conditions whereupon, condensation occurs. Wood moisture contents and the amount condensed at any node are tracked separately in order to allow drying to occur. In contrast, previous models balanced the bulk convective moisture flows to find the humidity ratio of the attic air and then used this value to calculate the moisture transferred to and from the wood surfaces.
- **Transient Model:** The current moisture model includes a transient moisture accumulation term in the mass balance of each node. A relationship for the rate of change of wood moisture content with time has been developed for this model so that the wood nodes are not assumed to be at steady state. Gorman and Cleary assumed a steady state solution for all the nodes. Ford did not assume a steady-state solution for the attic air but did not explicitly calculate wood moisture contents.
- **Calculated Ventilation Rates:** The attic ventilation rates as well as flow through the ceiling are different for each hour and are calculated using the two zone ventilation model. Previous models have either assumed a constant ventilation and ceiling flow rate or required them to be specified inputs; as such, these previous models were essentially limited to parametric studies and unsuited to simulating attic performance over long periods.

A lumped mass capacity analysis is used in the moisture model with the attic components separated into the nodes shown in Fig.4-1. The wood elements consist of the north and south roof sheathing, the joists and trusses, and the attic air. Following the work of Gorman, each of the north and south sheathing is separated into an inner (attic-side) layer, 3 mm thick and an

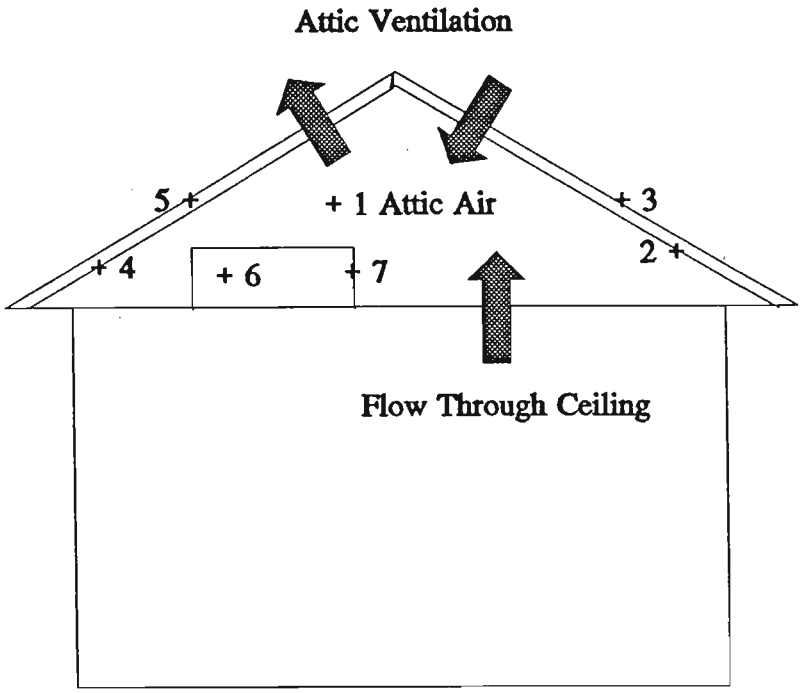

Figure 4-1 Node locations for the attic moisture model

1 is the attic air
2 is the north sheathing surface layer
3 is the north sheathing interior wood
4 is the south sheathing surface layer
5 is the south sheathing interior wood
6 is the interior ofjoists and trusses
7 is the joists and trusses surface layer

underlying layer comprising the remaining thickness (7 mm in the present study). The outer surface of the roof sheathing which is normally covered with building paper and shingles is assumed to be impermeable to water vapour movement. The remaining wood in the attic (joists and trusses) are likewise, separated into a 3 mm surface layer and the underlying mass of wood. The final node corresponds to the attic air which is assumed in this model, to be well mixed so that the humidity ratio of the air is uniform throughout the attic volume. Moisture flows associated with the bulk movement of air (ventilation and ceiling flows) are assumed to mix completely with the attic air. This neglects the possibility of localized deposition of moisture near the infiltration sites, particularly for ceiling flows that may deposit moisture within the ceiling insulation. This refinement could be added to the model but requires a detailed analysis of moisture deposition in porous media with imposed temperature differences. Finally, moisture diffusion through the ceiling and the gable ends is neglected in this model.

4.1 MOISTURE FLUXES

In a lumped capacity analysis, the time rate of change of moisture at node i is equated to the sum of all mass fluxes into and out of that node and the mass of water condensed or evaporated at the node. The transient moisture balance at node i is expressed as

$$\frac{dm_{v,i}}{dt} = \sum M_{v,i} + M_{\tau,i} \tag{4-1}$$

where $m_{v,i}$ is the mass of water at node i, $M_{v,i}$ are the corresponding mass fluxes, and $M_{\tau,i}$ is the mass of water condensed or evaporated at node i (for condensation the term is negative and positive for evaporation). For hour j, the time derivative in Eqn.4-1 is discretized as in the thermal model and approximated as $(m_{v,i}^{j}-m_{v,i}^{j-1})/\tau$ where the time increment is one hour.

As mentioned previously, there are three basic mechanisms for mass transfer. The first is diffusion of vapour through some material (in this case wood). For diffusion of vapour from node k to node i (temperature of the nodes may be different), the diffusive flux is expressed as

$$M_{W,i}=\frac{D_w A}{\Delta X R_{H2O} T_i}\left(\frac{T_i}{T_j}P_{v,j}-P_{v,i}\right) \tag{4-2}$$

where D_w is the diffusion coefficient of vapour in the material (m^2/s), A is the area across which diffusion occurs, ΔX is the distance across which diffusion occurs, R_{H2O} is the gas constant for

water vapour (462 J/kg K), T is the absolute temperature,and P_v is the vapour pressure. Equation 4-2 assumes that all diffusive fluxes are one-dimensional and that the temperature difference does not contribute an additional mass flux (ie. the "thermal-diffusion" effect is negligible). In this formulation, the vapour pressure is the "driving force" for diffusion. For wood, the vapour pressure can be interpreted as the vapour pressure of air that is in equilibrium with the wood at a given temperature and moisture content; the exact nature of this relation is discussed below (see Section 4.2). For wood, Siau (1984, Chap.6) has shown that the diffusion coefficient depends on temperature, moisture content, wood type and directional properties (when diffusion is parallel or perpendicular to the wood grain) and is of the order of 10^{-8} to 10^{-9} m^2/s. For simplicity, a constant diffusion coefficient is used in this study. In recent modelling of moisture transport in wood, Cunningham (1990) used a value of 3×10^{-10} m^2/s for pine. This value from Cunningham is used in this moisture transport model as pine is more typical of wood used in attic construction (fir and spruce are used in the attics that were tested). All of these values of diffusion coefficient are small enough that the exact value used is not critical for the moisture model. At very high moisture contents, the movement of water by capillary diffusion can result in large "diffusive" fluxes; however, this effect is neglected in the present model.

The second transfer mechanism is by the convective motion of air at a free surface eg. the inner surface of the sheathing. The rate of water vapour transfer at the wood surface is determined using a heat and mass transfer analogy as shown by Holman (1981, pg.492). Because phenomenological laws governing heat and mass transfer are similar, the relationship between heat and mass transfer coefficients can be expressed as

$$h_v = \frac{h_U}{C_{sh,\alpha}(Le)^{\frac{2}{3}}} \qquad (4\text{-}3)$$

where h_v is the mass transfer coefficient, m/s, h_U is the convective heat transfer coefficient, $C_{sh,\alpha}$ is the specific heat of air, and Le is the Lewis number for water vapour diffusing in air (ratio of thermal diffusivity to diffusion coefficient) which is assumed to be 0.92 (ASHRAE, 1989, pg.5). In the model developed for this study, Eqn.4-3 is assumed to apply to convective air flow over the wood surfaces in the attic. A similar relationship was used by Gorman (1987) to relate heat and mass transfer at the wood surface. Using a typical heat transfer coefficient of about 5 W/m^2 K, the corresponding mass transfer coefficient, calculated using Eqn.4-3 is approximately 5.3×10^{-3} m/s. Thus, the rate of mass transfer at the wood surface is given by

$$M_W = \frac{h_v A}{R_{H2O} T} \Delta P_v \qquad (4\text{-}4)$$

where ΔP_v is the difference in vapour pressure between the wood surface and the air flowing over it.

The final mass transfer mechanism is due to the "bulk" convective motion of air that transports moisture with it. This flux is equal to the mass flow rate of air multiplied by the humidity ratio of the air and is expressed as

$$M_v = \frac{M_{air}\ P_v}{\rho_{air}\ R_{H2O}\ T} \qquad (4\text{-}5)$$

where M_{air} is the flow rate of air determined from the ventilation model and ρ is the density of the air corresponding to the flow.

4.2 WOOD MOISTURE CONTENT RELATION

An important aspect of the moisture model is the relationship between wood moisture content, temperature, and the vapour pressure of air that is in equilibrium the wood. Measured values for this relationship (where the moisture content of air is expressed in various forms) are presented in the Wood Handbook (1982, Table 3-4) and Kollman and Côté (1968, pg.190) for temperatures ranging from -1°C up to approximately 100°C. Cleary (1985) developed an empirical equation to fit the data where the moisture content of the air was expressed as humidity ratio. By expressing the humidity ratio as vapour pressure, Cleary's equation becomes

$$P_v = \frac{P_\infty}{0.622} \exp\left(\frac{T}{B_3}\right)(B_4 + B_5 W_{MC} + B_6 W_{MC}^2 + B_7 W_{MC}^3) \qquad (4\text{-}6)$$

where P_∞ is atmospheric pressure, W_{MC} is wood moisture content (expressed as a mass ratio of water to dry wood, and T is the temperature in °C. The empirical constants have the following values:

B_3 = 15.8°C B_6 = -0.184
B_4 = -0.0015 B_7 = 0.233
B_5 = 0.053

Equation 4-6 is plotted in Fig.4-2a using vapour pressure and in Fig.4-2b using relative humidity. In each figure, the correlation has been extended to temperatures well below 0°C that are representative of attic temperatures during winter. Several important features are embodied in this correlation. First, from Fig.4-2b, the peak wood moisture content of 37% occurs near room temperature for saturated conditions. This represents the fibre saturation limit for wood where free water exists between the cells of the wood[1]. Second, as temperature falls below 0°C, the equilibrium wood moisture content decreases sharply. This decrease is based purely on an extrapolation of Cleary's correlation and is unsubstantiated by any measurements. At this point, it is unknown whether this correlation represents the actual behavior of wood at low temperatures (detailed measurements of wood moisture contents at low temperatures should be undertaken to confirm these predictions). In any case, the results shown in Fig.4-2b indicate that cooling wood tends to drive moisture out of the cell walls; for example, if a wood surface at a moisture content of 15% is cooled, the vapour pressure in the wood reaches saturation at approximately -13°C. Further cooling will force moisture to be condensed out of the wood as the vapour pressure cannot go above saturation. This leads to condensed water appearing within the wood by simple cooling of the wood and is an important factor in calculating mass condensation on attic surfaces. Finally, a mathematical consequence of Eqn.4-6 is that the lower limit for wood moisture content is 3.2% when the vapour pressure is zero.

4.3 NODE MOISTURE BALANCES

In this section, the transient moisture balance for each node of the attic is presented. The moisture balance for every node includes the rate of condensed mass, M_τ. It should be noted that this term is equal to zero if the vapour pressure at the node is less than the saturation vapour pressure (which is only a function of temperature).

4.3.1 Attic Air (node 1)

The moisture balance for the attic air, at hour j is

[1] The fibre saturation limit depends on wood species and would be approached when relative humidity nears 98%.

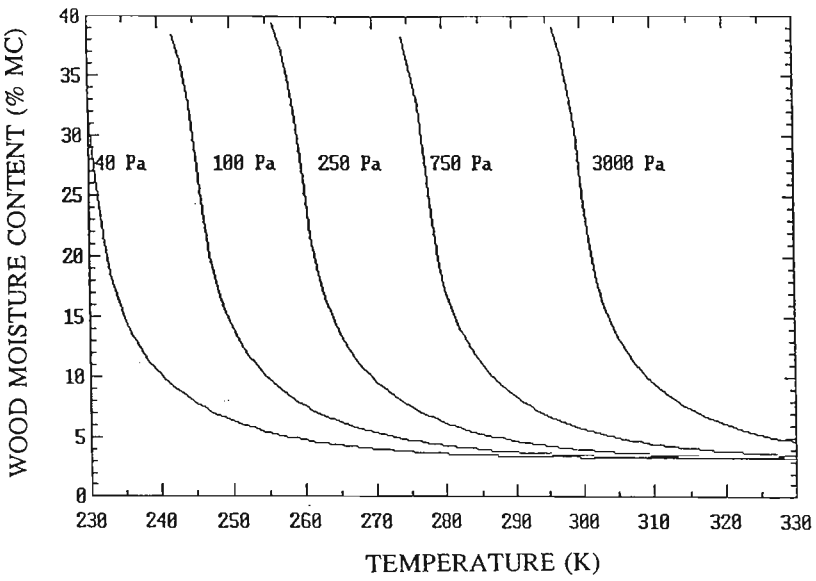

Figure 4-2a Wood moisture content versus temperature at varying equilibrium vapour pressures of air in contact with the wood.

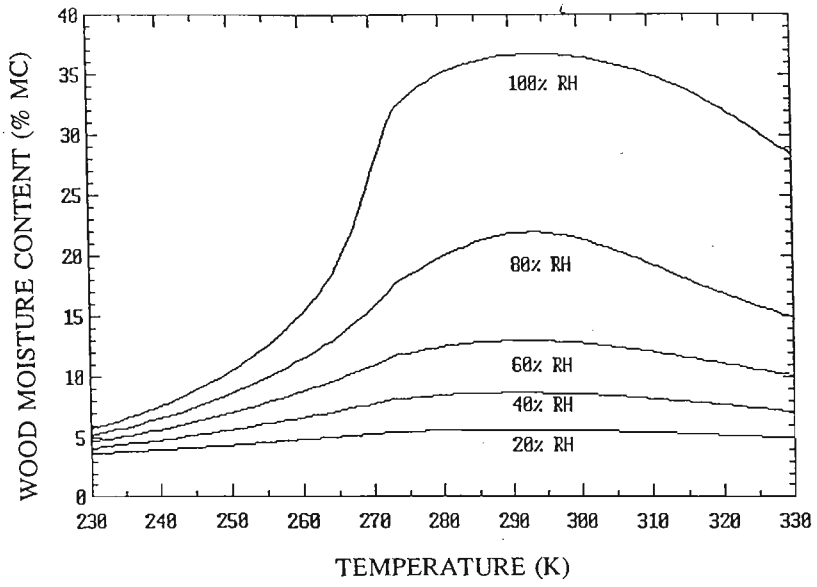

Figure 4-2b Wood moisture content versus temperature for varying equilibrium relative humidities of air in contact with the wood.

$$\frac{V_a(P_{v,1}^{j}-P_{v,1}^{j-1})}{R_{H2O}T_1^{j}\tau}=\frac{h_{v,4}^{j}A_4}{R_{H2O}T_4^{j}}\left(P_{v,4}^{j}-\frac{T_4^{j}}{T_1^{j}}P_{v,1}^{j}\right)+\frac{h_{v,2}^{j}A_2}{R_{H2O}T_2^{j}}\left(P_{v,2}^{j}-\frac{T_2^{j}}{T_1^{j}}P_{v,1}^{j}\right)$$
$$+\frac{h_{v,7}^{j}A_7}{R_{H2O}T_7^{j}}\left(P_{v,7}^{j}-\frac{T_7^{j}}{T_1^{j}}P_{v,1}^{j}\right)+\frac{M_c^{j}P_{v,in}^{j}}{\rho_{in}^{j}R_{H2O}T_{in}^{j}} \qquad (4\text{-}7)$$
$$+\frac{M_{in,a}^{j}P_{v,out}^{j}}{\rho_{out}^{j}R_{H2O}T_{out}^{j}}-\frac{M_{out,a}^{j}P_{v,1}^{j}}{\rho_a^{j}R_{H2O}T_1^{j}}-M_{\tau,1}^{j}$$

where V_a is the attic volume (61 m^3). The time rate of change of vapour mass within the attic air is equated to:

- the convective mass fluxes with nodes 2, 4, and 7
- the bulk convective flow of vapour associated with the ceiling flow rate, M_c, the outdoor ventilation flow, M_{in}, and the ventilation air leaving the attic, M_{out}
- the rate of vapour condensation in the attic air (discussed below).

For the convective air flows into and out of the attic, if M_c is into the attic and M_a is the total attic ventilation rate (measured value) then $M_{in,a}$ is equal to M_a - M_c and $M_{out,a}$ is equal to M_a; however, if M_c is out of the attic then $M_{in,a}$ is equal to M_a and $M_{out,a}$ is equal to M_a - M_c. In those situations where the ceiling flow is from the attic to the interior of the house, the moisture flow associated with the ceiling flow is negative.

4.3.2 Inner North Sheathing (node 2)

The inner sheathing layer exchanges vapour with the attic air by convective mass transfer and with the underlying wood, by diffusion. At hour j, the mass balance is

$$m_{W,2}\left(\frac{\partial W_{MC,2}^{j}}{\partial P_{v,2}^{j}}\frac{(P_{v,2}^{j}-P_{v,2}^{j-1})}{\tau}+\frac{\partial W_{MC,2}^{j}}{\partial T_2^{j}}\frac{(T_2^{j}-T_2^{j-1})}{\tau}\right)+M_{\tau,2}^{j}$$
$$=\frac{h_{v,2}^{j}A_2}{R_{H2O}T_2^{j}}\left(\frac{T_2^{j}}{T_1^{j}}P_{v,1}^{j}-P_{v,2}^{j}\right)+\frac{D_wA_2}{R_{H2O}T_2^{j}\Delta X_s}\left(\frac{T_2^{j}}{T_3^{j}}P_{v,3}^{j}-P_{v,2}^{j}\right) \qquad (4\text{-}8)$$

where $m_{W,2}$ is the mass of dry wood at node 2 (17.2 kg), W_{MC} is the wood moisture content, ΔX_s is the distance (5 mm) between sheathing nodes 2 and 3 for diffusion (1/2 the sheathing thickness since the nodes are located at the centre of each layer), $M_{\tau,2}^{j}$ is the rate of mass condensed or evaporated during hour j if this process occurs. The first term on the left hand side of Eqn.4-8 represents the time rate of change of wood moisture which is $m_W\, dW_{MC}/dt$. Using the empirical correlation for wood moisture content, temperature and vapour pressure, given in Eqn.4-6, dW_{MC}/dt can be expressed as

$$\frac{dW_{MC}}{dt}=\left(\frac{P_\infty}{0.622}\exp\left(\frac{T}{B_3}\right)(B_5+2B_6W_{MC}+3B_7W_{MC}^2)\right)^{-1}\frac{dP_v}{dt} + \left(\frac{-B_3(B_5+2B_6W_{MC}+3B_7W_{MC}^2)}{(B_4+B_5W_{MC}+B_6W_{MC}^2+B_7W_{MC}^3)}\right)^{-1}\frac{dT}{dt} \tag{4-9}$$

The time derivatives of vapour pressure and temperature in Eqn.4-9 are discretized over a one hour period, using the backward difference formulation. At hour j, the two factors in brackets involving temperature and wood moisture content must be evaluated. Since the moisture content at the current hour is not known (this is calculated by solving the node moisture balances), the moisture contents and temperatures from the previous hour are used to evaluate these factors.

4.3.3 Outer North Sheathing (node 3)

For this underlying node, the only mass flux is the diffusion exchange with surface node 2. For hour j, the mass balance is

$$m_{W,3}\left(\frac{\partial W_{MC,3}^{j-1}}{\partial P_{v,3}^{j-1}}\frac{(P_{v,3}^{j}-P_{v,3}^{j-1})}{\tau}+\frac{\partial W_{MC,3}^{j-1}}{\partial T_3^{j-1}}\frac{(T_3^{j}-T_3^{j-1})}{\tau}\right)+M_{\tau,3}^{j}= \frac{D_wA_2}{R_{H2O}T_3^{j}\Delta X_s}\left(\frac{T_3^{j}}{T_2^{j}}P_{v,2}^{j}-P_{v,3}^{j}\right) \tag{4-10}$$

where $m_{W,3}$ is the mass of dry wood (34.2 kg).

4.3.4 Inner South Sheathing (node 4)

The mass balance for this node is similar to that for node 2 and is expressed as

$$m_{W,4}\left(\frac{\partial W_{MC,4}^{j-1}}{\partial P_{v,4}^{j-1}}\frac{(P_{w4}^{j}-P_{w4}^{j-1})}{\tau}+\frac{\partial W_{MC,4}^{j-1}}{\partial T_4^{j-1}}\frac{(T_4^{j}-T_4^{j-1})}{\tau}\right)+M_{\tau,4}^{j} = \frac{h_{v,4}^{j}A_4}{R_{H2O}T_4^{j}}\left(\frac{T_4^{j}}{T_1^{j}}P_{v,1}^{j}-P_{v,4}^{j}\right)+\frac{D_w\,A_4}{R_{H2O}T_4^{i}\Delta X_s}\left(\frac{T_4^{j}}{T_5^{j}}P_{v,5}^{j}-P_{v,4}^{j}\right) \tag{4-11}$$

where $m_{W,4}$ is the mass of dry wood (17.2 kg).

4.3.5 Outer South Sheathing (node 5)

The mass balance for this node is similar to that for node 3 and is expressed as

$$m_{W,5}\left(\frac{\partial W_{MC,5}^{j-1}}{\partial P_{v,5}^{j-1}}\frac{(P_{v,5}^{j}-P_{v,5}^{j-1})}{\tau}+\frac{\partial W_{MC,5}^{j-1}}{\partial T_5^{j-1}}\frac{(T_5^{j}-T_5^{j-1})}{\tau}\right)+M_{\tau,5}^{j}= \frac{D_wA_4}{R_{H2O}T_5^{j}\Delta X_s}\left(\frac{T_5^{j}}{T_4^{j}}P_{v,4}^{j}-P_{v,5}^{j}\right) \tag{4-12}$$

where $m_{W,5}$ is the mass of dry wood at node 5 (34.2 kg).

4.3.6 Underlying Mass of Joists and Trusses (node 6)

This node exchanges moisture with surface node 7 by diffusion only. At hour j, the mass balance is

$$m_{W,6}\left(\frac{\partial W_{MC,6}^{j-1}}{\partial P_{v,6}^{j-1}}\frac{(P_{w6}^{j}-P_{w6}^{j-1})}{\tau}+\frac{\partial W_{MC,6}^{j-1}}{\partial T_{6}^{j-1}}\frac{(T_{6}^{j}-T_{6}^{j-1})}{\tau}\right) \qquad (4\text{-}13)$$
$$+M_{\tau,6}^{j}=\frac{D_w A_6}{R_{H2O}T_6^j\Delta X_w}\left(\frac{T_6^j}{T_7^j}P_{v,7}^{j}-P_{v,6}^{j}\right)$$

where $m_{W,6}$ is the mass of dry wood at node 6 (188 kg), ΔX_w is the mean distance between nodes 6 and 7 (for a 50mm by 100mm cross section truss component, ΔX_w is equal to 37.5 mm).

4.3.7 Surface of Joists and Trusses (node 7)

For this surface layer, a thickness of 1 mm was chosen. The moisture balance for hour j is

$$m_{W,7}\left(\frac{\partial W_{MC,7}^{j-1}}{\partial P_{v,7}^{j-1}}\frac{(P_{v,7}^{j}-P_{v,7}^{j-1})}{\tau}+\frac{\partial W_{MC,7}^{j-1}}{\partial T_{7}^{j-1}}\frac{(T_{7}^{j}-T_{7}^{j-1})}{\tau}\right)+M_{\tau,7}^{j} \qquad (4\text{-}14)$$
$$=\frac{h_{v,7}^{j}A_7}{R_{H2O}T_7^j}\left(\frac{T_7^j}{T_1^j}P_{v,1}^{j}-P_{v,7}^{j}\right)+\frac{D_w A_7}{R_{H2O}T_7^j\Delta X_w}\left(\frac{T_7^j}{T_6^j}P_{v,6}^{j}-P_{v,7}^{j}\right)$$

where $m_{W,7}$ is the mass of dry wood at node 7 (12 kg).

4.4 CALCULATION OF CONDENSED MASS

The above set of algebraic equations are easily solved if the vapour pressure at all nodes is below the saturation vapour pressure corresponding to the temperature at the node. If saturation conditions are reached at any one node, the solution of these equations becomes more complicated. The following section discuss condense water at the wood nodes and attic air.

4.4.1 Wood Surface Nodes

If the vapour pressure from the simultaneous solution of the mass transfer equations is

calculated to be greater than the saturation vapour pressure for a node, then the vapour pressure is set equal to the saturation vapour pressure. A new mass balance is performed with the vapour pressure held at the saturation vapour pressure for that node. Once all the other vapour pressures are found (other nodes may also be at saturation) the rate of mass condensation, M_τ, is calculated from the mass balance equation that includes fluxes to and from other nodes as well as mass changes due to temperature effects when the node is saturated. The effects of temperature are very important because a decrease in temperature for a node at saturation in cold winter weather implies a decrease in wood moisture content as can be seen in Fig.4-2b. The mass that was included as wood moisture content now appears as condensed mass at this wood node. Thus, the temperature change at a wood node can change its wood moisture content even if there is no net flux to the node. If the rate of condensed mass at a node is positive then mass accumulates at the node; this mass is not included in the wood moisture content (and therefore in finding the vapour pressure for the next hour) but is monitored using a separate term, m_τ, that is the total mass accumulated at the surface. If the net mass change is negative then m_τ is reduced. If this reduction makes the total accumulated mass negative then the difference between the net mass change and the accumulated mass from the previous hour is used to reduce the wood moisture content (and the vapour pressure) of the node. Thus, when all condensed mass has been evaporated or reabsorbed by the wood then $m_\tau = 0$ which implies that the vapour pressure is below saturation and the mass balance for the attic must be repeated as this node is now an unknown.

4.4.2 Attic Air Node

For the attic air, the vapour pressure is limited to the saturation vapour pressure as determined by attic air temperature. If there is a net mass flux to the attic air when it is saturated from the combination of attic wood surfaces and air flows then this net mass must result in condensed mass in the saturated attic air. Unlike the wood, there is no surface for this mass to accumulate on. Consequently, the condensed mass is assumed to be distributed to the wood surfaces and the air leaving the attic in proportion to their mass flux exchange with the attic air. Condensed attic moisture is only transferred to wood surfaces for which there is a positive flux from the attic air at the saturation vapour pressure to that node. This usually means positive fluxes from the attic air to colder sheathing surfaces which are at a lower vapour pressure. This usually leads to frost buildup on the interior of attic sheathing which is observed quite frequently during winter. The rest of the condensed attic air moisture

is advected out with the attic air ventilation flows. At the wood nodes, the additional condensed mass from the attic air is used to calculate a new wood moisture content and vapour pressure, and the mass balance for the attic is repeated with the vapour pressure for the attic air held at the saturation vapour pressure. If the mass transfer with the attic air at saturation makes the wood vapour pressure greater than its saturation vapour pressure then the procedure for considering condensed mass for the wood must also be performed (as discussed above). This process of finding which nodes are at saturation (then holding them at their saturation vapour pressure and recalculating the mass balance) is continued until no more nodes reach saturation.

4.5 SOLUTION PROCEDURE

If the vapour pressure is less than saturation at all nodes then the moisture model is a system of seven mass balance equations for the seven unknown vapour pressures. Gaussian elimination is used to simultaneously solve these seven equations. Problems occur because the vapour pressure has an upper limit of the saturation pressure. If a node is at saturation then its vapour pressure is known and is determined by the node temperature. This known vapour pressure must be substituted into the remaining equations for the other nodes and one less equation has to solved. This requires changing the number of equations in the gaussian elimination scheme and the procedure becomes even more complicated if more than one node is at saturation.

A solution to this problem is to use an iterative technique rather than gaussian elimination to solve the equations. Gaussian elimination is still used to provide initial estimates of vapour pressure which speeds up the iterative process. With an iterative technique, each node can be checked for saturation after every iteration and the appropriate vapour pressures held constant in the next iteration. The iterative technique used here makes estimates of the vapour pressure at a node by substituting the vapour pressures from the previous iteration for the other nodes. Each of the seven equations is solved consecutively. The process is speeded up by using the updated vapour pressures within each iteration as they become available; for example, after Eqn.4-7 is solved then $P_{v,1}$ is known. This vapour pressure is now substituted wherever it appears in the other six equations rather than waiting for the next iteration. Repeated estimates of vapour pressure are made by cycling through the seven equations until all the vapour pressures change by less than 0.1 Pa. Each node at each iteration is checked to see if the calculated vapour pressure is greater than saturation. If it is then this vapour pressure is set equal to the saturation vapour pressure corresponding to the temperature at that node. The mass balance is then

performed with this fixed vapour pressure to find the condensed mass as outlined in Sections 4.4.1 and 4.4.2. If saturated conditions do not exist, only one iteration is required since the initial estimates from the gaussian elimination method are already the solution to the set of non-saturated equations.Once the vapour pressure is found for each node the wood moisture content is calculated for the wood nodes using Eqn.4-6.

SECTION FIVE

MEASUREMENTS AND MODEL PREDICTIONS

The complete attic thermal and moisture simulation model was verified with data taken in a full-size field test facility located at the Alberta Home Heating Research Facility, Edmonton, Alberta. The attic monitoring program was carried out over a two year period from 1990 to 1992. In Section 5.1, details of the test houses and more specifically, the test attics are presented along with the procedures for measurement of attic ventilation rates, temperatures, and air and wood moisture contents. Since attic ventilation rates are central to this study, Section 5.2 first provides some trends observed in the measured attic ventilation rates and ceiling flow rates and their dependence on ambient conditions. Section 5.3 then presents a comparison of the measurements and predictions in order to verify the models.

5.1 TEST FACILITY AND MEASUREMENT PROCEDURES

The field monitoring program was carried out over a period covering two heating seasons in 1990-91 and 1991-92 at The Alberta Home Heating Research Facility (AHHRF), located south of Edmonton, Alberta. The facility consists of six houses situated in an east-west row, each house having a full basement with a single storey and gable-end attic. The houses are spaced approximately 2.6 m apart. At each end of the row, false end walls were constructed about 3.7 m high but without roof gable peaks, to provide wind shelter and solar shading similar to that experienced by interior houses in the row. The attic ventilation tests were carried out in houses 5 and 6 which are the last two houses at the east end of the row. Table 5-1 lists the pertinent details of houses 5 and 6 which are essentially identical in construction and insulation levels; Figure 5-1 shows a series of photographs of houses 5 and 6, detailing their layout and the false end wall. All houses at the test site are heated electrically and a centrifugal fan operates continuously, recirculating 4.5 house interior volumes per hour. Since the indoor ventilation rates

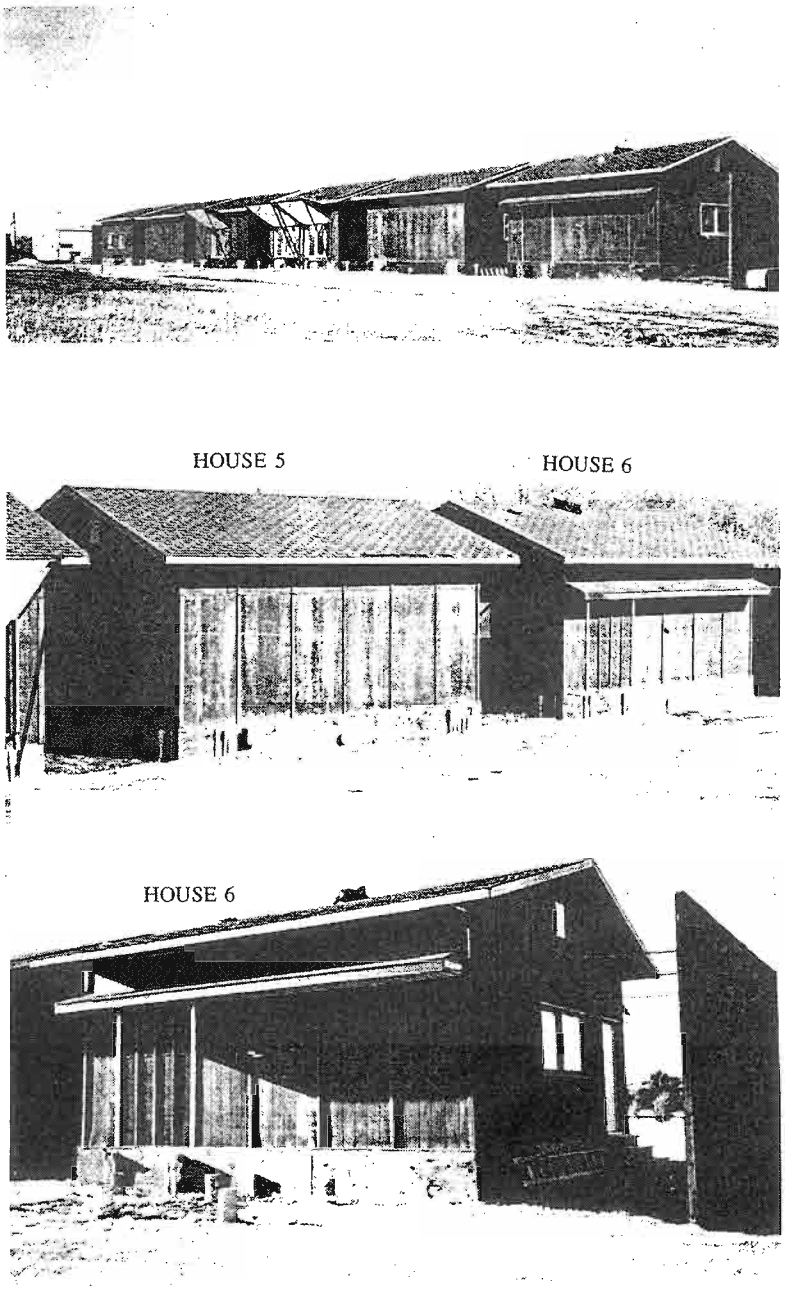

Figure 5-1. Houses 5 and 6 at AHHRF showing building orientation and false end wall.

Table 5-1
Construction Details of Houses 5 and 6

Floor Area	6.7 m x 7.3 m (22′ x 24′)
Wall Height	2.4 m (8′)
Basement Height	2.4 m, 1.8 m below grade (8′,6′ below grade) Exterior insulation RSI 1.76 (R10) to 0.61 m (2′) below grade
Walls	9.5 mm (3/8") Prestained Rough Tex Plywood 64 mm (2-1/2") Glass fiber batts 51 mm x 102 mm (2" x 4") studs, 40 cm (16") o/c 4 mil poly vapour barrier 12.7 mm (1/2") drywall, painted
Wall Area/Floor Area	1.39/1
Windows	N 99 cm x 193 cm (39" x 76") double glazed sealed S none E 101 cm x 193 cm (40" x 76") double glazed sealed W same as E
Window Area/Floor Area	11.9%
Ceiling	152 mm (6") Glass fiber batts 4 mil poly vapour barrier 12.7 mm (1/2") drywall, painted
Roof	CMHC approved trusses with 76 cm (2-1/2") stub 210# asphalt shingles 9.5 mm (3/8") Ext. GD plywood sheathing roof pitch 3.0:1 61 m^3 attic volume
Basement	20 cm (8") concrete wall 10 cm (4") concrete slab on 6 mil poly
Electric Furnace Capacity	12 kW

are continuously measured using SF_6 tracer gas, the fan ensures that the air inside the house is well mixed. All houses, except #3 (conservation unit with enhanced insulation levels) have a 15.2cm ID flue pipe that extends from 145 cm above the basement floor through the ceiling and

roof to terminate in a rain cap level with the roof ridge. The flue is not attached to the furnace but does allow indoor air to escape outdoors. During the 1990-92 test period, the flue was blocked off in houses 5 and 6; however, prior to this period, house ventilation rates were measured in a number of configurations including flue, windows, and vents in open and closed positions. The houses are totally exposed to south and east winds and partially sheltered by trees and buildings for north and west winds. Because wind speeds are measured close to the buildings, wind shelter by trees and buildings is accounted for directly in the wind measurements.

The attic space in houses 5 and 6 are identical in construction. Each attic has plan dimensions of 6.7 m by 7.3 m (including the eaves makes it 7.3 m by 7.8 m) with a roof design of gable end walls and a full length ridge oriented along the east-west direction. Thus, the sloped roof sections face north and south while the gable ends of the attic are vertical extensions of the east and west walls. The roof trusses are constructed of 38 mm by 89 mm spruce joists and are spaced at 61 cm intervals. The sloped roof section (with a pitch of 3:1) is raised 0.67 m above the attic floor to accommodate various levels of ceiling insulation for other tests that have been conducted at AHHRF. The sloped section was covered with 9.5 mm exterior plywood sheathing and 210# brown asphalt shingles. The ceiling consisted of 12.7 mm painted drywall, 4 mil polyethylene vapour barrier, and 89 mm glass fibre batts between the trusses. The total enclosed attic volume was estimated to be 61 m^3. Figure 5-2 shows the truss detail and a photograph detailing the heel section of the trusses.

The two attics selected for the study had different venting arrangements. Attic 5 was selected as a "tight" attic where there were no intentional openings such as roof or soffit vents in the exterior portion on the attic envelope. The only leakage area in attic 5 was the unavoidable leakage associated with construction of the attic envelope. Attic 6 was fitted with continuous soffit vents along the north and south eaves and two flush-mounted attic vents. The soffit vents were mounted on false eaves that were aligned with the floor of the attic; this was done to have the soffit leakage area in a location that was representative of conventional residential construction. Photographs of this detail are shown in Fig.5-3; the first photo shows the false eave from outside, while the second photo shows the detailing from inside the attic. Short pieces of roof sheathing were positioned near the soffits to mimic the sloped roof of a conventional attic without the raised truss. The total soffit area on each side of the house was 2.6 m^2, with 3875 perforations per square metre of soffit area. Each perforation measured 8 mm by 0.5 mm resulting in a gross open area of 403 cm^2 on each side of the house. The flush-mounted roof vents were standard vents purchased at a local hardware store and had a gross opening area of

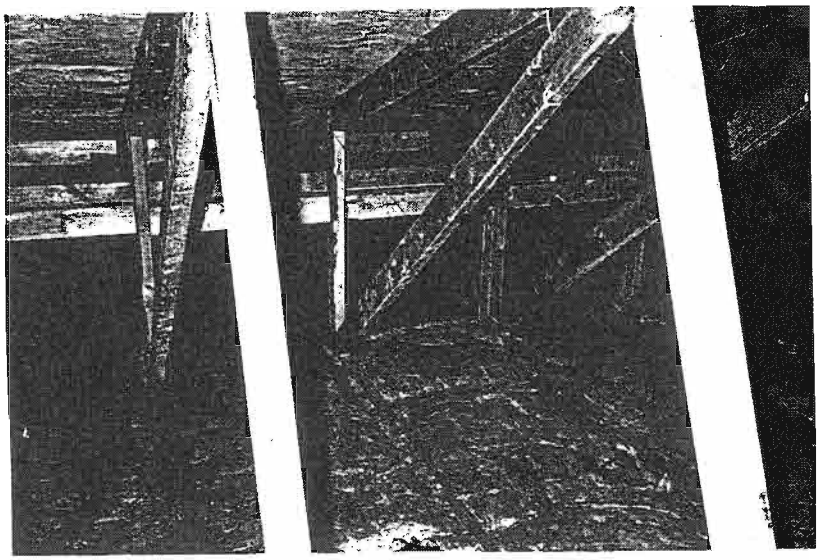

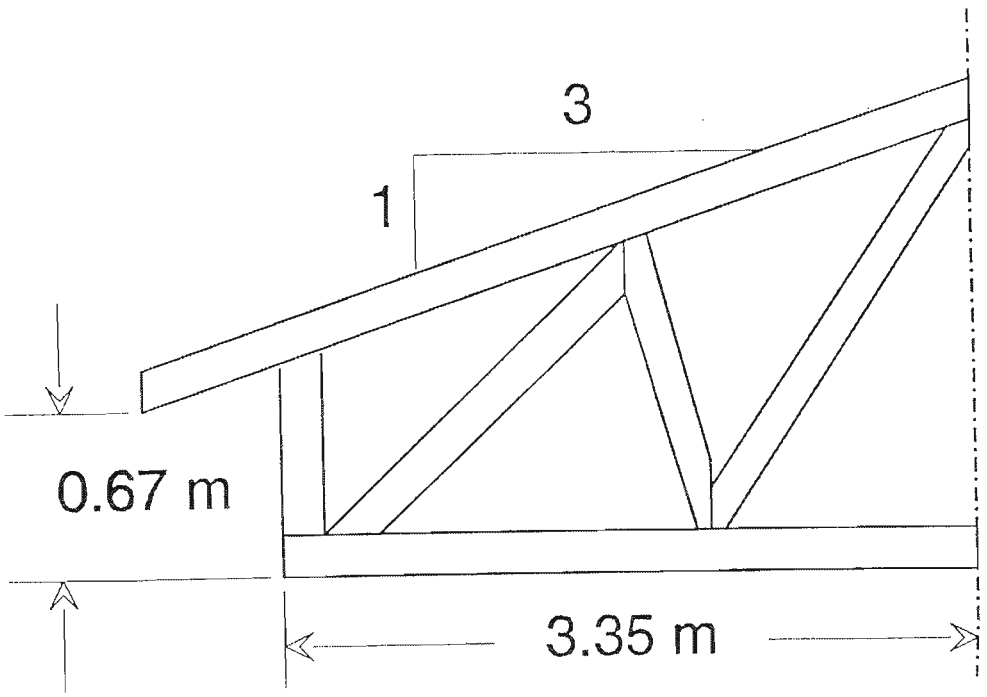

Figure 5-2. Attic interior showing detail of trusses.

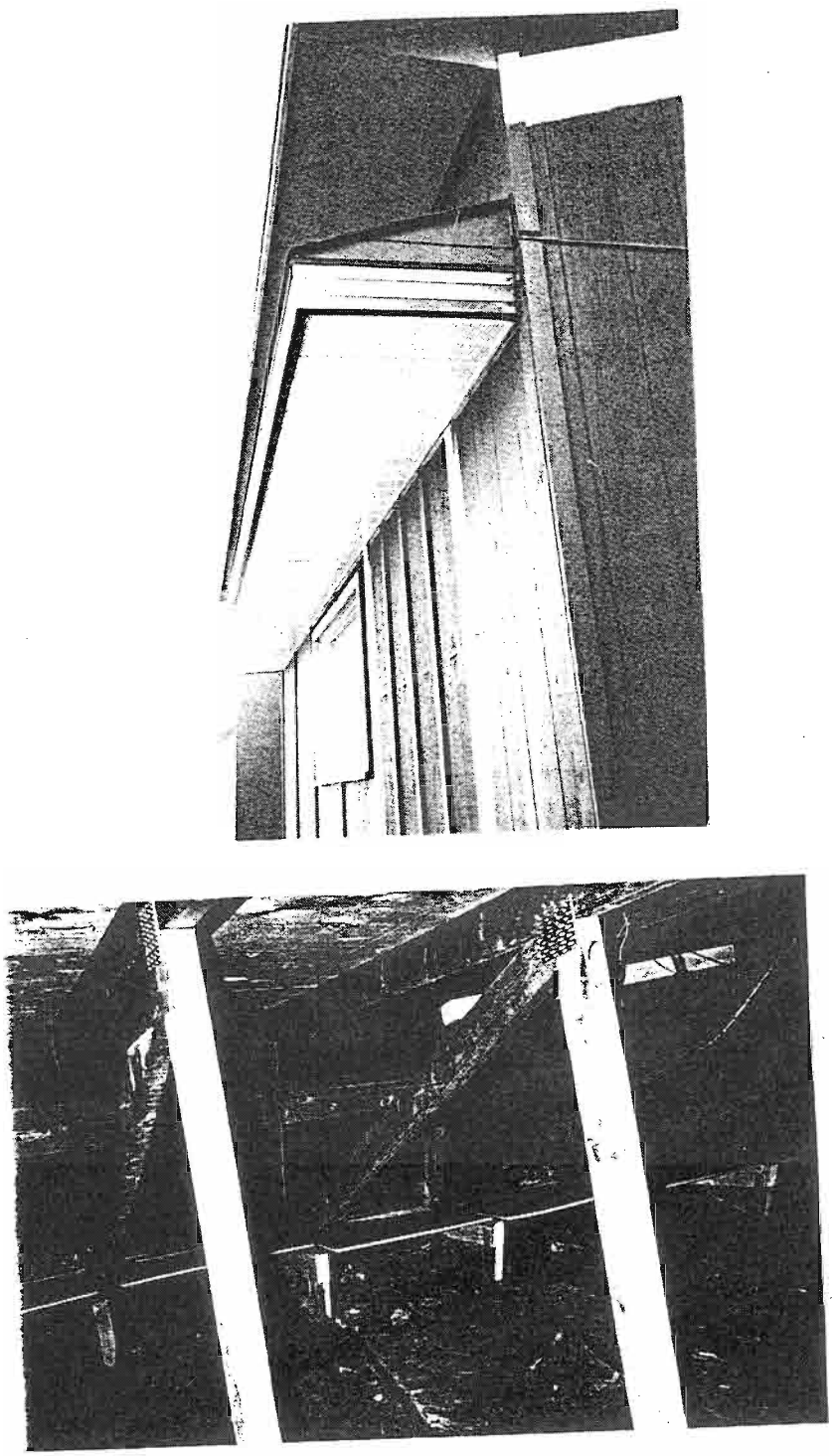

Figure 5-3. False eaves on house 6 from outside and inside.

384 cm^2. The net area was reduced by a screen which was used to prevent the entry of insects. On the north face of the roof, one vents was placed 0.81 m down from the peak of the roof and 1.57 m in from the east edge of the roof; on the south face, the vent was placed 0.81 m down from the peak and 1.57 m in from the west edge. Details of the roof vents are also shown in Fig.5-4.

During the second heating season, attic 6 was retro-fitted with a commercially available, roof-mounted fan (Broan Model 334). The attic fan was located on the north-east section of the roof, 0.81 m from the roof peak and 2.84 m in from the east edge of the roof. Normally, the fan exhausts attic air to outdoors (depressurize the attic). The fan was initially installed and tested in this orientation; however, it was decided to also test the fan in the reverse mode where the fan blows outdoor air into the attic (pressurize the attic). This required that the fan be physically turned upside down in order to reverse the flow direction. In this configuration, the fan inlet would be exposed to the outdoor environment. In order to protect the fan, a short length of 15 cm diameter pipe (1 m long) was attached to the inlet of the fan with a rain cap at the opposite end (the discharge side of the fan was protected with a large rain cap, supplied by the manufacturer). It was necessary to test the fan with this inlet duct arrangement so as to maintain the same flow characteristics of the fan in both orientations. This fan-inlet duct system was initially installed on the roof of attic 6 on November 4, 1991 and tested in the exhaust mode between November 4, 1991 and January 30, 1992. During the tests, the fan was cycled on-off over each 24 hour period with a timer; the fan was on between 10:00 am and 4:00 pm and off for the rest of the day. On January 30, 1992 the fan was reversed and ventilation rate measurements have been continuing since that time. A photograph of the fan in this orientation is shown in Fig.5-5. Prior to installation, the fan-duct system was tested in a calibrated flow apparatus where the flow-pressure difference characteristic was measured; the rated flow, Q_{rated} and pressure, ΔP_{rated} were 0.164 m^3/s and 175 Pa, respectively. Thus, the constant speed characteristic for this fan was

$$Q_{fan} = 0.164 \left(\frac{175 - \Delta P_{fan}}{175} \right)^{0.3} \qquad (5\text{-}1)$$

where Q_{fan} is flow rate in m^3/sec and ΔP_{fan} is pressure difference in Pa. The maximum air flow that the fan can deliver is) 0.164 m^3/s which corresponds to an attic ventilation rate of 9.6 air changes per hour (ac/h) based on an attic volume of 61 m^3. When the fan is connected to the attic there are additional flow resistances through the vents and soffits resulting in a decrease in

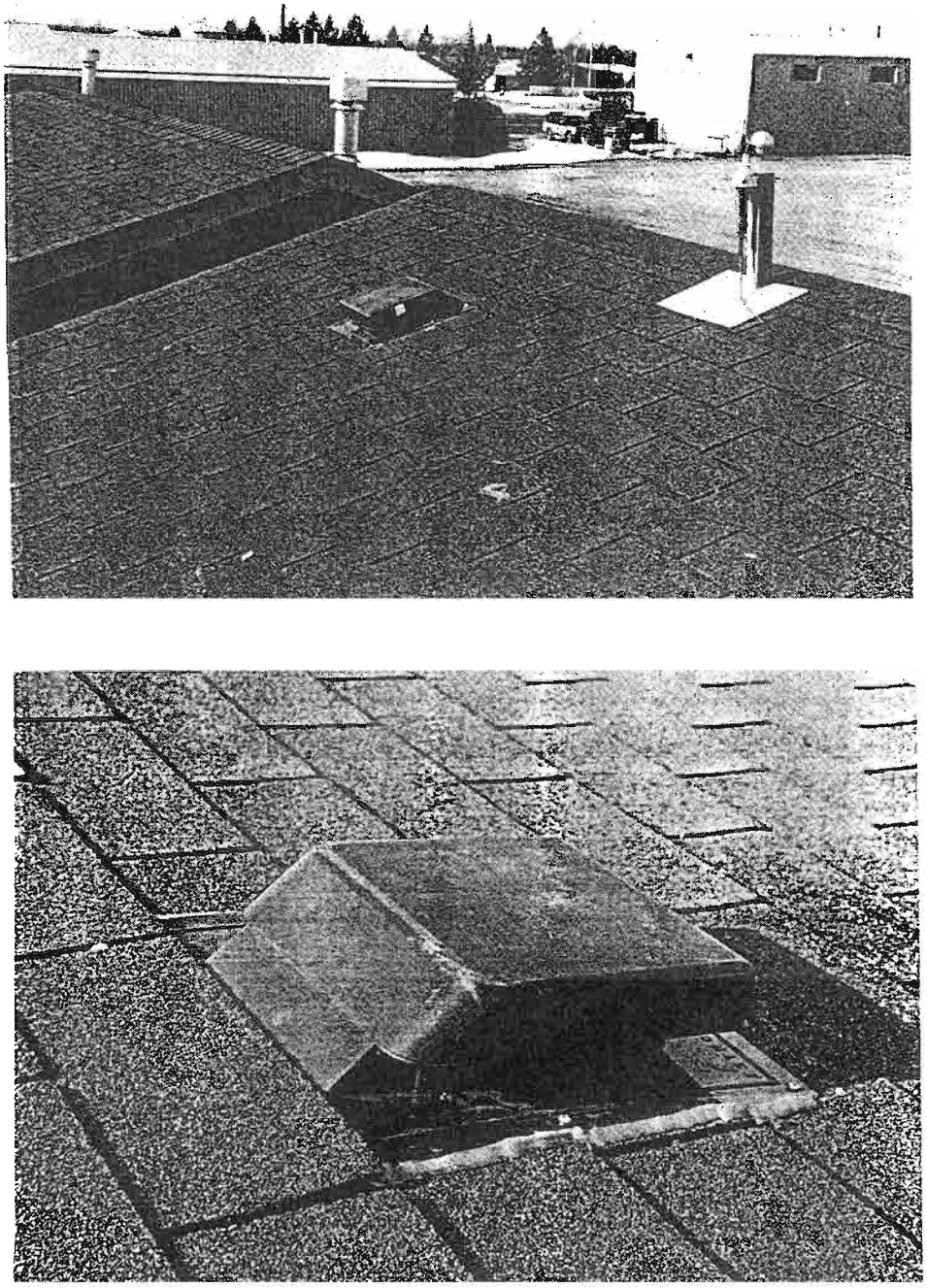

Figure 5-4. Location and installation of roof vents for attic 6.

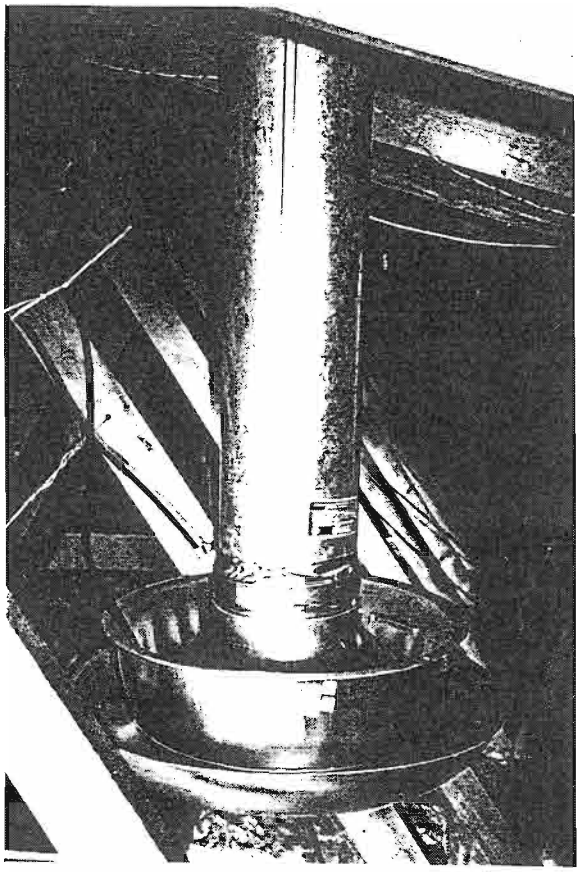

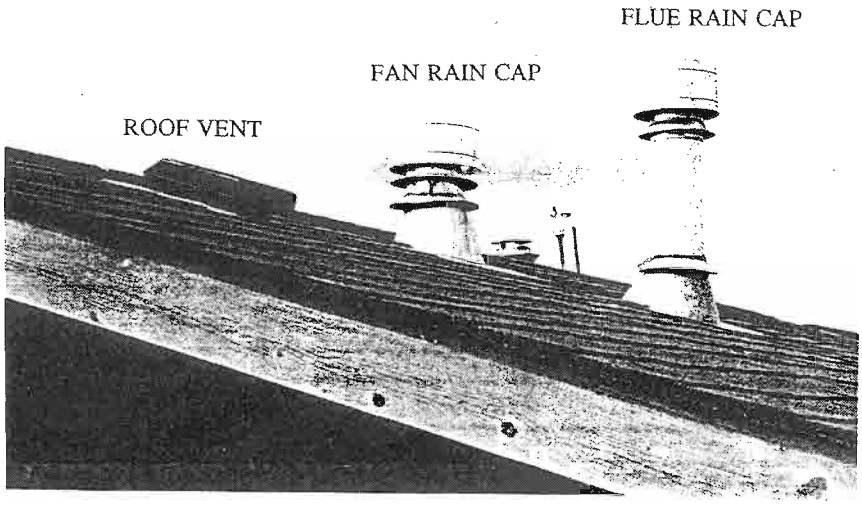

Figure 5-5. Ventilation fan in attic 6 in supply orientation showing interior view and exterior protective rain cap (same as the flue beside it).

the flow delivered by the fan.

The leakage area in the ceiling interface between the heated interior space of the house and the attic allows air exchange between the two zones. During cold weather, indoor air exfiltrating into the attic may impose a significant moisture load on the attic. One of the objectives of the test protocol was to measure the indoor-attic exchange rate. The ceilings in houses 5 and 6 were essentially identical in construction with drywall, vapour retarder, and glass fiber batt insulation. There was some unintentional leakage area, particularly around the electrical junction boxes for the two fluorescent light fixtures in each house. In addition, a 0.5 m by 0.89 m ceiling panel, shown in Fig.5-6 was placed approximately in the centre of the ceiling in both houses and a 7.6 cm diameter hole was placed in the centre of the panel to provide a large leakage site. This intentional leakage site was part of an orifice flow meter which was used to monitor the flow through this leakage area. The ceiling in house 5 had an additional ceiling panel which had three separate leakage sites, 7.6 cm, 2.5 cm, and 0.64 cm diameter, respectively which was used for a separate study on moisture accumulation in the ceiling insulation.

5.1.1 Fan Pressurization Tests

One of the first series of tests conducted on the attics was pressurization measurements to determine the leakage characteristics of the exterior envelope of the attic and of the ceiling. The houses were also pressure tested since the house leakage needs to be known as an input to the two zone attic-house ventilation model. The attic tests were carried out using two separate blowers, one connecting the attic with the interior of the house and the other connecting the interior the house with the outdoors. Figure 5-7 shows the two blowers in house 6; the attic blower was connected through the plexiglass ceiling panel which had been temporally removed for these tests. The flowrate through each blower was obtained by measuring the pressure drop across a laminar flow element which was in series with the fan and pressure difference measurements were taken with calibrated diaphragm transducers (Validyne). The first set of measurements was to determine the background leakage area of the exterior portion of the attic envelope (not including the ceiling). For these tests, the attic was pressurized to a certain level relative to the outdoors and the blower connected to the interior of the house was adjusted until the attic-indoor pressure difference was zero; this procedure required careful manipulation to reach the desired operating point. These measurements were repeated at several pressure differences to obtain a complete flow-pressure difference characteristic. Typical results of these tests are shown as log-log plots in

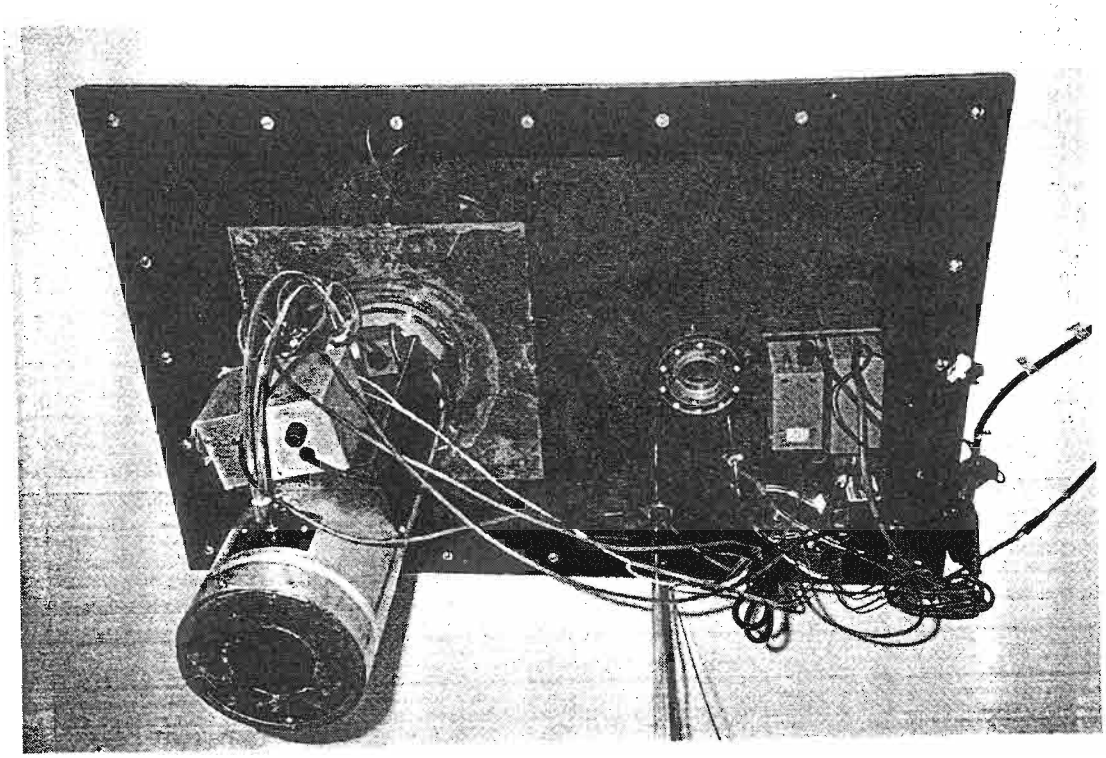

Figure 5-6. Ceiling panel and orifice flow meter.

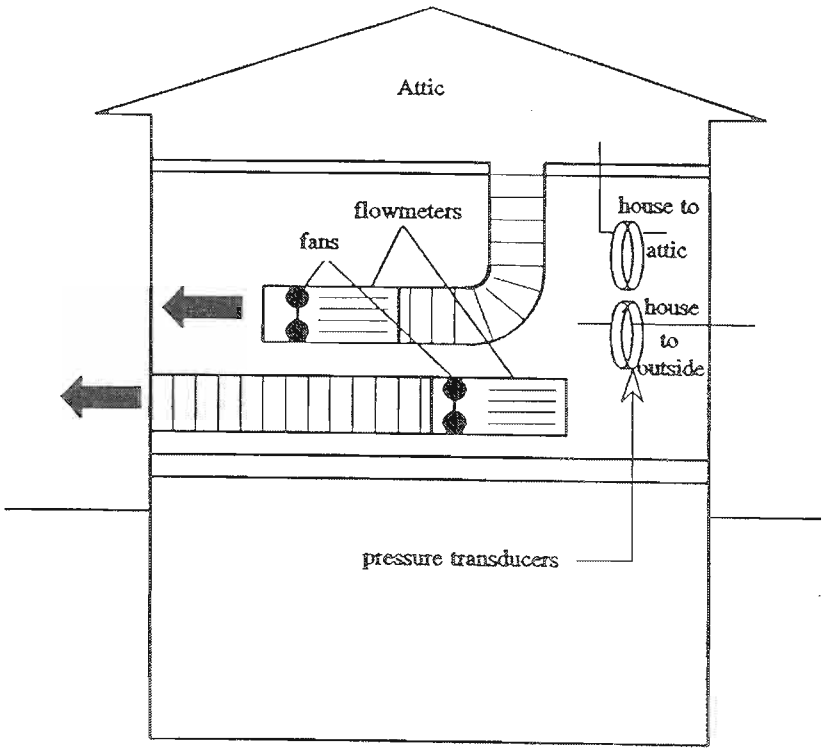

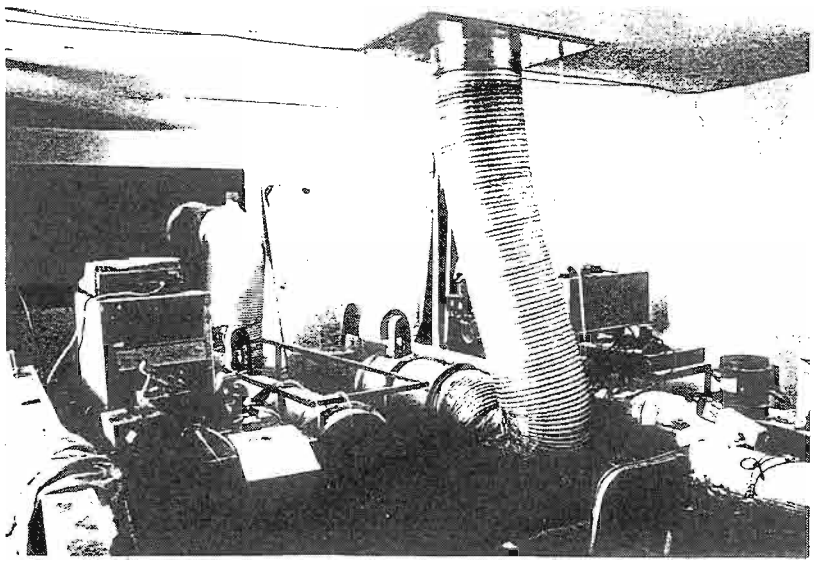

Figure 5-7. Fan pressurization system for attic leakage testing.

Figs.5-8a and 5-8b for attic 5 and 6, respectively. For these tests, the two roof vents were sealed and the soffits were left open so that only the background leakage area was being measured. In order to reduce the scatter in these data, all fan pressurization tests were carried out only when the prevailing wind speed was less than 1 m/sec. The figures show the individual data points as well as a linear least squares fit to the data. The linearity of these curves indicates that the flow characteristic follows a power law where

$$Q = C\Delta P^{n} \tag{5-2}$$

Note that the pressure difference range for attic 6 was 3 to 7 Pa; whereas, attic 5 was tested from 7 to 30 Pa. These pressure ranges were dictated by the maximum flow capacity of the attic fan (approximately 0.7 m^3/sec) and the leakage area of the attic. Since the leakage area of attic 6 was substantially larger than attic 5 (mainly due to the soffits), the maximum pressure difference that could be reached in attic 6 was much less than in attic 5. The derived values of C and n for the exterior portion of each attic envelope is given in Table 5-2 together with the equivalent leakage area based on a pressure difference of 4 Pa. A 4 Pa pressure difference was used for equivalent leakage area since this is a typical average pressure difference that the envelope would experience under natural conditions. The leakage area at 4 Pa can be converted to other pressure differences using

$$A_{\Delta P} = Al_4 \left(\frac{\Delta P}{4}\right)^{n-1/2} \tag{5-3}$$

where $A_{\Delta P}$ and Al_4 are the leakage areas at a pressure difference ΔP and 4 Pa, respectively, and n is the flow exponent. The results clearly show the large difference in leakage areas of the two attics and with the roof vents included attic 6 has approximately four times the leakage are of attic 5. In addition, the values of the flow exponents for the two attics agree with what one might expect. The leakage in attic 5 is dominated by small cracks that arise from the construction of the attic envelope and flow through these cracks is probably developing flow because the cracks are short compared with their width. The value of 0.707 is close to values measured for the interior envelope of a house. Attic 6, on the other hand, includes soffit and roof vents, all of which behave as orifice flow and the measured value of 0.597 supports this observation.

The ceiling leakage area was not included in the first set of measurements since the attic-indoor pressure difference was maintained at zero by the indoor fan. In order to measure the ceiling leakage characteristics, the simplest method was to carry out a pressurization test on

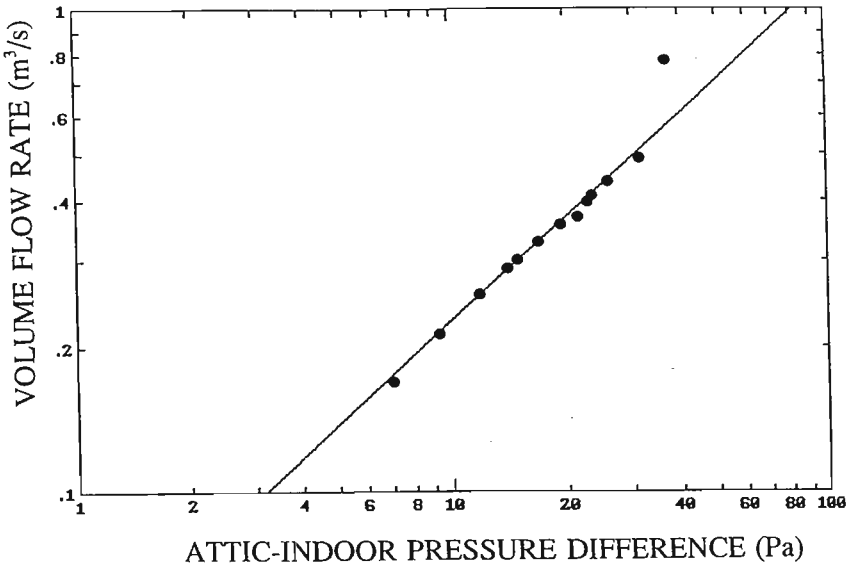

Figure 5-8a. Fan pressurization test results for attic 5.

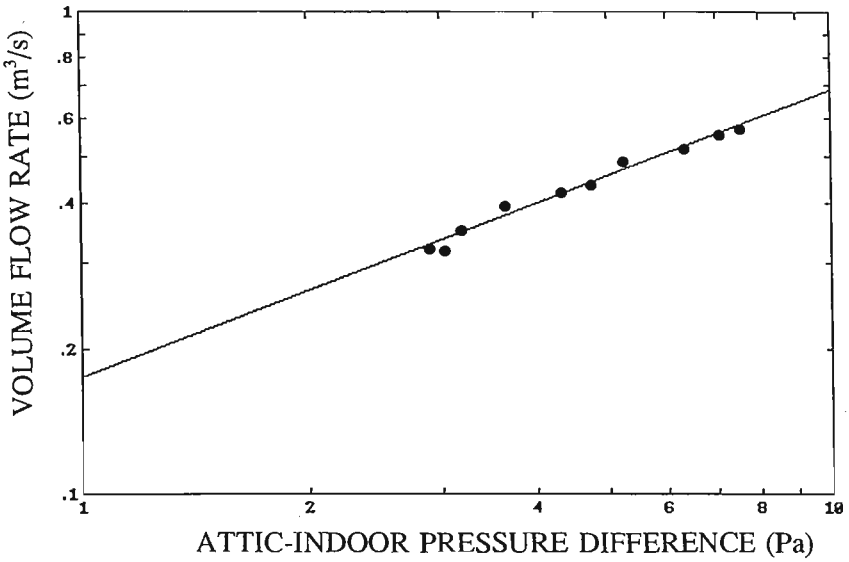

Figure 5-8b. Fan pressurization test results for attic 6.

the interior of the house with the ceiling exposed (as it is normally) and repeating the test with the ceiling leakage area sealed. For both houses 5 and 6 this was possible since almost all the ceiling leakage was concentrated in the intentional openings in the ceiling panel and the unintentional openings around the light fixtures, which were located near the ceiling panel. In a more conventional house, there would tend to be other leakage paths such as, plumbing stacks and gaps between the flue pipe and the duct leading up to the attic, that are inaccessible and would make this method impractical. A different approach to measuring ceiling leakage, such as that proposed by CMHC (1989b), would have to be employed. However, this test protocol requires balancing of indoor-outdoor, attic-outdoor and attic-indoor pressures. This is extremely difficult because wind pressures cause fluctuations in flow and pressure that are the same magnitude as the flows and pressures that one is attempting to measure. The required balancing of flows and pressures was found to be impractical and produced large scatter in the measurements. Blower tests on the interior of the house were performed by an automated system that only carried out the tests when wind speeds were below 1 m/sec. In order to seal the ceiling leakage, a large polyethylene sheet was placed over the central portion of the ceiling, covering the ceiling panel and the two light fixtures and taped along its edge. Interior pressurization tests were then performed (depressurization tests were not performed since the plastic sheet would be blown off the ceiling even when small pressure differences are applied) over a range of pressures from 1 to 100 Pa. The blower test system and measurement methods are described in detail by Modera and Wilson (1989). The most important features of the AHHRF blower test system are:

- a large range of test pressures from 1 to 100Pa. This more than covers the range required by ASTM (1982) and CGSB (1986) standards. Testing at windspeeds below 1m/s allows the extension of the low pressure range down to 1 Pa, which is much lower than either of the above standards.
- pressures across the envelope due to wind and stack effects are corrected by taking a reference pressure at every data point.
- outdoor pressures are spatially averaged by having a pressure tap outside each of the four walls of the building.

Results of these tests are shown in Figs.5-9 and 5-10 for houses 5 and 6, respectively, where flowrate is plotted versus pressure difference; each figure shows results with the ceiling uncovered and with the ceiling leakage sealed. From a least squares fit to the data

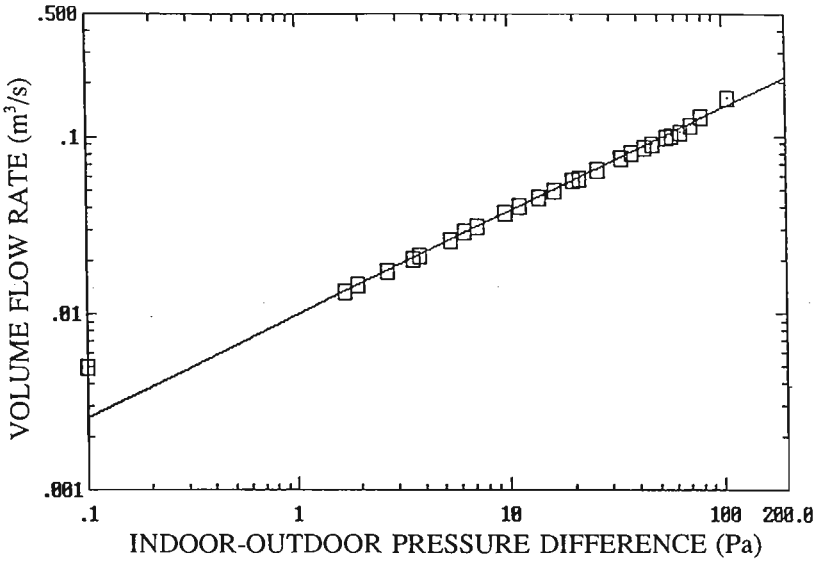

Figure 5-9a. Fan pressurization test results for house 5 with ceiling leaks uncovered.

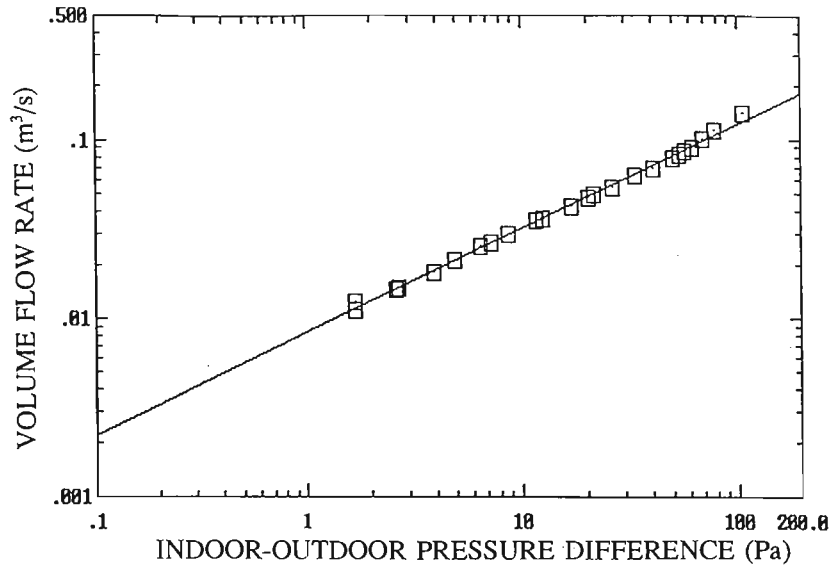

Figure 5-9b. Fan pressurization test results for house 5 with ceiling leaks sealed.

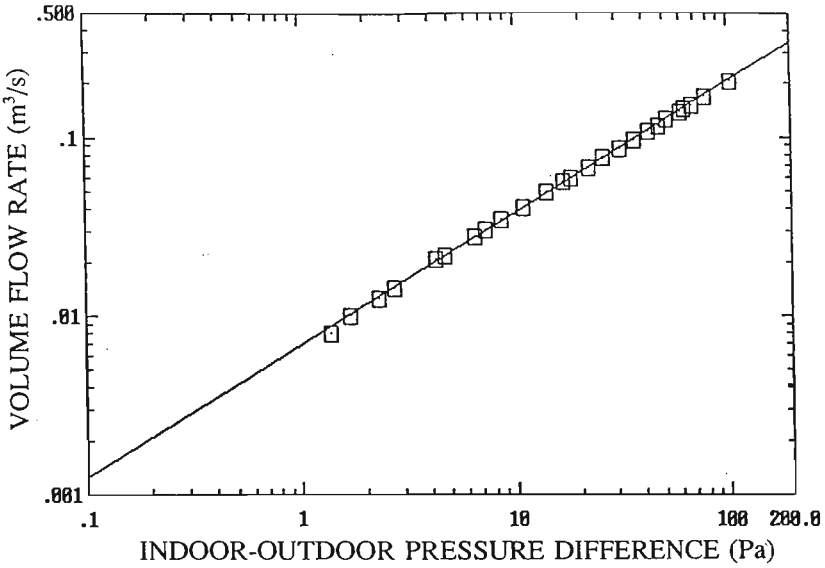

Figure 5-10a. Fan pressurization test results for house 6 with ceiling leaks uncovered.

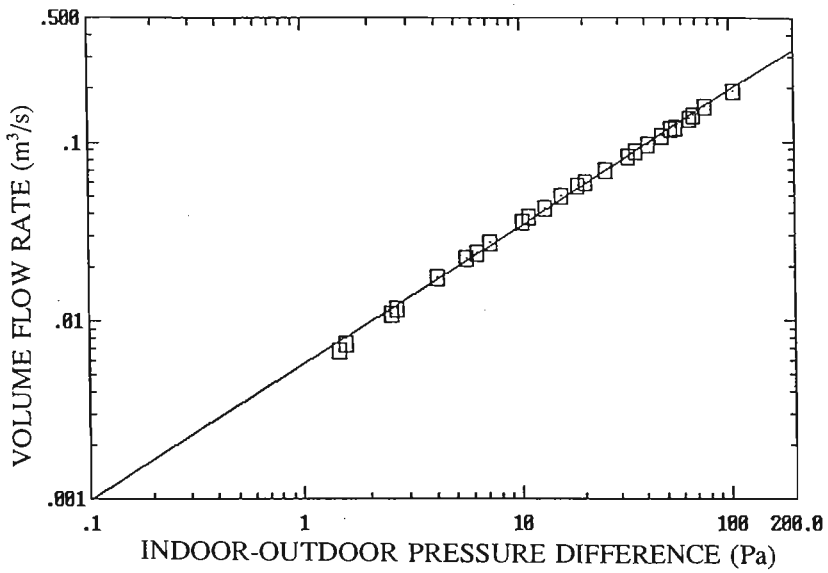

Figure 5-10b. Fan pressurization test results for house 6 with ceiling leaks sealed.

(solid lines in these figures), values of C, n, and A_4 were obtained and these results are tabulated in Table 5-2. The ceiling leakage areas at 4 Pa were estimated by subtracting the house leakage areas with the ceiling leaks covered and uncovered; the ceiling leakage areas

Table 5-2
Leakage Characteristics of Attic, House and Ceiling in Houses 5 and 6

House Zone	Flow Coefficient $m^3/sec.(Pa)^n$	Flow Exponent n	Leakage Area @ 4 Pa cm^2
Attic 5 - exterior envelope	$4.416x10^{-2}$	0.707	456
Attic 6 - exterior envelope	$1.740x10^{-1}$	0.597	1542
House 5 - ceiling (uncovered)	$9.842x10^{-3}$	0.583	85.5
House 5 - ceiling (covered)	$8.446x10^{-3}$	0.580	73.1
House 6 - ceiling (uncovered)	$6.903x10^{-3}$	0.737	74.3
House 6 - ceiling (covered)	$5.730x10^{-3}$	0.766	64.2

for house 5 and 6 were 12 and 10 cm^2, respectively. These leakage areas can be compared with the area of the 7.6 diameter orifice flowmeter in the ceiling panel, which is 26.5 cm^2. This area together with the additional leakage of the light fixtures corresponds to a considerably larger gross area than the measured values. The discrepancy is due to the additional flow resistance of the 89 mm thick glass fibre batt ceiling insulation resulting in smaller effective ceiling leakage areas. These results point out the fact that actual leakage areas are quite different from visible leakage areas and fan pressurization tests are required to accurately measure these areas.

5.1.2 Measurement of Ventilation Rates

The ventilation rates of attics 5 and 6 were measured using a tracer gas injection system that measured the amount of gas required to maintain a constant concentration within the attic space. Gas concentrations were measured with an infra-red gas analyzer (MIRAN 1A) that had the capability of measuring concentration of different tracer gases by adjusting the wavelength of the infra-red radiation. This capability was necessary because two different tracer gases were used to separately measure the indoor infiltration rates (using sulphur

hexaflouride, SF_6) and the attic ventilation rates (using Freon gas, R22). Indoor infiltration rates have been measured in all six houses at AHHRF over approximately the past ten heating seasons which have seen several improvements made to the measurement procedure. Computer controlled gas injections are made several times each hour to maintain the gas concentration inside the house at a nominal value of 5 ppm; infiltration rates were inferred from the amount of gas injected into the interior space. Details of this system can be found in Wilson and Walker (1991).

Attic ventilation rates were monitored separately from the indoor infiltration rates using R22 as a second tracer gas in the attic. The ventilation rates were measured using the same procedures as used for measuring indoor infiltration rates. The R22 concentration in the attic was maintained at a nominal concentration of 5 ppm. The attic air was mixed by two small fans shown in the foreground and background in Fig.5-11, to ensure uniform conditions within the attic space. The fans provided a combined flow of approximately 10 attic air changes per hour (ac/h). A four point sampling system and manifold was used to draw equal volumes of air from distributed locations in the attic in order to obtain a more representative average sample of the tracer gas concentration. All air samples were drawn through a heated water bath to remove the effects of the sensitivity of the infra-red gas analyzer to temperature fluctuations. The gas analyzer was used to measure the concentrations of both R22 and SF_6 in air samples drawn from the attic and indoors. By measuring both concentrations, attic ventilation rates along with the indoor-attic exchange rates were measured. In order to carry out these measurements, the infra-red radiation passing through the air sample in the gas analyzer was adjusted to the wavelength corresponding to maximum attenuation for either R22 or SF_6. To do this, the gas analyzer was modified by connecting a DC motor to the mechanism that adjusts the variable wavelength filter. The motor (and hence, the wavelength setting) was controlled by the computer in the data acquisition system. The MIRAN 1A was calibrated by preparing gas mixtures of R22-air and SF_6-air of varying concentrations in the range 0 to 5 ppm. This calibration procedure has been repeated four times over the course of the past two heating seasons.

For attic sampling, the gas analyzer was first tuned to the R22 wavelength, then the sample pump was turned on and the solenoid valve to the attic was opened to draw an air sample from the attic. Air was drawn through the hoses and gas analyzer for a prescribed length of time to purge the system of the previous sample. During this time, the DAS was recording temperatures, relative humidities, windspeed, wind direction. After this purging

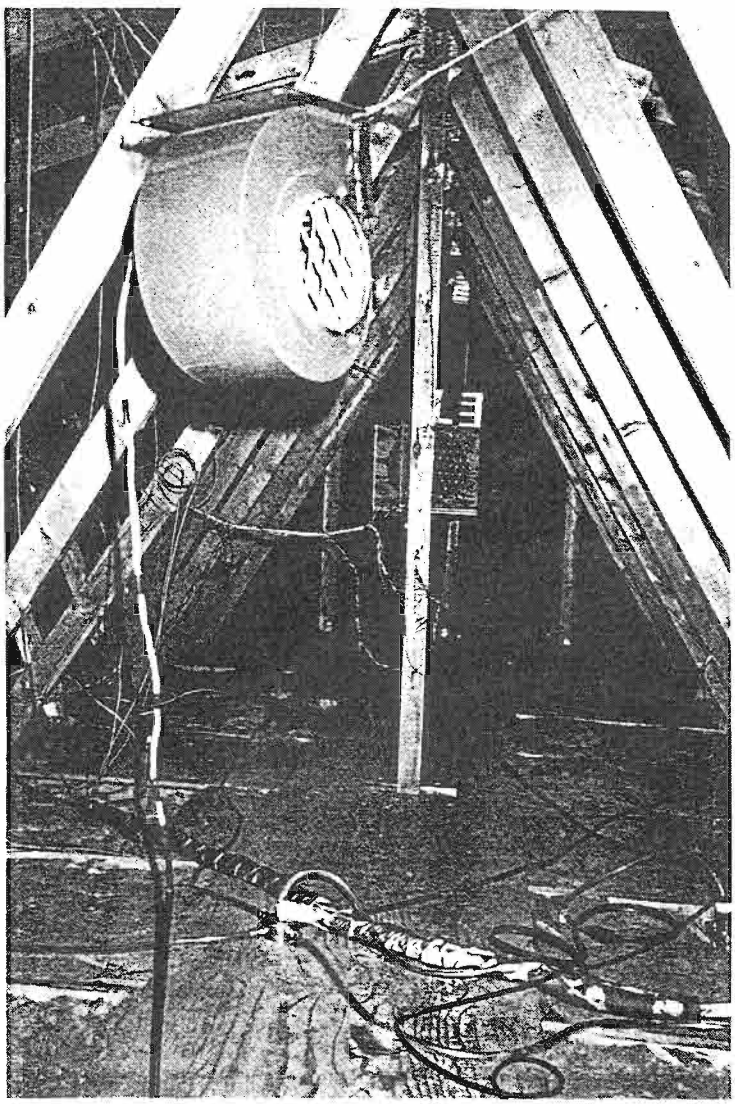

Figure 5-11. Interior of attic 6 showing mixing fans.

period, the pump was turned off and 10 seconds elapsed to equalize pressure in the gas analyzer. The R22 attic concentration was measured and the computer calculated the amount of tracer gas (based on the attic volume) required to maintain 5 ppm. The gas analyzer was then adjusted to the SF_6 wavelength; whilst the gas analyzer stabilized at the new wavelength, the temperatures, relative humidities, etc., were measured. The SF_6 concentration was then measured for the same sample of attic air. The concentration of SF_6 in the attic will of course, depend on the magnitude and direction of the ceiling leakage flow and, therefore, these concentrations will be either zero if ceiling flow is from the attic to indoors or some value (probably less than 5 ppm) if ceiling flow is from indoors to the attic. This made it necessary to calibrate the voltage output of the gas analyzer over the entire range of 0 to 5 ppm for both R22 and SF_6. For room sampling, the gas analyzer was switched to the R22 wavelength and the solenoid to the room opened to draw air from the room. The same procedure as described above for the attic space, was followed to draw a room air sample. The gas analyzer was adjusted to the R22 wavelength and while it was stabilizing, the R22 injection required to maintain 5 ppm in the attic was carried out (the number of injections required was calculated when the attic was sampled). Finally, the room SF_6 was measured. Tracer gas to maintain the 5 ppm nominal concentration in each attic was injected from a bottle of pure R22, stored inside the house, by pulsing a pair of closely spaced solenoid valves in series to produce puffs of tracer gas. The injector volumes for attic 5 and 6 produced 5.0 and 7.4 ml of R22 gas (at room temperature and pressure), respectively and were calibrated by counting the number of pulses required to produce 1 litre of gas which was measured by bubbling the gas through water and collecting the gas in an inverted graduated cylinder. The R22 tracer gas was fed into the attic were it was injected at the inlet of a small centrifugal fan located near the centre of the attic. This small fan was used to help disperse the tracer gas within the attic volume. Since the tracer gas was released at the prevailing temperature within the attic, the volume of gas released was corrected to the measured attic temperature by multiplying the room temperature injector volumes (5.0 and 7.4 ml, respectively) by the attic to room temperature ratio. Since there were a total of four spaces to sample (two attics and interior spaces in houses 5 and 6), air sampling was carried out using the following protocol. An air sample was taken from attic 6 for 35 seconds in order to purge the lines and gas analyzer of the previous sample; during this period, the DAS injects the calculated amount of R22 tracer gas into attic 5 to bring the concentration back to 5 ppm. After a 10 second pause, the R22 and SF_6 concentrations are measured. An air sample from attic 5 is then taken for 50 seconds (the purging time is longer for attic 5 since the sample lines are longer than for attic 6); during this period, R22 injections are made in

attic 6; gas concentrations are then measured by the gas analyzer. An air sample is now taken from the interior of house 5 for 60 seconds to purge the sample lines and the gas concentrations are then measured. Finally, the interior of house 6 is sampled by drawing an air sample for 35 seconds. During these latter two sampling periods, tracer gas injections continue in both attics 5 and 6 if required. The entire air sampling and measurement cycle took approximately 260 seconds resulting in 12 to 13 samples for each zone per hour. At the end of each hour, all measurements were averaged and recorded on a floppy disc. At midnight, the first 5 minutes of the hour was used to take a sample of outdoor air to provide a continuous check on the gas analyzer drift. This reading gave a check on the instrument zero setting, and on the presence of background contaminants (such as ammonia from fertilizers that are applied in the surrounding area during certain times of the year) that occasionally produce a false tracer gas reading in the incoming outdoor air.

The ventilation rates in the two zones were inferred from a mass balance on the tracer gas used in each zone:

$$Q = \frac{N\ V_{inj}}{\bar{c}} \tag{5-4}$$

where Q is the ventilation rate in m^3/hr, N is the number of gas injections made during an hour, V_{inj} is average volume in m^3 of tracer gas released per injection, and $\bar{c}$ is the hourly-averaged tracer gas concentration in the zone expressed as a volume ratio. These ventilation rates were converted to air changes per hour by dividing Q by the zone volume; for both houses, the interior and attic volumes were 220 and 61 m^3, respectively. Estimates of the uncertainty in the injection and concentration measurements indicated that the measured ventilation rates were within ± 6% of the true value for both the interior and attic zones. The indoor-attic exchange rate was inferred from the concentration of SF_6 in the attic using a mass balance for SF_6 in the attic:

$$Q_{IA} = \left(\frac{T_I}{T_A}\right)\left(\frac{C^{A}_{SF6}}{C_{SF6}{}^{I}}\right) Q_I \tag{5-5}$$

where the designation I, and A refer a quantity to the interior or attic zone and Q_{IA} is the indoor-attic exchange rate. In the result section, this exchange rate is expressed as air changes per hour by dividing by the attic volume.

5.1.3 Other Measurements

Temperatures and wood moisture contents were measured at six locations in each attic. A schematic of the sensor locations is shown in Fig.5-12. Four of these measuring points were placed on the inner surface of the roof sheathing in the middle of the NE, NW, SE, and SW quadrants of the sloped roof. Two sets of thermocouples and moisture pins were placed near the large opening in the ceiling panel. One set was located on the upper end of the horizontal ceiling joist next to the opening, while the second set was placed directly above this location in the roof truss.

Wood moisture content At each measurement location a thermocouple was glued to the wood surface and wood moisture content was measured with a pair of stainless steel metal pins imbedded in the wood. The electrical resistance across the pins was measured and moisture contents inferred from the calibration of the resistance readings. The pins measured 6.4 mm in length and 3.2 mm in diameter and were spaced at a distance of 31.8 mm, centre-to-centre. The pins were inserted into pre-drilled holes so that the top of each pin was flush with the surface. The top exposed surface of each pin was sealed by applying a thin coat of epoxy glue. This was done to prevent surface condensation from creating a low resistance path between the pins and produce a false reading. In this way, each pair of pins was recording the moisture content of the underlying layer of wood. The resistances were measured with a wood moisture meter (Lignometer) which had been calibrated on small samples of roof sheathing and joist sections. These samples had been pre-soaked to known moisture contents (determined gravimetrically). In addition to the resistance measurement, the measured temperature at each location was used to correct the wood moisture content reading using the correction factors given by Pfaff and Garrahan (1986).

Temperature Temperatures were measured using type K thermocouples. The thermocouples were epoxied to the wood surface at every wood moisture pin location. In addition the attic air, house interior air and the outside air temperature were monitored. The outside air temperature was measured inside a ventilated box on the north wall of house 6.

Relative Humidity A polymer film capacitance sensor (General Eastern) was used to measure the relative humidity. Air vapour pressures were calculated based on these relative humidity measurements and the saturation pressure based on the air temperature. The relative humidity sensors were calibrated over three different saturated salt solutions which spanned

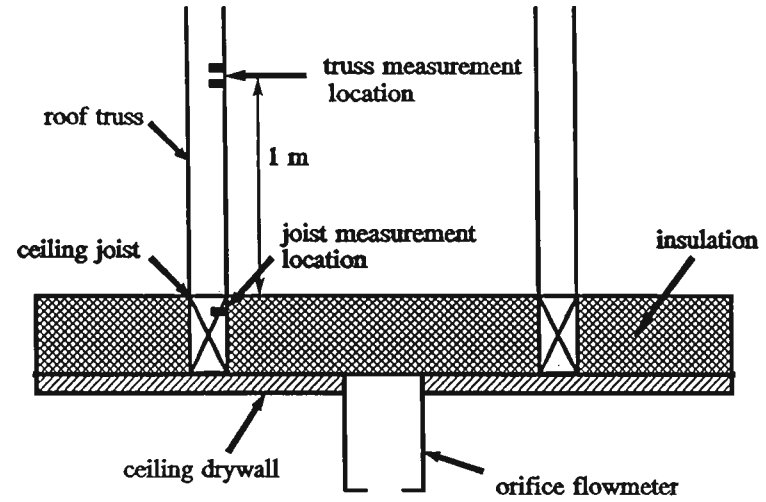

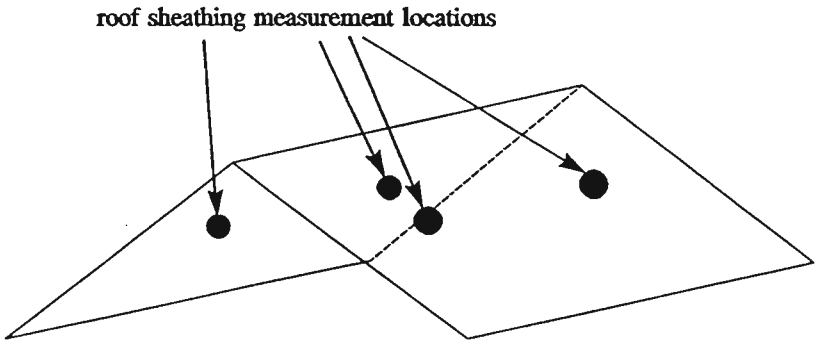

Figure 5-12 Schematic of the attic space showing location of thermocouple/moisture pin sensors

a relative humidity range from 12% to 98%. The relative humidity of the air in both attics and houses was measured in addition to the outside air.

Wind Speed and Direction The sensors for wind speed and direction were placed on top of a 10 m tall tower located midway along the row of houses and approximately 30 m north of the houses. Wind speed was measured with a low-friction cup anemometer which had been calibrated in a low speed wind tunnel while wind direction was measured with a rotating vane (Windflow 540 - Athabasca Research Corp.). The data acquisition system recorded the average wind speed and east and north vector components for each hour. These east and north vector components were used to calculate the true average wind direction.

Solar Radiation Incoming solar radiation on the north and south facing sections of the roof was measured with two pyranometers (Kipp and Zonen), one on each of the sloped roof sections of attic 6. One was placed on the north and the other on the south section of the pitched roof surface. The two pyranometers are oriented parallel to the roof slope so that the measured values can be entered directly to the heat transfer model without geometric conversion.

5.2 MEASURED DATA

Prior to the presentation of a comparison of measured results and predictions, a sample of attic ventilation rates, indoor-attic exchange rates, attic temperatures, and sheathing moisture contents are presented in this section in order to identify certain trends in the data.

5.2.1 Attic Ventilation Rates

Attic ventilation rates were found to be dominated by wind speed, increasing as wind speed increased. Ventilation rates in attic 5 varied between 0 up to approximately 7 ac/h (air changes based on attic volume per hour) at average wind speeds of 9 m/sec, while ventilation rates in attic 6 varied from 0 to an inferred value of 50 ac/h. With ventilation rates approaching 50 ac/h there may not be sufficient mixing of R22 tracer gas in the attic by the two attic fans to yield accurate values of ventilation rate. In order to investigate this effect, ventilation rates in attic 6 were plotted on a log-log plot. When the data are plotted in this way, a straight line should result ie. there is a power law-type dependence of ventilation rate on wind speed. A power law exponent of 2n is expected because the wind driven pressure

difference is proportional to wind speed squared and the flowrate is proportional to pressure difference to the power n. In addition, a single wind direction must be chosen to reduce the effects of shelter that change wind pressures at the same wind speed. Results for attic 6 with southeast winds only (in the range of 120° to 150°) are shown in Fig. 5-13 where the measured data has been binned every 1m/s and the mean value is plotted with the error bars showing one standard deviation within the bin. The dashed line in Fig.5-13 simply connects the average values of ventilation rate in ascending order to compare with a straight line. The results for attic 6 generally follow a power law that is linear in this figure up to an average wind speed of approximately 6 m/sec where the mean ventilation rate is about 20 ac/h. Beyond this wind speed, there is a significant deviation in ventilation rates from the power-law relation. If the problem is one of incomplete mixing of tracer gas in the attic then more gas would be injected than is necessary to maintain a constant concentration of 5 ppm. This would yield higher inferred ventilation rates than the true values. Since this is what is observed in the data, the conclusion is that this must be the limit for accurately measuring ventilation rates in the attics with the current measurement technique. One possible method of increasing this limit would have been to increase the flow rate of the mixing fans in the attic. Larger fans may have created pressures on the attic interior surfaces which would affect the ventilation rate. It was decided not to alter the measurement technique but invoke a simple criterion to stop ventilation rate measurements if the wind speed was greater than 6 m/s. This corresponds to a maximum ventilation rate in attic 6 of about 20 ac/h. The same criterion of a 20 ac/h maximum was applied to attic 5.

The ventilation of attics is driven by a combination of wind-induced pressures on the attic envelope and the attic "stack" effect which depends on the attic-outdoor temperature difference. Figures 5-14 and 5-15 show the ventilation rates in attic 5 and 6 as a function of wind speed and include wind from all directions and all attic-outdoor temperature differences. The maximum measured ventilation rate for attic 6 was limited to approximately 20 ac/h due to non-uniform mixing of tracer gas in the attic at high ventilation rates; thus, the ventilation rates shown in Fig.5-14 correspond to wind speeds less than approximately 5 m/sec. For all wind speeds, the ventilation rates in attic 5 are much less than in attic 6 and reflect the difference in leakage areas, attic 5 having approximately one third the leakage area of attic 6. Both sets of data show a general increase in ventilation rate with wind speed although there is considerable scatter in these data. A large part of this scatter is due to the variation in wind direction which alters both the shelter and pressure coefficients on the attic envelope. Both attics are essentially unsheltered for winds from the north or south and would

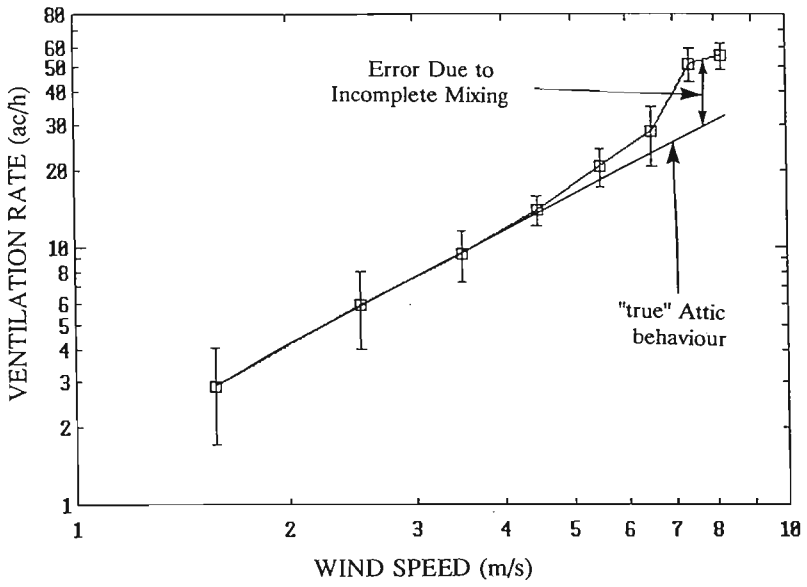

Figure 5-13 Measured ventilation rates in attic 6 versus wind speed for south-east winds between 120° and 150° (0° is north).

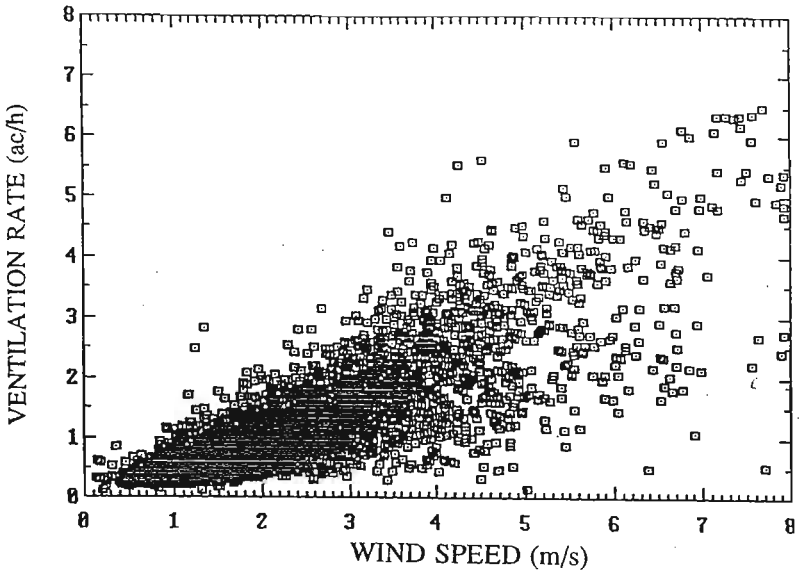

Figure 5-14. Measured ventilation rates in attic 5 for all wind speeds and temperature differences (3758 data points).

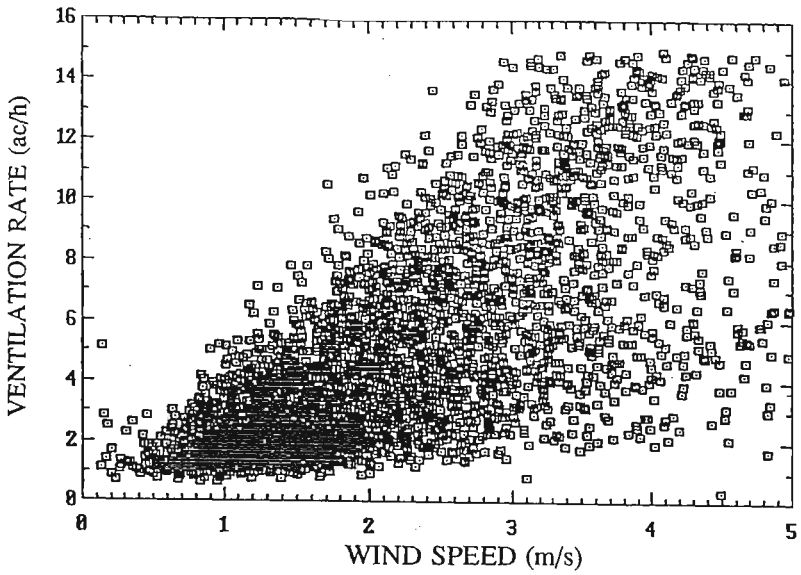

Figure 5-15. Measured ventilation rates in attic 6 for wind speeds up to 5 m/s and all temperature differences (3522 data points).

therefore, have relatively large ventilation rates, while strong shelter occurs for east and west winds producing lower ventilation rates. For attic 6 which has a total vent area sized according to the building code, ventilation rates for south (unsheltered) and west (sheltered) wind directions are shown in Figs.5-16a and 5-16b, respectively. Each data set only includes wind directions ±22.5° about the nominal direction. For south winds, attic 6 is totally unsheltered resulting in the highest ventilation rates which increase approximately linearly with wind speed at 3 ac/h per m/s wind speed. For west winds, the attic is sheltered by the other houses in the row resulting in ventilation rates which are noticeably less than for south winds and much less dependent on wind speed than the unsheltered case. A similar comparison for attic 5 is shown in Figs.5-17a and 5-17b for south and west winds, respectively. With approximately one quarter the leakage area of attic 6, attic 5 ventilation rates are approximately 1/3 that of attic 6.

The dependence of attic ventilation on stack effect is shown in Figs.5-18 and 5-19 for attics 5 and 6, respectively where attic ventilation rates are plotted versus the attic-outdoor temperature difference. In these two figures there is a point for each hour. To elucidate the trend in these figures, the data has been binned every 5°C of attic-outdoor temperature difference. The mean is shown by the squares and the error bars represent the standard deviation in each bin. These data have been selected from the time period between December 1, 1990 and October 31, 1991 and include only those hourly-averaged ventilation rates when the wind speed was below 2 m/sec. Although the data show considerable scatter, there is a weak dependence of ventilation rate on attic-outdoor temperature difference with stack driven ventilation rates reaching a maximum of approximately 0.5 ac/h in attic 5 and 2 ac/h in attic 6; the data in Figs.5-18 and 5-19 show a small offset ventilation at zero attic-outdoor temperature difference which is due to wind speeds less than 2 m/s that are included in this dataset. A comparison of Figs.5-14 and 5-18 and Figs.5-15 and 5-19 for attics 5 and 6, respectively indicates that "stack" driven ventilation is much less than ventilation generated by wind-induced pressure on the attic envelope except at very low wind speeds. One of the immediate observations from the data presented in Figs.5-14 and 5-15 is that to "see" the expected increase in ventilation rate with increasing wind speed, a large number of measurements need to be taken. Figure 5-14 for attic 5, contains 3758 hourly averages, while Fig.5-15 contains 3522 data points. Datasets that contain a limited number of measurements (on the order of 10 hourly averages) could display any type of variation with wind speed, increasing, decreasing, or constant. Thus, sufficiently large number of measurements are generally required to uncover true trends in the data.

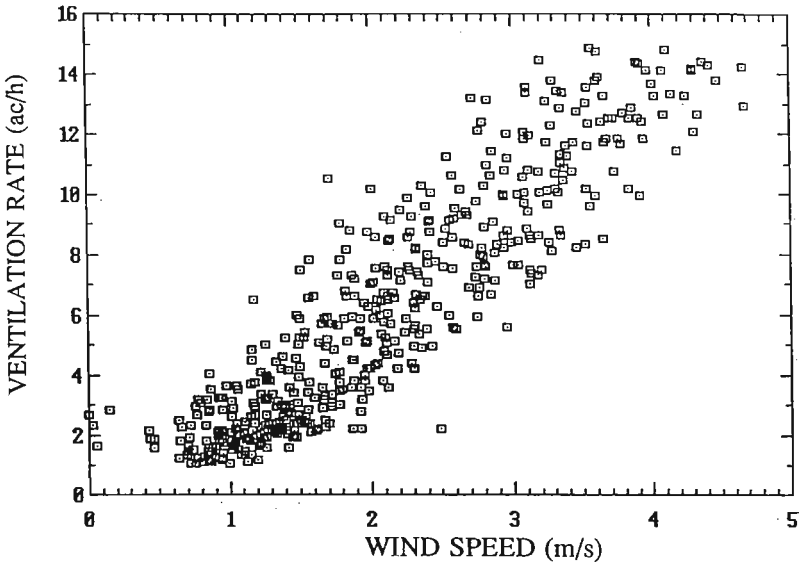

Figure 5-16a. Measured ventilation rates in attic 6 for south winds only (unsheltered direction) (497 data points).

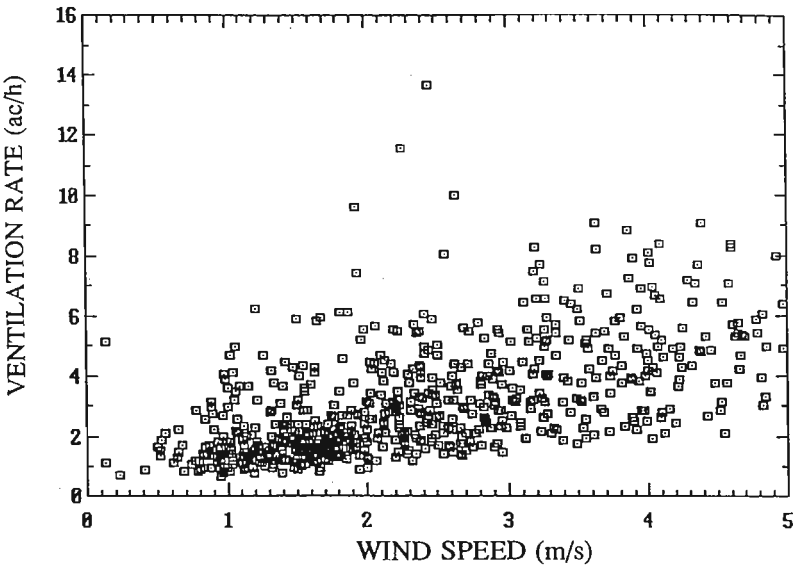

Figure 5-16b. Measured ventilation rates in attic 6 for west winds only (sheltered direction) (697 data points).

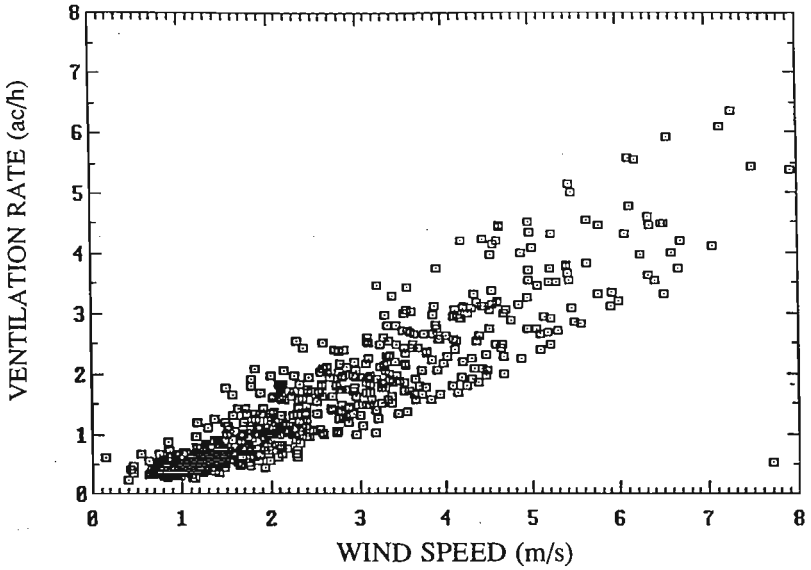

Figure 5-17a. Measured ventilation rates in attic 5 for south winds only (unsheltered direction) (641 data points).

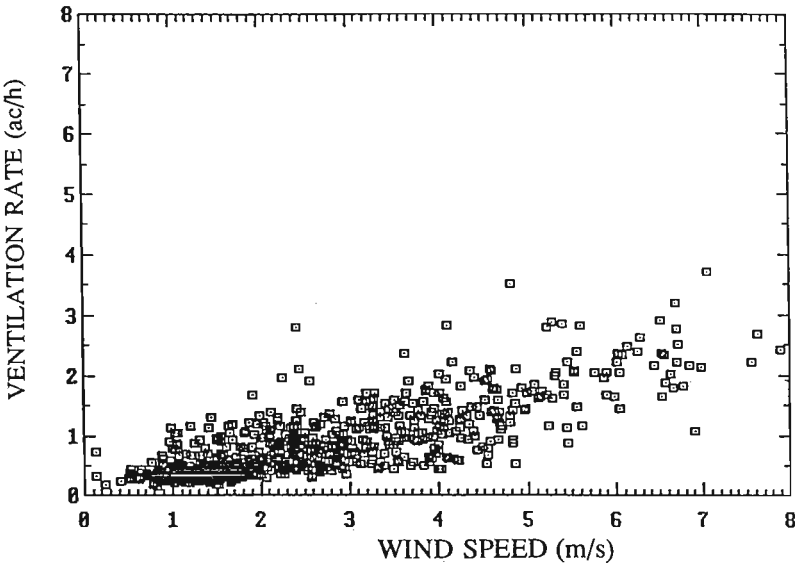

Figure 5-17b. Measured ventilation rates in attic 5 for west winds only (sheltered direction) (784 data points).

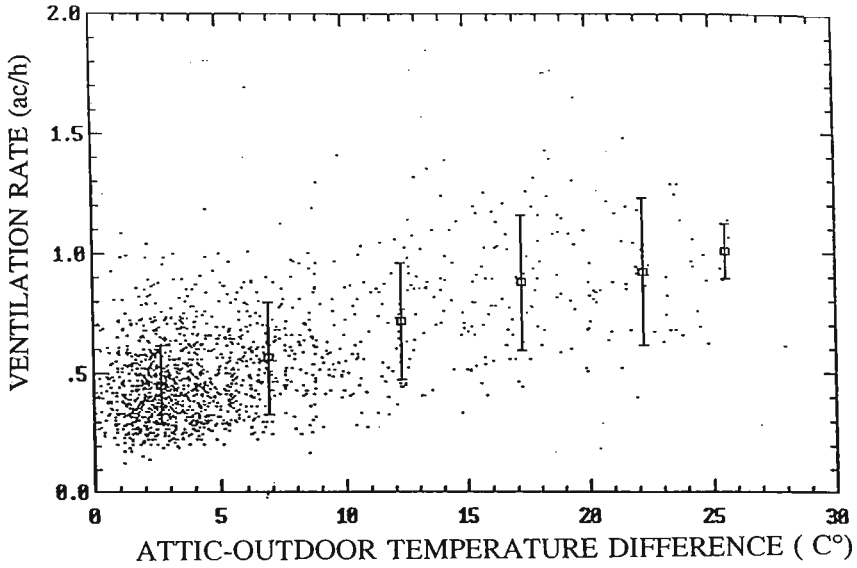

Figure 5-18. Attic-outdoor temperature difference effect on measured ventilation rates in attic 5 for wind speeds less than 2 m/s (1573 data points).

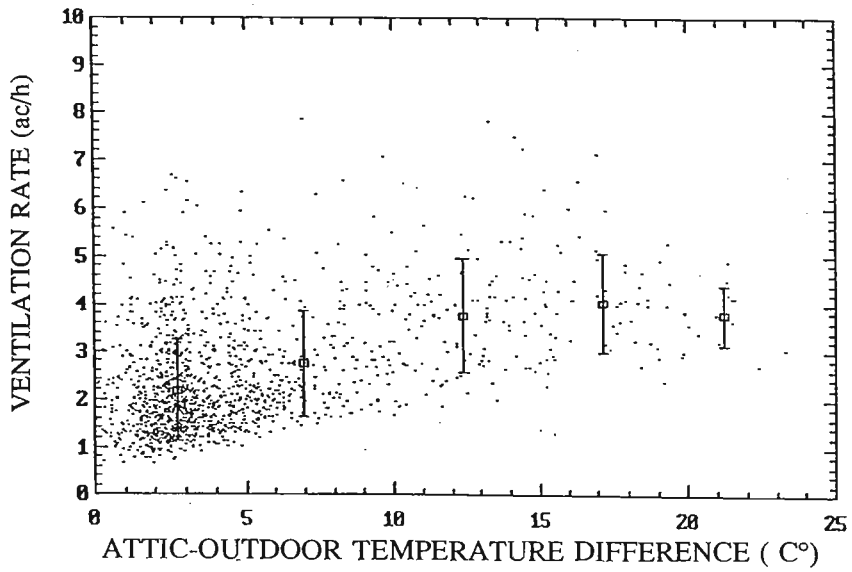

Figure 5-19. Attic-outdoor temperature difference effect on measured ventilation rates in attic 6 for wind speeds less than 2 m/s (1444 data points).

The effect of wind direction on ventilation rates was partially illustrated in Figs.5-16 and 5-17 for attics 6 and 5 where data was selected for sheltered and unsheltered wind directions. To isolate the effect of wind direction on ventilation rates, the data was plotted as a function of wind angle (0° being north and positive angles measured in a clockwise sense). The measured results for attics 5 and 6 are presented in Figs.5-20 and 5-21, respectively; the upper plots shows individual data points, while the lower plot shows the average and standard deviation of the measurements when data was sorted into 22.5° wind angle bins and help to accentuate the dependence of ventilation rates on wind direction. In both sets of plots, the individual ventilation rates have been divided by the wind speed at eave height (which is used as the reference wind speed in the ventilation model) raised to the power 2n where n is the flow exponent obtained from the fan pressurization measurements on each attic. This normalization procedure factors out the variation of ventilation rate with wind speed for a given direction and helps to reduce some of the considerable scatter that is evident in both plots. Finally, the normalized ventilation rates are divided by the mean normalized ventilation rate for the southerly direction (180°); the southerly direction was chosen since this direction contained a large amount of data and the houses experience the least wind shelter. Both data sets for attics 5 and 6 show a reduction in ventilation rate of approximately 50% for easterly winds (90°) and 70% for westerly winds (270°). The reduction in ventilation rates for westerly winds was slightly larger than for easterly winds and this small asymmetry is due to the air flow pattern over the houses which affects the surface pressure coefficients. For westerly winds, both attics 5 and 6 are sheltered by four identical houses; for easterly winds, attic 5 is sheltered by house 6 and attic 6 is only sheltered by the windbreak shown in Fig.5-1. The exact nature of the differing flow patterns and their effect on pressure coefficients would require detailed experimentation in a wind tunnel (or perhaps numerical simulation) and is beyond the scope of this study. Nonetheless, Figs.5-20 and 5-21 clearly show the large sheltering that the neighbouring houses provide for attics 5 and 6.

5.2.2 Mechanical Attic Ventilation

During the second year of testing, a ventilating fan was installed in attic 6 and tests were carried out for two modes of operation, fan depressurizing the attic (normal mode of operation) and pressurizing the attic. As mentioned previously, the fan itself provided a maximum ventilation rate of 9.6 ac/h and was cycled on between 10:00 am and 4:00 pm and off for the remaining portion of the day. The effect this has on ventilation rates in attic 6 can be seen in Fig.5-22a which covers a three day period from November 20 to 22, 1991.

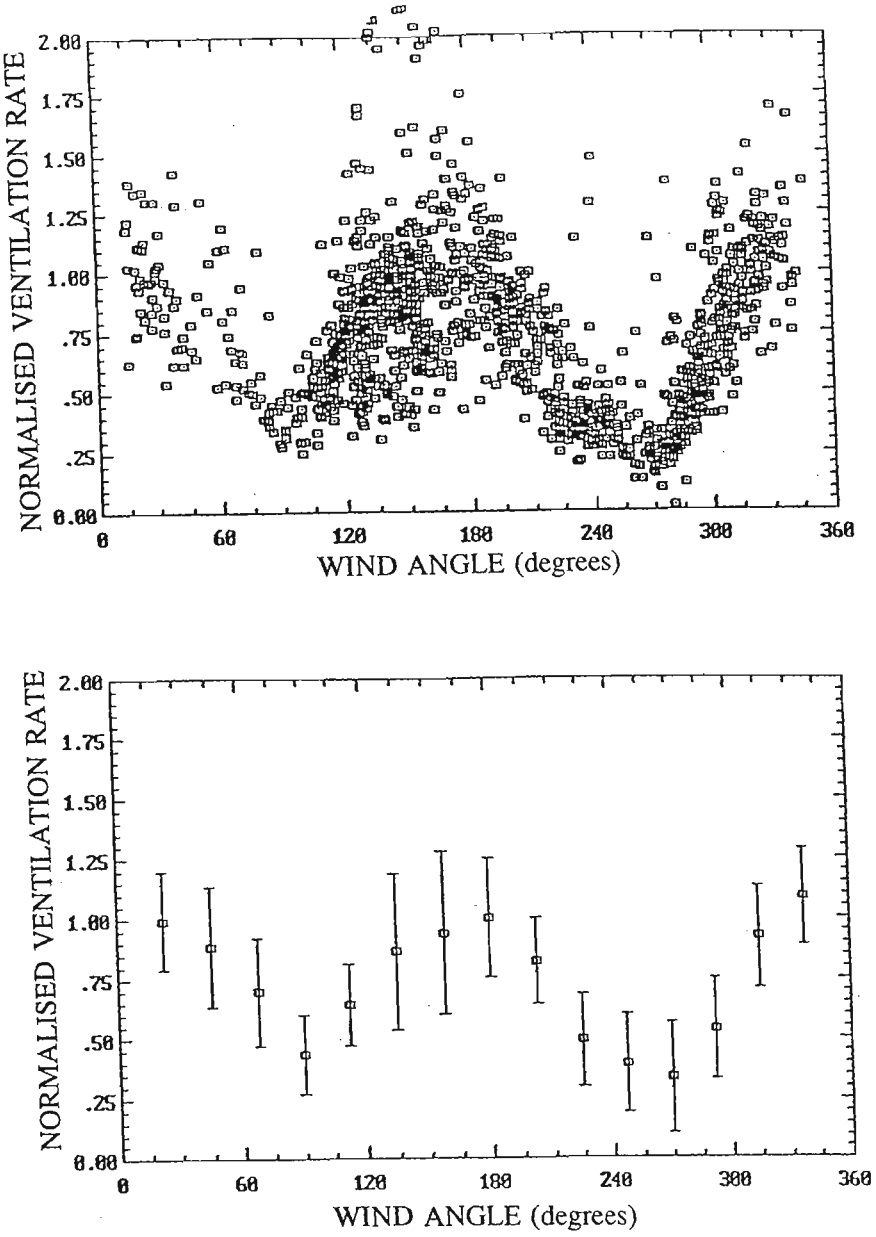

Figure 5-20. Effect of wind direction on ventilation rates for attic 5 (1302 points). Upper plot shows individual data points: lower plot shows averages and standard deviations for binned data.

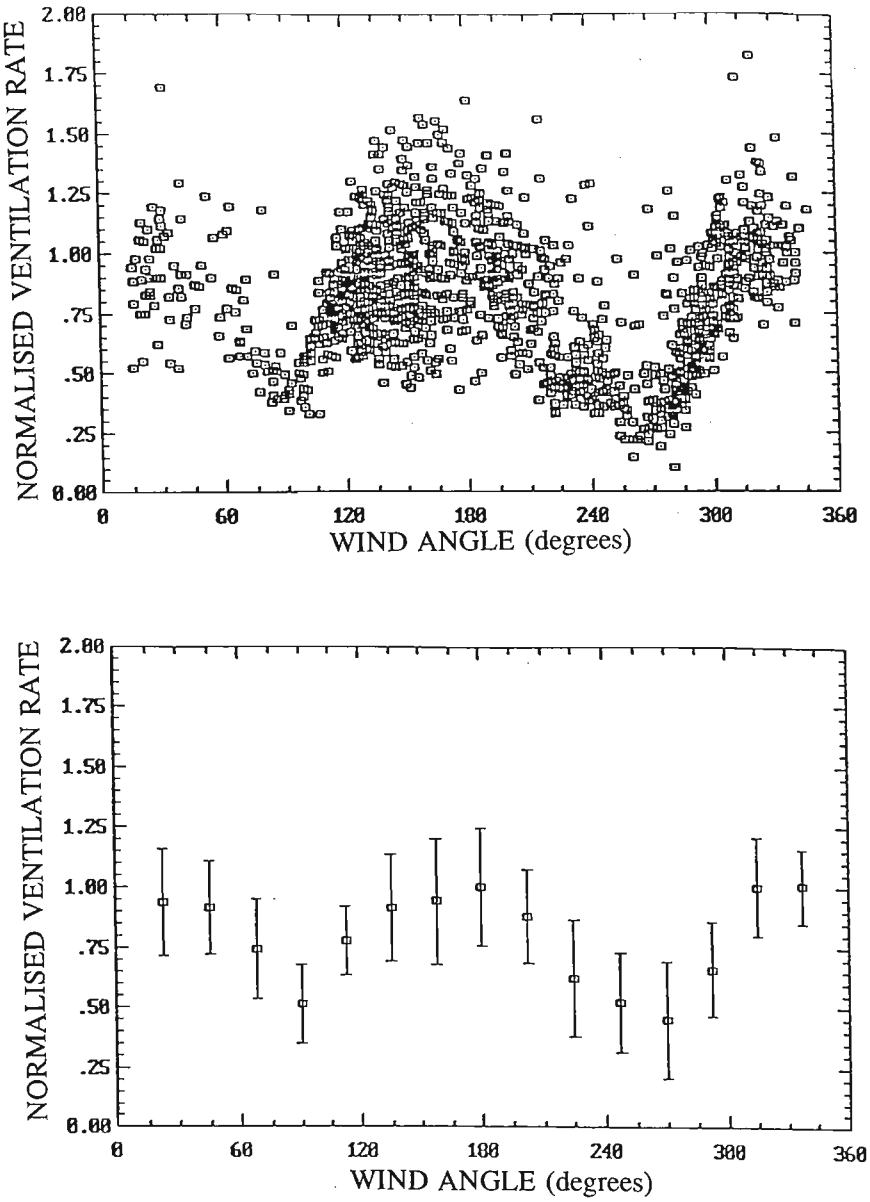

Figure 5-21. Effect of wind direction on ventilation rates for attic 6 (1302 points). Upper plot shows individual data points: lower plot shows averages and standard deviations for binned data.

This period was selected because the ventilation rates for the first two days were relatively constant, while ventilation rates increased significantly on the third day. For comparison purposes, the ventilation rates in attic 5 over the same period are shown in Fig.5-22b and indicate relatively calm conditions the first two days with low ventilation rates and increased ventilation on the third day. During low wind speeds where ventilation rates are low, the attic fan creates pressure differences across the attic envelope that are much larger than wind-induced pressure differences and for these situations attic ventilation rates are dominated by the fan. Over the first two days, the ventilation rates with the fan on averaged approximately 11 ac/h and with the fan off, approximately 4 ac/h. The fan contribution was therefore, 7 ac/h which is close to the maximum capacity of the fan. On the third day, the wind speed increased during the day resulting in an increase in the "background" ventilation rate to approximately 13 ac/h while the measured rate was approximately 16 ac/h. In this case, the fan did not increase the ventilation rate to the same extent as on the previous days since the wind-induced pressures on the attic envelope were relatively large.

5.2.3 Indoor-Attic Exchange Rates

One of the important measurements obtained during the field monitoring program was the magnitude of the indoor-attic exchange rate and its dependence on outdoor conditions. A large amount of moisture can be transported into the cool attic space when there is a sustained exchange of air from indoors to the attic and the interior heated space has a large relative humidity. During cold weather, this moisture will deposit as frost which steadily accumulates; a sudden thaw will melt the frost with resultant water damage to the ceiling and an increase in sheathing and joist wood moisture content. However, there are very few field measurements of the magnitude of this flow let alone its dependence on ambient conditions.

Measured indoor-attic exchange rates (expressed as ac/h based on the attic volume) in attics 5 and 6 are shown in Figs.5-23a and 5-23b, respectively and are correlated with the indoor-outdoor temperature difference. Data have been selected for wind speeds less than 2 m/sec to help reduce the scatter; the individual hourly averages are shown together with the average and standard deviation in each increment of 5 C°. During extremely cold weather, there is a large sustained pressure difference across the ceiling due to the stack effect which results in relatively large exchange rates, on the order of 0.20 to 0.25 ac/h (12 to 15 m^3/hr); at the interior conditions of 20°C and relative humidity of 40%, this maximum leakage flow will convect on the order of 100 grams water per hour. Of course, the magnitude of these

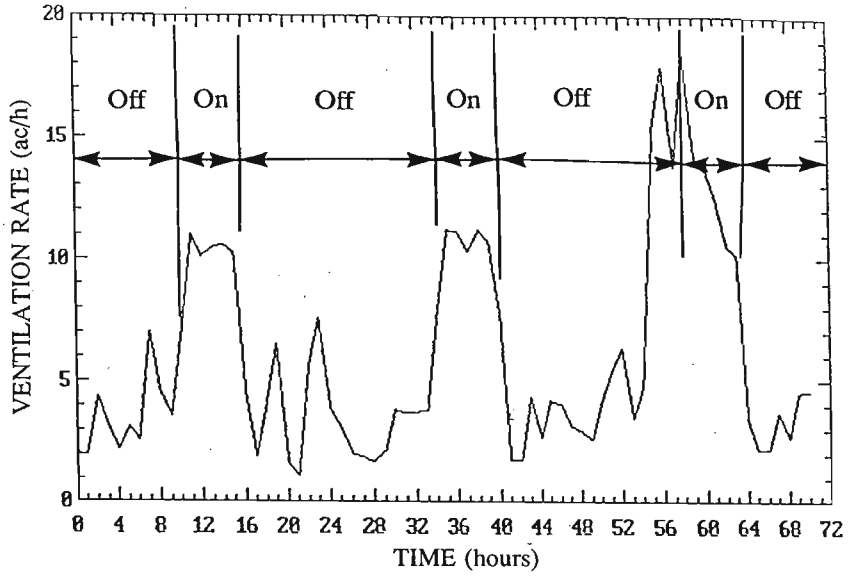

Figure 5-22a. Effect of ventilation fan on attic 6 ventilation rates. Fan is on during hours 11-15, 35-39, and 59-63.

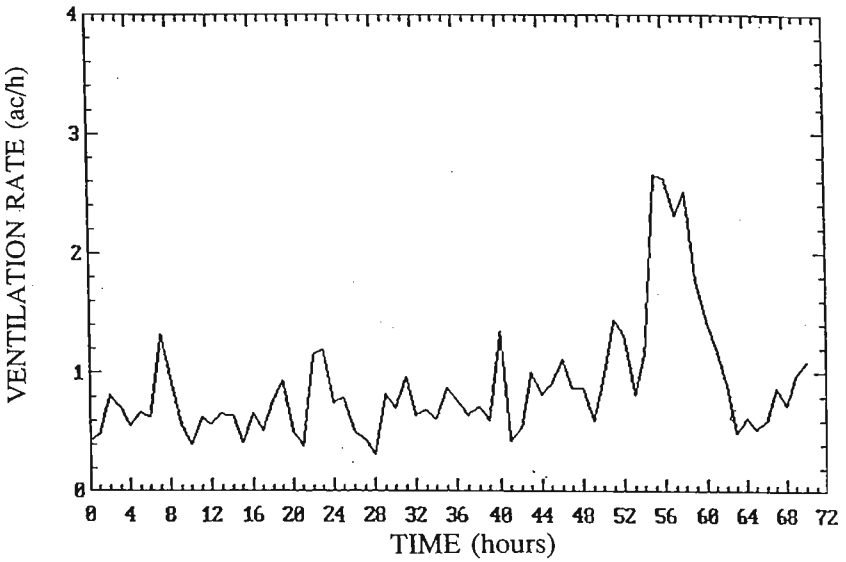

Figure 5-22b. Ventilation rates in attic 5 for the same time as Fig.5-22a, showing the increase in ventilation rates for the third day caused by increased wind speed.

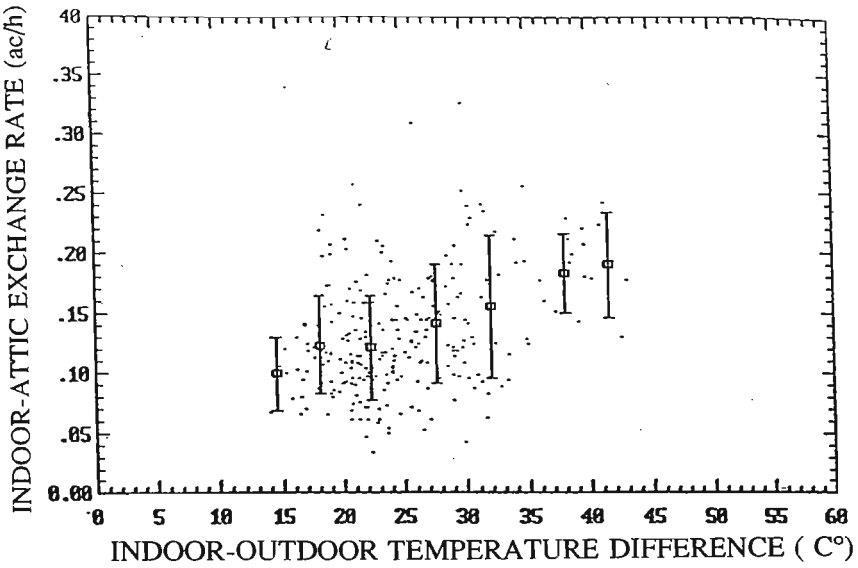

Figure 5-23a. Indoor-outdoor temperature difference effect on measured indoor-attic exchange rates for attic 5 for wind speeds less than 2 m/s.

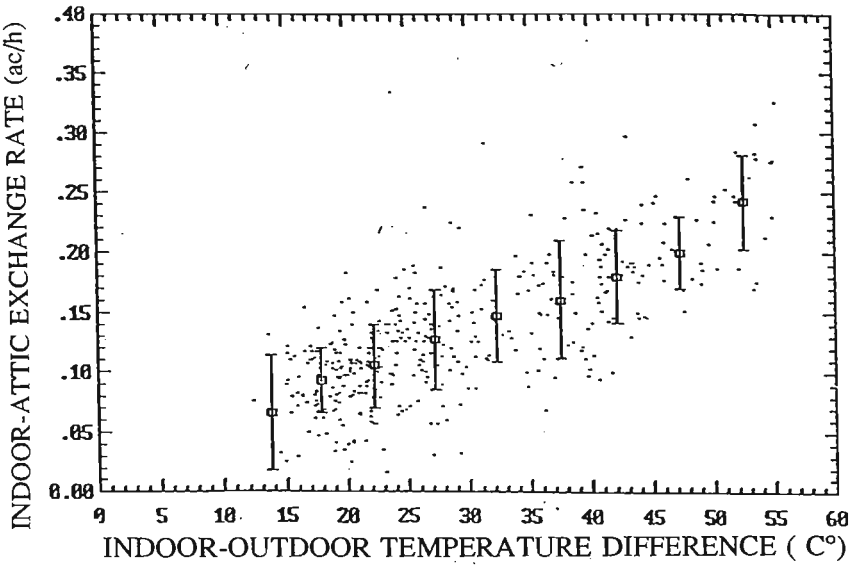

Figure 5-23b. Indoor-outdoor temperature difference effect on measured indoor to attic exchange rates for attic 6 for wind speeds less than 2 m/s.

rates will be dependent on the total indoor-attic leakage area and hence, these measuredvalues are characteristic of test houses 5 and 6 at AHHRF. The results shown in Fig.5-23 are for wind speeds less than 2 m/sec and an obvious question arises if indoor-attic exchange rates are correlated with wind speed. A typical set of measurements is shown in Fig.5-24 for attic 5 exposed to winds from the south (180°±45°); a relatively large wind angle bin was selected to provide enough data points. The data suggests that there is no obvious correlation of exchange rates with wind speed. The large scatter in the data probably obscures any correlation that exists and may indicate that exchange rates are sensitive to wind direction.

5.2.4 Attic Temperatures

The measured attic temperatures exhibit a strong diurnal cycle due to daytime solar gains and night time radiative losses. Figure 5-25 shows typical results on a spring day for attic 5. The south facing sheathing is heated the most and is more than 30°C higher than the outdoor temperature at its peak value at 2 p.m. (hour 15) in the afternoon. The truss and attic air temperatures are less than the sheathing temperature because they are not directly exposed to the radiative gains. The peak values do not occur at the same time due to the thermal masses involved and the attic air and the trusses lag behind the sheathing by approximately two hours. In addition, after the sun has set at about 7 p.m. (hour 19) the low thermal mass of the sheathing and its exposure to the cold sky temperature means that it cools faster than the attic air and the trusses. This is important because it implies that a steady state model of heat transfer that does not account for the thermal masses will not predict the correct magnitude or time variation of attic temperatures.

The night time cooling of attic sheathing due to radiation to the sky is illustrated further in Fig.5-26 on a spring day for attic 6, where hour 1 is noon. The outer sheathing temperature drops 3 to 4 degrees below the ambient temperature and 4 to 5 degrees below the attic air. The inner sheathing shows less temperature depression of about 2 degrees below the attic air but is still the coldest attic surface. This is important for night time moisture deposition on the sheathing surfaces.

5.2.5 Wood Moisture Content

Typical results for the north and south roof sheathing moisture contents of attic 5 are shown in Fig.5-27 for a heating season (5 months). At these low values of wood moisture

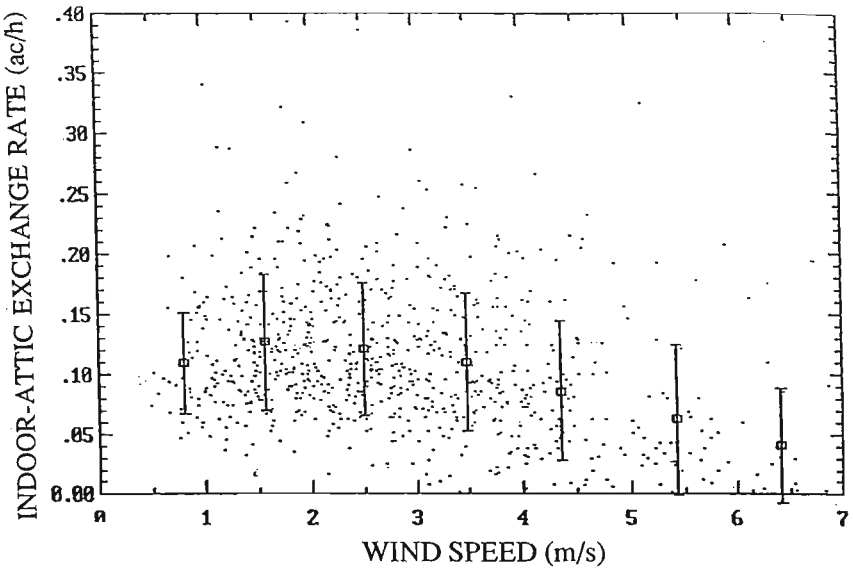

Figure 5-24 Effect of wind speed on indoor-attic exchange rates for attic 5 for south wind (180°±45°)

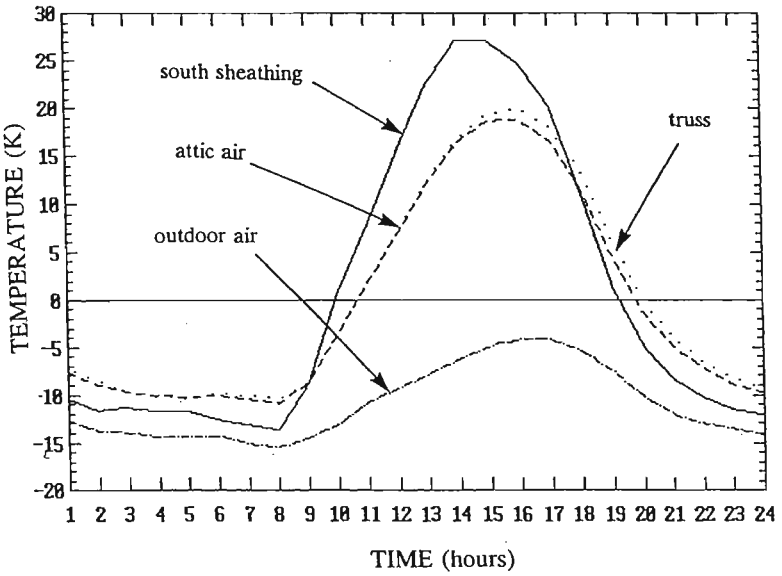

Figure 5-25 Diurnal variation of temperatures in attic 5 for March 12, 1991 (hour 1 is mid-night).

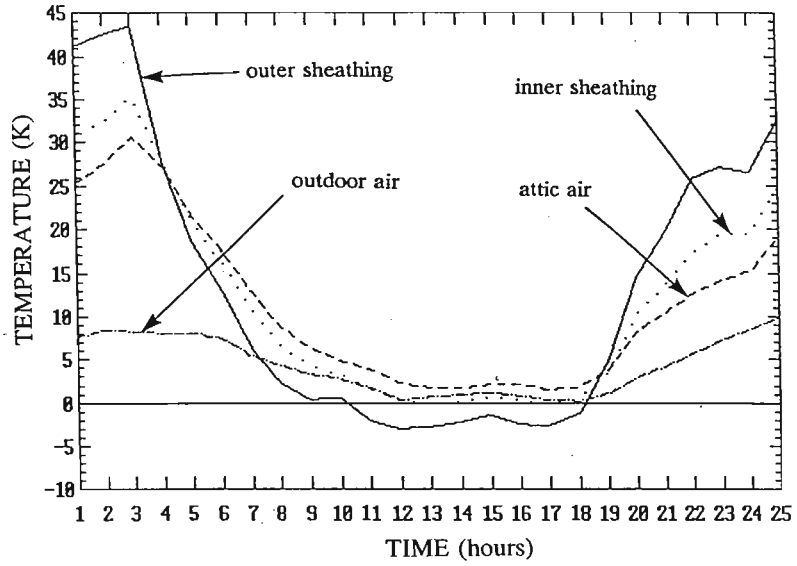

Figure 5-26 Diurnal variations of temperatures in attic 6 over the night time for April 9 and 10, 1991 (hour 1 is noon).

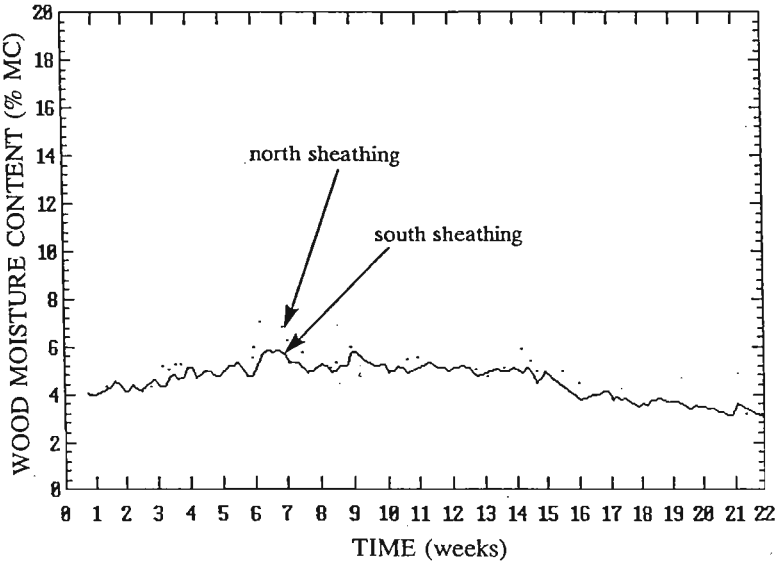

Figure 5-27 Measured daily-averaged wood moisture contents in the north and south roof sheathing from December, 1991 through April, 1992.

content (below 7%), the wood moisture meter is at its operating limit and therefore all that can be realistically inferred about the measured values is that they are at or below about 7%. Because of the uncertainty in these low values of wood moisture content the small rise and fall of about 2% over the heating season does not imply any seasonal moisture storage in the sheathing. These low values result from the moisture pins being sealed below the surface and therefore, not responding to the larger changes in moisture content at the surface. These measurements are only useful for verification in that the moisture model should indicate that the wood remains dry. Therefore, it will not be possible to verify model predictions for the surface layer, except to see if the model predicts condensed moisture (as was occasionally observed by visual inspection of the attics during winter months).

5.3 COMPARISON OF MEASUREMENTS AND PREDICTIONS

In this section, predictions of the three models presented in Sections 2, 3, and 4 are compared with the measured data. The principle component of the combined model is the two zone ventilation model which is first tested separately using the measured attic air temperature. The thermal and moisture models are then tested using the combined model with predicted ventilation rates. The basic philosophy used in the verification process was to compare measurements and predictions without adjusting model inputs to "fit" the data. Model deficiencies are noted and suggestions are made for further refinement of the model.

5.3.1 Attic Ventilation Rates

The attic ventilation model was verified by comparing model predictions to measured data described in Section 5.2. In order to make predictions of ventilation rates in the two attics some assumptions were made about the leakage distribution over the attic envelope. The total distributed leakage was presented in Table 5-2 and a reasonable distribution of this leakage is summarised in Table 5-3, together with the additional area provided by the vents in attic 6. The ventilation model also computes the house ventilation rates and the indoor-attic flow through the ceiling and thus, requires an estimate of leakage distributions of the interior zone; the distribution of the house leakage used to perform these calculations is summarised in Table 5-4. As with the attic, these leakage distributions are only estimates except for the fraction of leakage in the ceiling which was estimated from the difference in leakage areas found from the pressurization tests for the house with the ceiling holes open and covered (see Table 5-2). The wall and floor level leakage is assumed to be equally distributed over the

Table 5-3.
Assumed Distribution of Background Leakage
Area and Leakage Location Dimensions For Attics 5 and 6

2 Surface or Point on Attic Envelope	Attic 5		Attic 6	
	%	height above grade [m]	% (or area in bold)	height above grade [m]
eaves on roof surface 1	25	3	45	3
eaves on roof surface 2	25	3	45	3
gable - surface 3	5	distributed	0	-
gable - surface 4	5	distributed	0	-
roof surface 1	20	distributed	5	distributed
roof surface 2	20	distributed	5	distributed
vents on roof surface 1	-	-	**0.036 m^2**	4.5
vents on roof surface 2	-	-	**0.036 m^2**	4.5
roof peak	-	5	-	5

four sides of the building. The other inputs to the model include wind speed, wind direction (to calculate Cp and S_w) and house, attic, and outdoor temperatures. The measured attic temperature was first used so that the ventilation model could be tested independently of the heat transfer model.

Figures 5-28 and 5-29 show how the attic predictions compare to measured values for attic 5 and attic 6 respectively, for all temperatures (this is the same measured data as shown in Figs.5-14 and 5-15). In order to compare measured values and predictions more clearly, the measured data has been binned every 1 m/s of wind speed and the average is shown as a square and the error bars indicate the standard deviation of each bin. The ventilation rates are predicted for every hour based on measured weather data and their mean values at the mean windspeed for each hour are connected by a straight line in the figures. The trend in increasing ventilation rate with wind speed shown by the measured values is followed by the model predictions with a general tendency towards underprediction. The magnitude of the error is found by averaging the difference between measured and predicted values for each

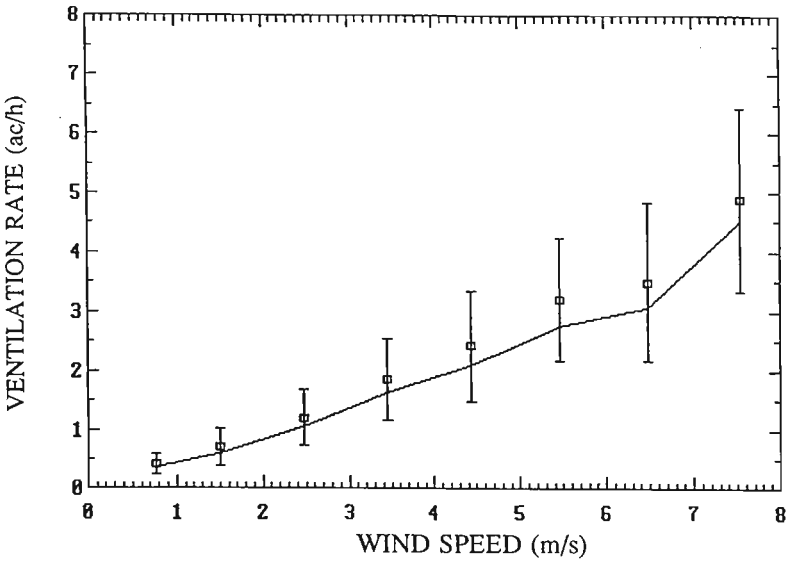

Figure 5-28. Measured binned attic 5 ventilation data (3758 hours) with predicted line for all wind directions and temperatures.

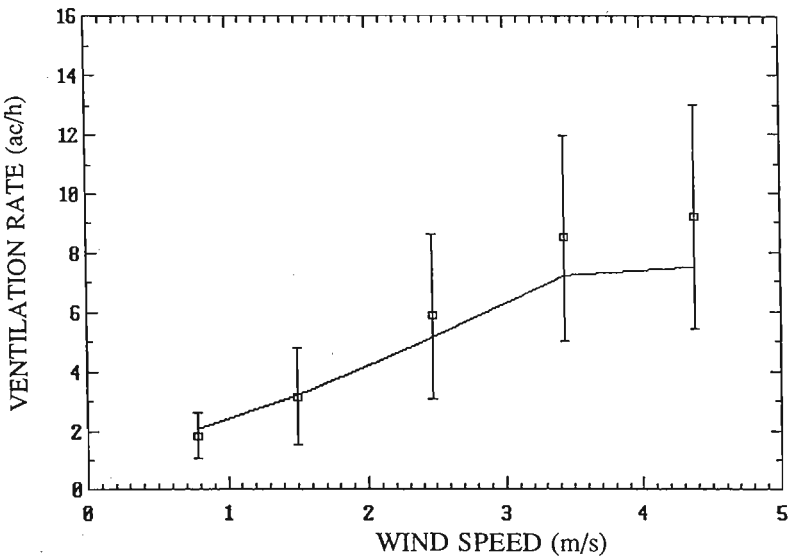

Figure 5-29. Measured binned attic 6 ventilation data (3522 hours) with predicted line for all wind directions and temperatures.

Table 5-4.
Assumed Leakage Distributions and Locations for House 5 and 6

Location on Building Envelope	House 5		House 6	
	%	height above grade [m]	%	height above grade [m]
Floor Level	20	0.6	15	0.6
Ceiling	15	3	15	3
Walls	65	distributed	70	distributed

hour rather than the difference in the averages shown in Fig.5-28 and 5-29. For attic 5 the underprediction is -0.017 ac/h on average and for attic 6 it is -0.5 ac/h. Most of this underprediction occurs when the wind blows along the row of houses (as will be shown later). When expressed as an average percentage error the results are -9.3% and +4.3% for attics 5 and 6, respectively. The attic 6 percentage error is positive because its overpredictions occur at lower ventilation rates where the percentage overprediction is high but the ventilation rate overprediction is relatively small. Considering the uncertainty in pressure coefficients, wind shelter and leakage distributions, these errors are about as small as could be reasonably expected. The values of these parameters could have been altered to reduce the errors but then the model would have been "fitted" to the measured data for AHHRF and this procedure would not have validated the model in a general sense.

The wind direction has a strong effect on ventilation rate because it changes the wind pressure coefficients and the wind shelter. The magnitude of this effect is about a factor of 3 to 4 reduction in ventilation rate from sheltered to unsheltered conditions, as shown by Figs.5-20 and 5-21. To test if the model has the correct variation of pressure coefficient and shelter, the measured and calculated ventilation rates for attic 6 are shown in Figs.5-30a and 5-30b, respectively. Both figures illustrate the same trends with much less ventilation for east and west winds (90^{o} and 270^{o}) than for north and south winds (0^{o} and 180^{o}). The large spread of data for a given wind direction is due to the effects of changing windspeed and outdoor temperatures. There is less scatter in the predicted data because the measured data has included all the variations in parameters such as wind speed, wind direction and temperatures during the hour that are not included in the hourly averages input to the model. This trend of less scatter in measured data is seen in all data comparisons of this type where

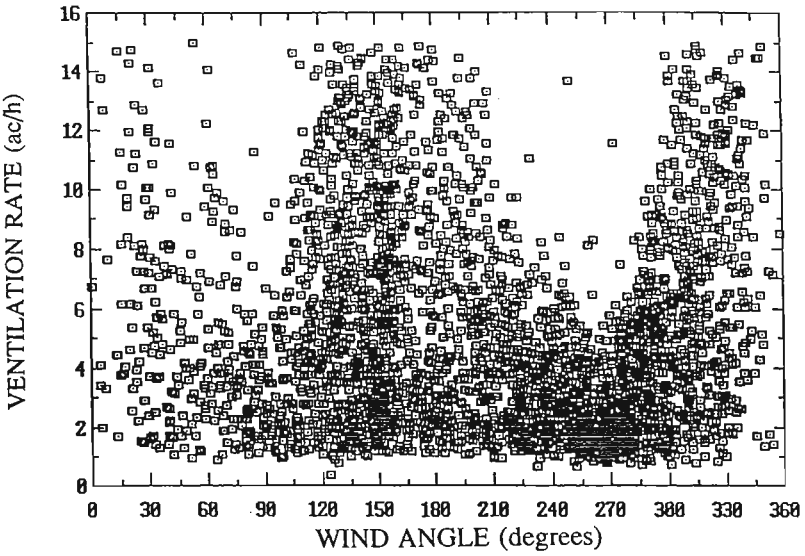

Figure 5-30a. Variation of measured ventilation rates for attic 6 with wind direction (3522 hours).

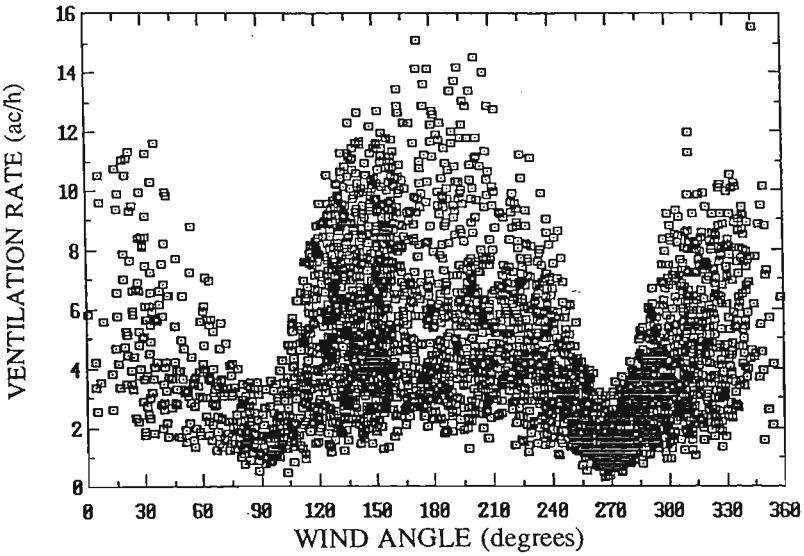

Figure 5-30b. Variation of predicted ventilation rates for attic 6 with wind direction (3522 hours).

points are "unpaired" and individual data points for each hour are displayed in the figures. Attic 5 ventilation rates show the same trends in measured and predicted values, as illustrated in Figs.5-30a and 5-30b and are not presented here. To highlight the model performance, the measured and predicted data has been binned every 22.5° to provide 16 wind direction bins and normalised as in Figs.5-20 and 5-21. Figures 5-31 and 5-32 show the results of this procedure for attic 5 and attic 6. For attic 5, the normalised air exchange rates are about 50% less for east and west winds than for north and south winds due to the sheltering effects of the neighbouring buildings. For attic 6 the sheltering effect is asymmetric with a reduction of almost 60% for west winds and only 40% for east winds. Attic 6 is sheltered by other buildings in the row of houses for west winds but for east winds, is sheltered only by a rectangular vertical wall which is 3.7m high and the same width as the houses. The data shows that this sheltering wall does not have the same shelter effect as an upwind house. The model follows the change in normalised air exchange with wind direction and for both attics the largest error is an underprediction when winds are from the east or west. The ventilation model errors are summarised in Table 5-5 including the variation of error with wind angle.

Table 5-5.
Mean Errors in Predicted Ventilation Rates for Attics 5 and 6

	Attic 5 ac/h (%)	Attic 6 ac/h (%)
For stack dominated ventilation	0.07 (19)	0.34 (21)
For wind dominated ventilation (all wind directions)	-0.02 (-9.3)	-0.5 (+4.3)
North winds only	-0.04 (+2.2)	-1.7 (-14.1)
South winds only	0.15 (14.2)	0.08 (18.9)
East winds only	-0.24 (-25.8)	-1.50 (-27.1)
West winds only	-0.28 (-28.8)	-0.75 (-17.1)

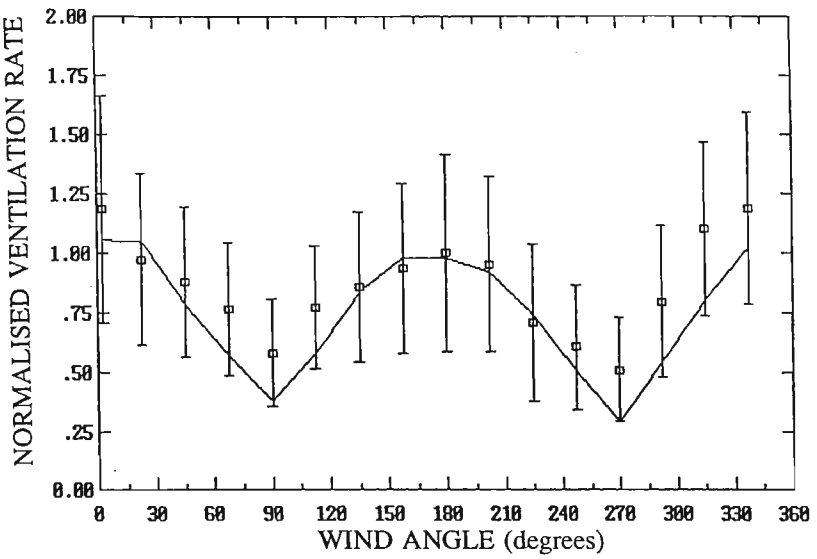

Figure 5-31. Comparison of predicted (line) and measured (binned) normalised ventilation rates as a function of wind direction for attic 5 (3758 hours) showing mean and standard deviation of binned measured data and a line connecting the mean predicted values for each bin.

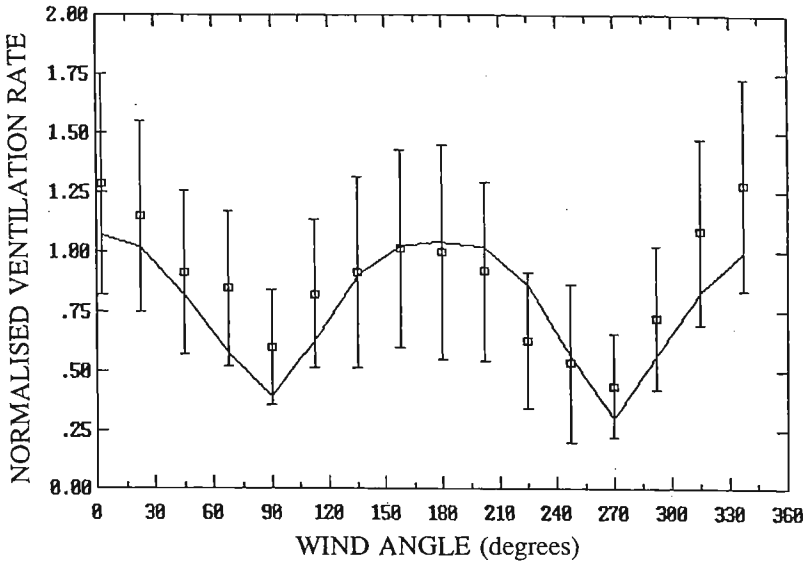

Figure 5-32. Comparison of predicted (line) and measured (binned) normalised ventilation rates as a function of wind direction for attic 6 (3522 hours) showing mean and standard deviation of binned measured data and a line connecting the mean predicted values for each bin.

5.3.2 Indoor - Attic Exchange Rates

For the thermal and moisture models, the flow through the ceiling is an important parameter. The ventilation model calculates this flow based on the leakage area attributed to the ceiling and the pressure difference between the house and attic. From the measurements, the indoor-attic exchange rate was mainly dependent on the temperature difference between the house and attic; the effect of wind speed was small because the mean pressures in both zones caused by the wind, were approximately equal. To reduce scatter, the data was sorted for windspeeds less than 2 m/s. The resulting measured data was then binned every 5 C° of indoor-attic temperature difference. The mean and standard deviation of the measured data are shown in Figs.5-33 (990 hours) and 5-34 (722 hours) for attic 5 and 6, respectively. The mean exchange rate predicted by the model for each bin, is shown connected by the solid line. These figures show good agreement between measured and predicted values considering the small magnitude of these exchange rates. For both attics, the peak exchange is about 0.25 ac/h which is only a few percent of the total attic ventilation rate. Typically, the indoor-attic exchange rate is about 5% of the total ventilation rate for attic 5 and only 1% of the total for attic 6. The mean errors between predicted and measured exchange rates is -0.015 ac/h or 4.5% for attic 5 and 0.0014 ac/h or 14.3% for attic 6. Given the large scatter in the measured data and the relative small magnitudes of these flows, the two zone ventilation model is able to predict the general trends observed in the measured data.

5.3.3 Attic Ventilation Rates with Fans

For the winter of 1991-1992 attic 6 was equipped with a ventilation fan, described in Section 5.1, to find the increase in ventilation created by a fan. The fan was included in the ventilation model using a fan curve and the "rated" flow and pressure difference for the fan. The fan was operated on a cycle, switching on at 10:00 a.m. and off at 4 p.m. Figure 5-35 shows four days of measured and predicted ventilation rates for the fan in exhaust mode (depressurizing the attic). From November 1991 to February 1992 there were a total of 1035 ventilation measurements made, with 259 when the fan was on and 776 with the fan off. The ventilation model is able to track the measured ventilation rates with reasonable accuracy. For this entire dataset, the mean error between measurements and predictions was an under prediction of 0.37 ac/h with the fan off (6% of the mean measured value), and an under prediction of 0.32 ac/h (3% of the measured value) with the fan on. The performance of the fan can be clearly seen in Fig.5-35; for the first two days the natural ventilation due to stack

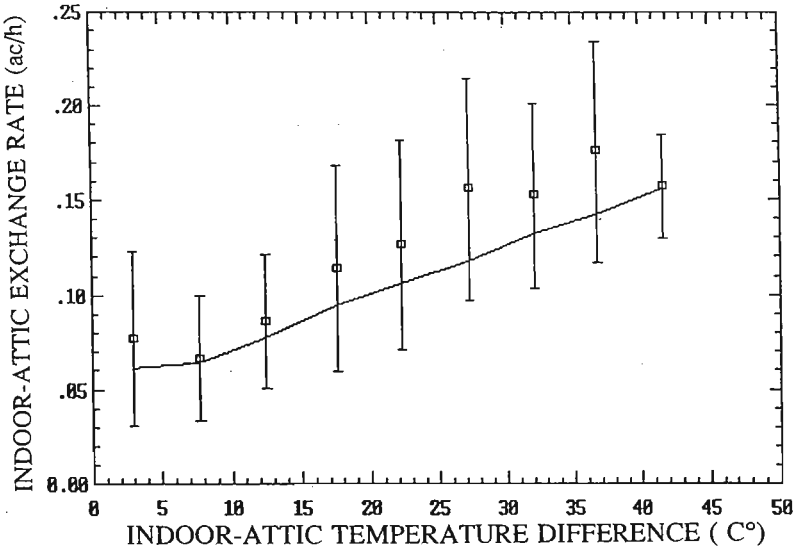

Figure 5-33. Comparison of measured (binned) and predicted (line) indoor-attic exchange rates for attic 5 for wind speeds < 2 m/s (990 hours) showing mean and standard deviation of binned measured data and a line connecting the mean predicted values for each bin.

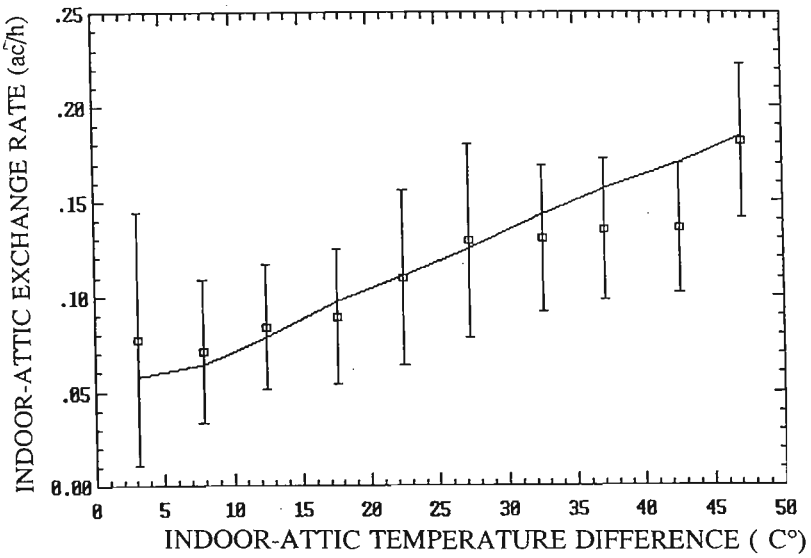

Figure 5-34. Comparison of measured (binned) and predicted (line) indoor-attic exchange rates for attic 6 for wind speeds < 2 m/s (722 hours) showing mean and standard deviation of binned measured data and a line connecting the mean predicted values for each bin.

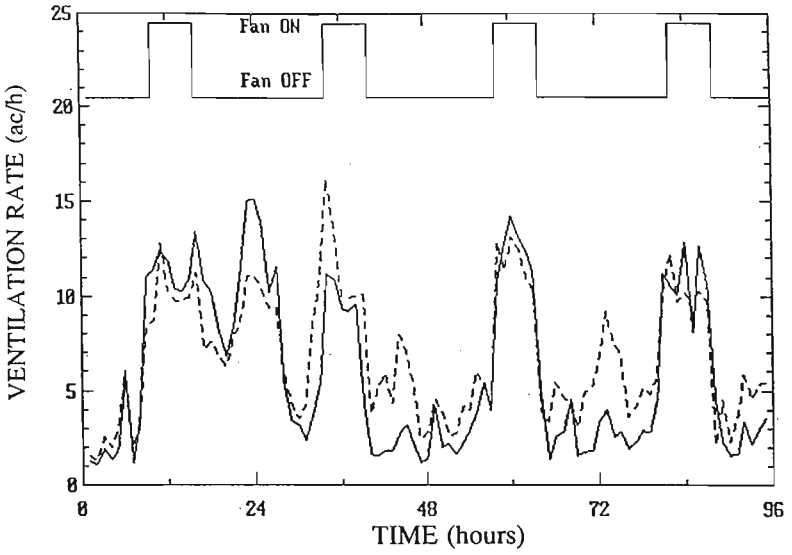

Figure 5-35 Measured (solid line) and predicted (dashed line) attic 6 ventilation rates with an exhaust fan providing 9.6 ac/h from 10:00 am to 4 pm each day. January 17 through 20, 1992.

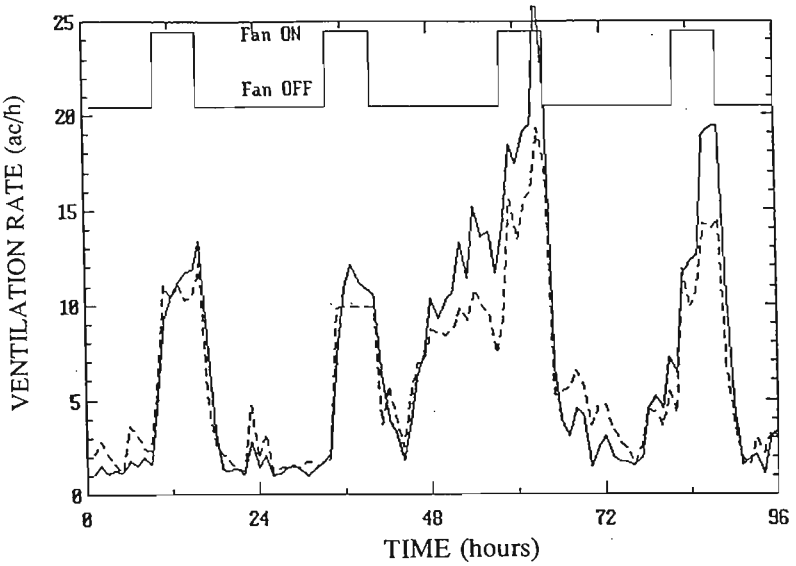

Figure 5-36 Measured (solid line) and predicted (dashed line) attic 6 ventilation rates with a supply fan providing 9.6 ac/h from 10:00 am to 4 pm each day. March 13 through 16, 1992.

and wind effect was large and then decreased for the last two days. The data show that the fan does not add linearly to the natural ventilation rate as the ventilation rate when the fan is on, is about the same each day. When the natural (mostly wind driven) pressure differences across the attic leaks were large then the fan did not increase the ventilation rate significantly. Conversely, at low natural ventilation rates, the fan provided a minimum ventilation rate that was close to the rated capacity of the fan (9.6 ac/h); under these conditions, the fan-generated pressure differences were much larger than the natural pressure differences. These results show that adding the fan does not change the errors in predictions so that the model is combining the fan and natural ventilation rates correctly.

From March to June, the fan was reversed and acted as a supply fan to pressurize the attic. A total of 1359 hours in ventilation data were measured; 326 hours with the fan on and 1033 with the fan off. Figure 5-36 shows four days of typical results and were selected to show low natural ventilation for the first two days then higher natural ventilation rates for the last two days. As in the extraction mode, the fan did not combine linearly with the natural ventilation but provided a guaranteed minimum ventilation rate of 9.6 ac/h. The magnitudes of the differences between measured and predicted ventilation rates were about the same as for the extractor fan and are summarised in Table 5-6.

Table 5-6.
Summary of Attic Fan Performance and Model Prediction Errors

	Supply Fan		Exhaust Fan	
	ON	OFF	ON	OFF
Number of hours	326	1033	259	776
Mean measured ac/h	12.22	5.38	11.16	6.04
Mean predicted ac/h	12.54	5.15	10.84	5.67
Mean error ac/h (%)	0.32 (2.6%)	-0.23 (-4.3%)	-0.32 (-2.9%)	-0.37 (-6.1%)

These results show that there is no systematic error in model predictions when fans are included. With and without the fan, the mean errors are about the same. The increased ventilation rates with the fan on, leads to reduced percentage error because the fan is a well

defined leak in the model with small uncertainty in its flow rate.

5.3.4 Attic Thermal Model

In this section, predictions of the temperature-time variation at various node locations are compared with measured data. For this comparison, attic ventilation rates (which strongly affect attic temperatures) are predicted from the two zone ventilation model. This is a somewhat more stringent test since errors in the two models are combined when the predictions are made. The solution of the combined ventilation and thermal model requires an iterative procedure where the initial estimate of ventilation rate (with the attic air temperature set equal to the outdoor temperature) is used to find the attic temperatures; the attic air temperature is then used to calculate a new attic air density for the attic stack effect and mass balance calculations. Since ventilation rates are not strongly dependent on attic air temperature, the model calculations seldom required more than 5 iterations.

To illustrate the model performance, six days have been chosen (May 15 through 20, 1991) that cover a wide range of wind speeds and ventilation rates, and have a reasonable range of outdoor temperatures and high solar radiation gains. For this period, Fig.5-37 shows that the wind speed varies over a range of 0.8 m/s to 10 m/s and changes rapidly from hour to hour. The variation of outdoor temperature is shown in Fig.5-38 and has a diurnal cycle with peak temperatures in the afternoon 10 to 15 ^{o}C higher than at night. The measured solar radiation on the two pitched roof surfaces is shown in Fig.5-39 and as expected, the south face has greater solar gains than the north face. The third, fourth, and fifth days (hours 48 to 120) show the effect of clouds which reduced the incoming solar radiation. Cloud cover was not measured at the test facility and for the model predictions, it was assumed that the sky was half covered for all hours of the day and night. This assumption about cloud cover means that for clear skies the solar gains and night sky losses are underpredicted and for cloud covered skies, they are overpredicted by the model. Over this period, attic ventilation rates in attic 5 ranged from 0.5 to 10 ac/h while in attic 6, ventilation rates ranged from 2 to well over 20 ac/h. Finally, the various inputs to the thermal model such as, the masses and heat capacities associated with each node, the inner and outer roof surface emissivities, and thermal transport properties of the attic components were given in Section 3.

Figure 5-40a shows predicted and measured air temperatures in attic 5 using predicted attic ventilation rates. The combined model was able to track the large change in measured

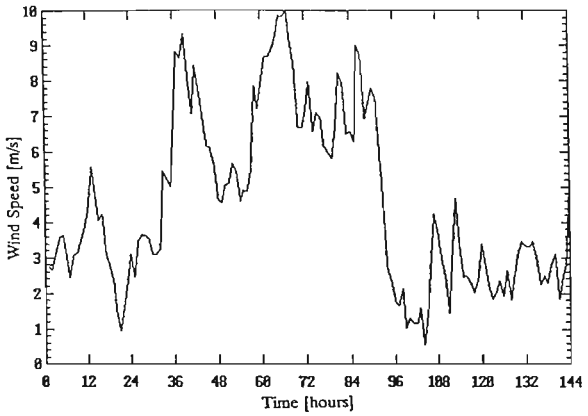

Figure 5-37 Variation in wind speed over the 6 day period from May 15 through 20, 1991.

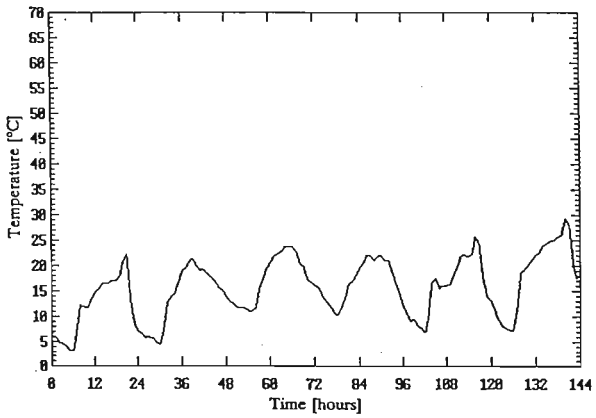

Figure 5-38 Variation of outdoor temperature over the 6 day period from may 15 through 20, 1991.

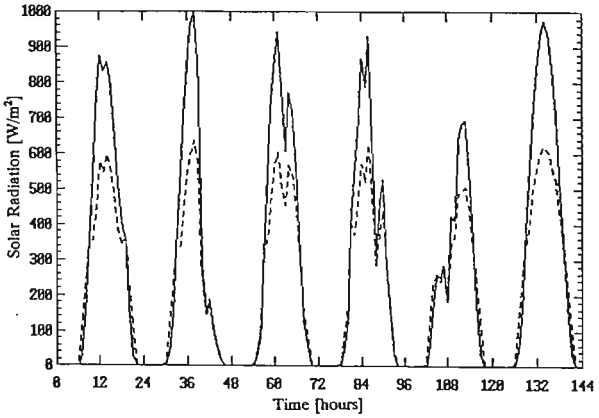

Figure 5-39 Total solar radiation flux on north (dashed line) and south (solid line) roof over the 6 day period from May 15 through 20, 1991.

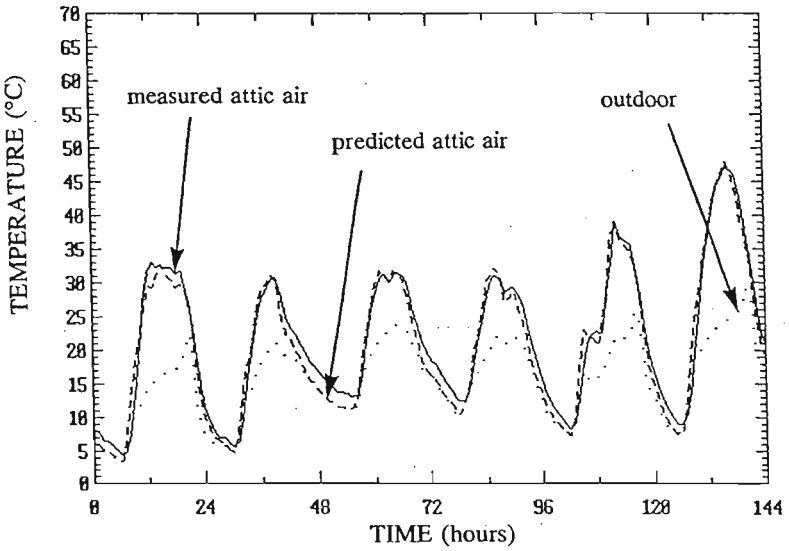

Figure 5-40a Measure (solid line) and predicted (dashed line) air temperatures in attic 5 using predicted ventilation rates over the 6 day period for May 15 through 20, 1991.

attic air temperatures quite closely, although there was a small systematic under-prediction of temperatures, particularly during the night. Over this entire period, the mean error was -0.68 C° while the absolute error was 1.75 C°. Model predictions were made with different values for the shingle emissivity; however, this did not change the predictions significantly unless unrealistic values were used. The other major unknown was the cloud cover since this was not directly measured, particularly at night. Had the cloud cover been greater than 0.5 (the fixed value used in the thermal model), then the model would have predicted less night time cooling resulting in a warmer attic air temperature. Figures 5-40b and 5-40c compare the measured and predicted inner and outer south sheathing temperatures; these components were selected since they experience the largest temperature variations of any of the attic components. For both nodes, the model over-predicts during the day and under-predicts at night. The mean and absolute errors for the inner node were 0.55 and 4.33 C°, respectively; for the outer node, the errors were 0.96 and 3.85 C°, respectively. The reason for this large error is the thermal masses associated with these nodes. The original mass of the outer node was twice that of the inner node in order to account for the mass of shingles; however, this should probably be much higher. Additional mass at the outer node will not only affect the temperature response of the outer node but also, that of the inner node. The model was run with the outer mass ten times that of the inner node which reduced the absolute error by 24%, although the systematic under-prediction was not eliminated. For the remaining nodes, the mean and absolute errors were -1.14 and 2.75 C° for the inner north sheathing, -0.23 and 4.15 C° for the outer north sheathing, and -0.74 and 1.80 C° for joists and trusses, respectively.

A similar comparison is presented in Figs.5-41a, 5-41b, and 5-41c for the temperatures of the attic air, inner, and outer south sheathing in attic 6. A similar trend to that in attic 5 is observed in attic 6, where the predictions tend to over-predict during the day and under-predict at night, although the deviations are not quite as large. The results show the temperature variations in attic 6 are not as large as in attic 5. This is due to the dominant effect of the ventilation rate as it becomes the largest term in the heat balance for the attic. For typical conditions in attic 6, the total convective heat flux is estimated to be 660 W, while the energy flow due to ventilation ranges from 500 to 2000 W over the period shown in Figs.5-40 and 5-41. From these comparisons of measured and predicted temperatures, it was concluded that the combined ventilation and thermal model was giving reasonable results considering that the errors are a combination of those from the thermal and ventilation models.

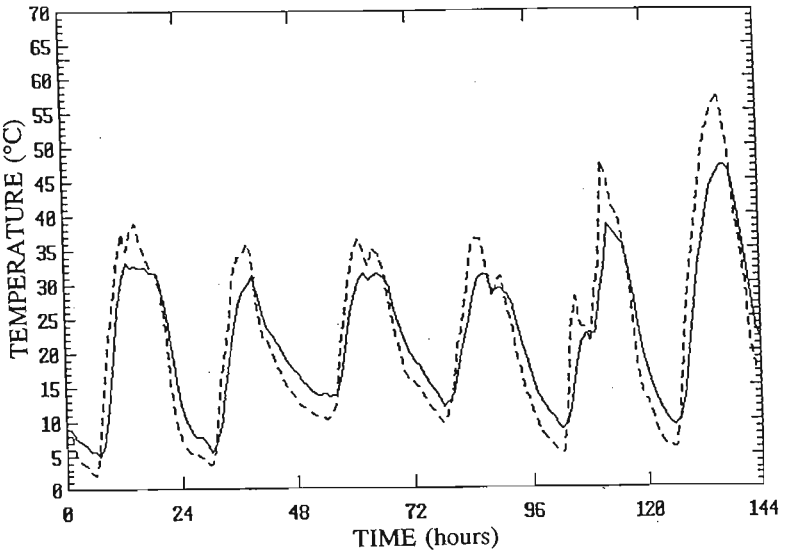

Figure 5-40b Measured (solid line) and predicted (dashed line) inner south sheathing node temperature for attic 5 using predicted ventilation rates for May 15 through 20, 1991.

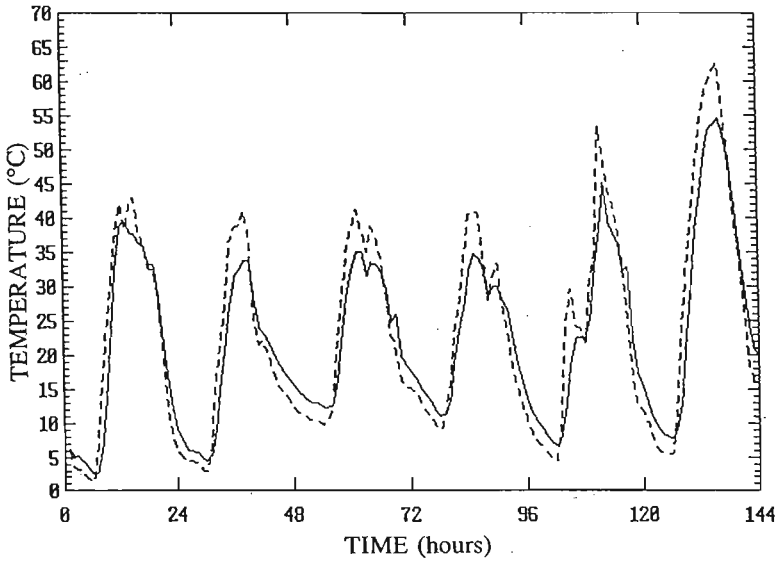

Figure 5-40c Measured (solid line) and predicted (dashed line) outer south sheathing node temperature for attic 5 using predicted ventilation rates for May 15 through 20, 1991.

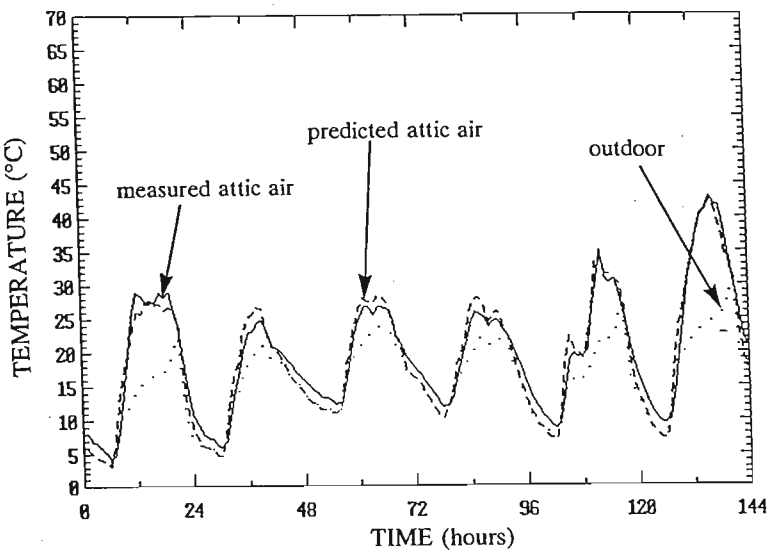

Figure 5-41a Measure (solid line) and predicted (dashed line) air temperatures in attic 6 using predicted ventilation rates over the 6 day period for May 15 through 20, 1991.

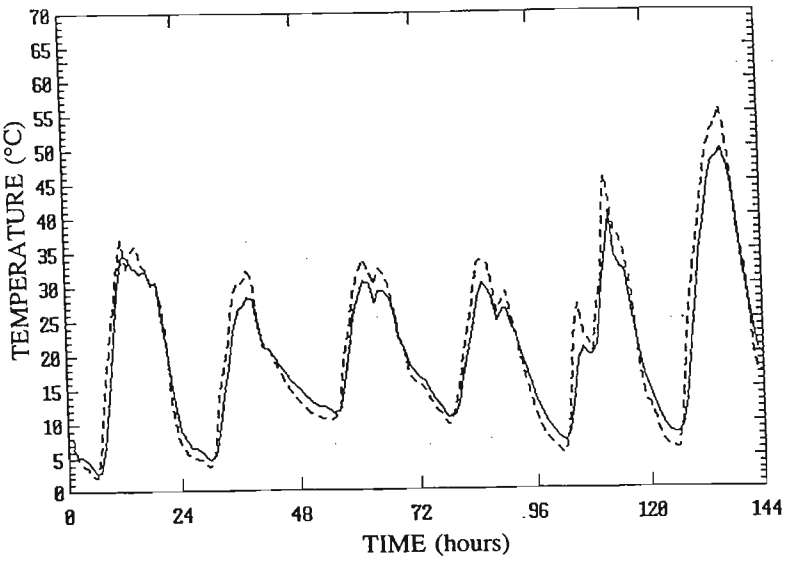

Figure 5-41b Measured (solid line) and predicted (dashed line) inner south sheathing node temperature for attic 6 using predicted ventilation rates for May 15 through 20, 1991.

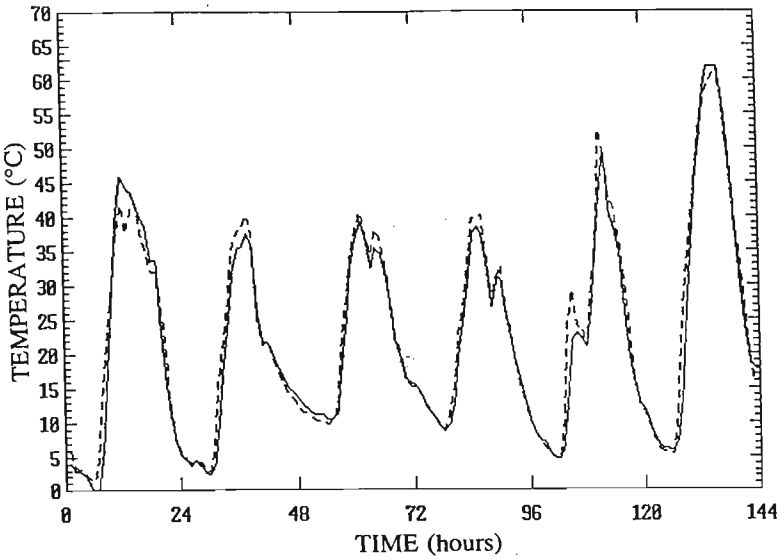

Figure 5-41c Measured (solid line) and predicted (dashed line) outer south sheathing node temperature for attic 6 using predicted ventilation rates for May 15 through 20, 1991.

5.3.5 Attic Moisture Model

Predictions from the attic moisture model were based on the complete model where both ventilation rates and temperatures were predicted and these were compared with the measured data. For moisture measurements (described in Section 5.1), the only data recorded was the attic air relative humidity and the underlying sheathing and truss moisture contents. Unfortunately, the sheathing and truss wood moisture contents remained at a very low moisture content (below 7%) throughout the winter period; hence, these data can only be used to verify that the moisture model predicts low and unchanging moisture contents in the underlying wood layers for the given ambient conditions. The surface layers of the wood however, undergo large changes in moisture content since moisture condenses and evaporates from these surfaces but, there was no way of reliably measuring these moisture contents. The attic air however, undergoes large changes in moisture content which is reflected in changing relative humidity. Thus, the only verification of the moisture model was a comparison of measured and predicted attic air moisture content. This comparison was based on the attic air vapour pressure instead of relative humidity since the latter quantity depends not only on vapour pressure but also, on temperature; if temperature changes are large (as can happen in an attic), this can obscure the changes in vapour pressure which is the air property that is of interest.

The moisture model uses predictions from the ventilation and thermal models as input to the moisture model. Additional inputs include the ambient and house interior relative humidity, both of which were measured at the test site, and initial estimates of attic relative humidity, wood moisture content and condensed mass at each node. For the purposes of verification, the initial moisture conditions for the inner wood nodes were given by the first measured value for each test. The initial condensed masses were set to zero for each surface and the initial relative humidity was taken from the first measured value. The surface wood moisture contents had to be estimated because they were not measured; for winter conditions in attic 6, the initial surface wood moisture content was set equal to the inner wood moisture content and for spring or summer conditions an extra 5% wood moisture content was added to the inner wood moisture content. For attic 5, 5% was added to the inner wood moisture content to obtain estimates of the surface moisture content in all seasons. These values were chosen based on the providing the smallest initial transient for the model calculations. Initial moisture contents that are too high produce a transient period that disappears after a few days.

In order to test the model over a wide range of conditions, three sets of data covering 6 days each, were used to verify the attic air vapour pressure predictions. The three sets of data were for summer (August 13 through 18, 1991), spring (May 15 through 20, 1991), and winter (January 1 through 6, 1991). The range of weather conditions covered by these data are summarised in Table 5-7 and show the wide range of mean outdoor temperatures from -24°C to 20°C. With the diurnal temperature variation added to the means, the total temperature range based on individual hours was -40°C to 30°C. A large range of measured ventilation rates was also covered ranging from 0.2 to about 60 ac/h (predicted).

Table 5-7
Range of test conditions for moisture model verification

	Mean Tout (°C)	Ventilation Rate (ac/h)		
		Mean	Minimum	Maximum
Attic 5				
Summer	20	1.2	0.2	3.4
Spring	16	2.5	0.3	6.8
Winter	-24	0.8	0.4	2.3
Attic 6				
Summer	20	5.4	0.7	17.4
Spring	16	15.3	0.8	~30
Winter	-24	4.0	1.3	18.9

The measured and predicted vapour pressure in attic 5 are shown in Figs.5-42a, 5-42b, and 5-42c for the three date ranges chosen; the large "spikes" in the measured data on days 4 and 5 are due to errors in the data acquisition system. For the summer period (Fig.5-42a), the diurnal vapour pressure changes are large indicating that the attic air exchanges moisture with the wood surfaces in the attic; the wood absorbs moisture from the air during the night and releases moisture to the air during the day. In this figure, the outdoor vapour pressure is also plotted and indicates that the attic air does not simply follow the outdoor variations.

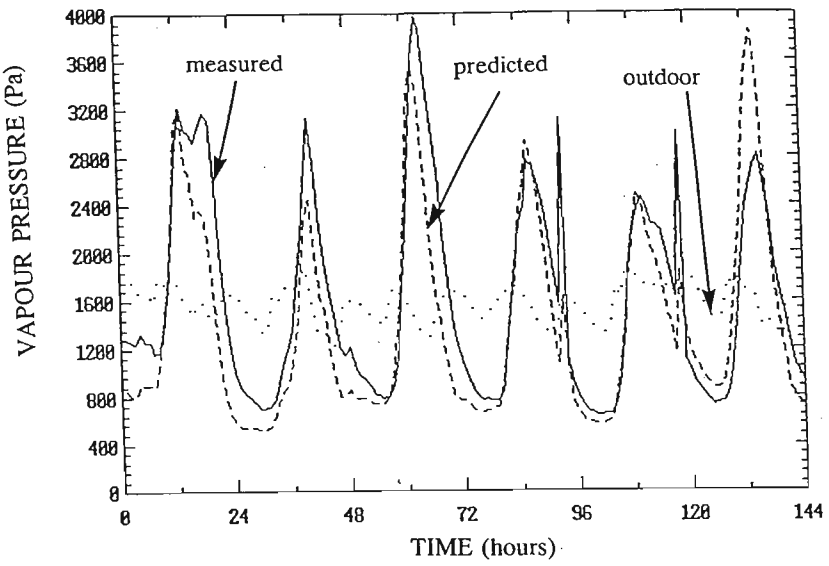

Figure 5-42a Measured (solid line) and predicted (dashed line) vapour pressure for attic 5 and outdoor vapour pressure (dotted line) over 6 day period from August 13 through 18, 1991.

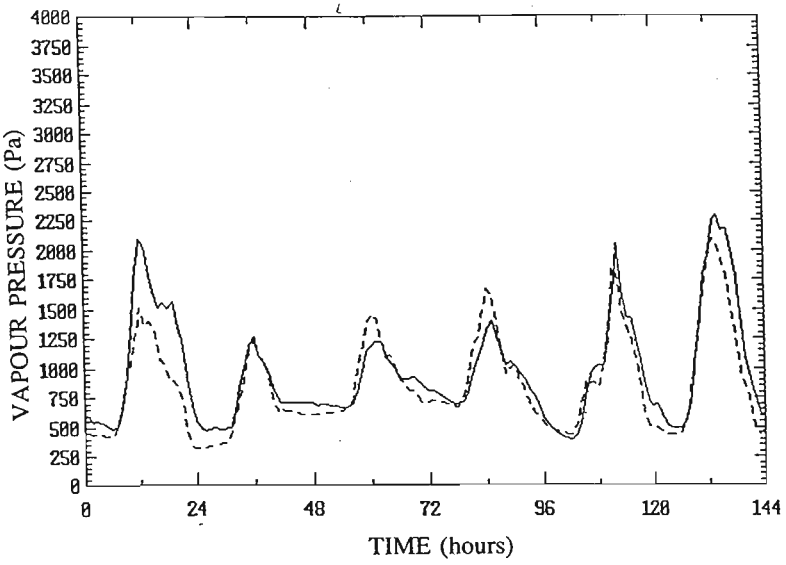

Figure 5-42b Measured (solid line) and predicted (dashed line) vapour pressure for attic 5 over 6 day period from May 15 through 20, 1991.

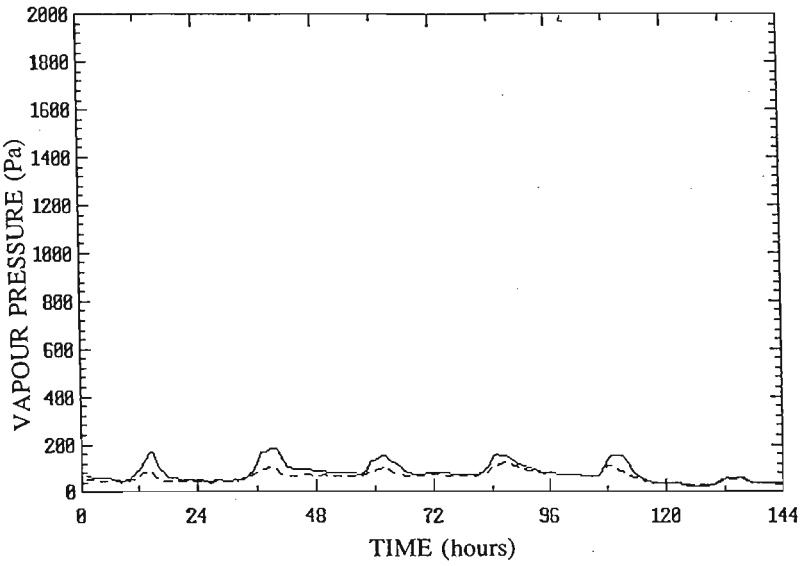

Figure 5-42c Measured (solid line) and predicted (dashed line) vapour pressure for attic 5 over 6 day period from January 1 through 6, 1991.

The model predictions are able to follow the diurnal variations in vapour pressure quite closely and demonstrates the skill of the model. Given the errors in predicted ventilation rates and temperatures, the results are very good and give added confidence to the model predictions. A similar diurnal variation in attic vapour pressure is seen in both the spring and winter but with a much reduced amplitude, particularly during the winter period. This simply reflects the fact that as outdoor temperature decreases the air holds less water vapour. In both cases, the model predictions are very close to the measured data and are able to track both the short term, diurnal changes as well as the seasonal changes in vapour pressure. A similar set of comparisons for the same date ranges is presented in Figs.5-43a, 5-43b, and 5-43c for attic 6. Again model predictions agree quite well with the measurements for all three data sets. The diurnal variation in vapour pressure in attic 6 is not as large as in attic 5 (particularly in summer) since attic 6 has a much higher ventilation rate than attic 5. The high ventilation rates allow the attic air temperatures and vapour pressures to be closer to the outdoor conditions.

The mean and absolute errors for the attic air vapour pressure are summarised in Table 5-8. In both attic 5 and attic 6 there is a tendency to underpredict the attic air vapour pressure with the error increasing from about 7% in summer to 20% to 30% in winter. These large percentage errors in winter must be kept in perspective because the vapour pressures in winter are extremely low and an error of only 16 Pa in vapour pressure corresponds to a 20% error. The magnitude of the errors shown in Table 5-8 are acceptable considering the cumulative errors generated by the ventilation and thermal models.

For the underlying wood moisture contents (which showed little or no change in value during the winter), the model predictions are shown Fig.5-44 for the north and south sheathing and the joists. These predicted wood moisture contents remain low and change very slowly. The model predicts that the inner wood remains at low wood moisture content for both attics over all weather conditions. This relatively constant low value of wood moisture content corresponds qualitatively with the measured wood moisture contents.

The combined ventilation, thermal, and moisture model has been successfully verified with the measured data, although some errors were noted which would point to some further refinements. This combined model will be used in the Section 6 to perform simulations to evaluate the effect of climate, attic leakage distribution and mechanical ventilation on moisture in attics.

Table 5-8
Comparison of measured and predicted attic air vapour pressures

	Figure Number	Mean Measured P_w [Pa]	Mean Error		Absolute Error	
			Pa	%	Pa	%
Attic 5						
Summer	5-42a	1632	-133	-8	318	19
Spring	5-42b	970	-102	-11	152	16
Winter	5-42c	111	-18	-16	23	21
Attic 6						
Summer	5-43a	1692	-126	-7	247	15
Spring	5-43b	995	-108	-11	134	13
Winter	5-43c	82	-16	-20	17	21

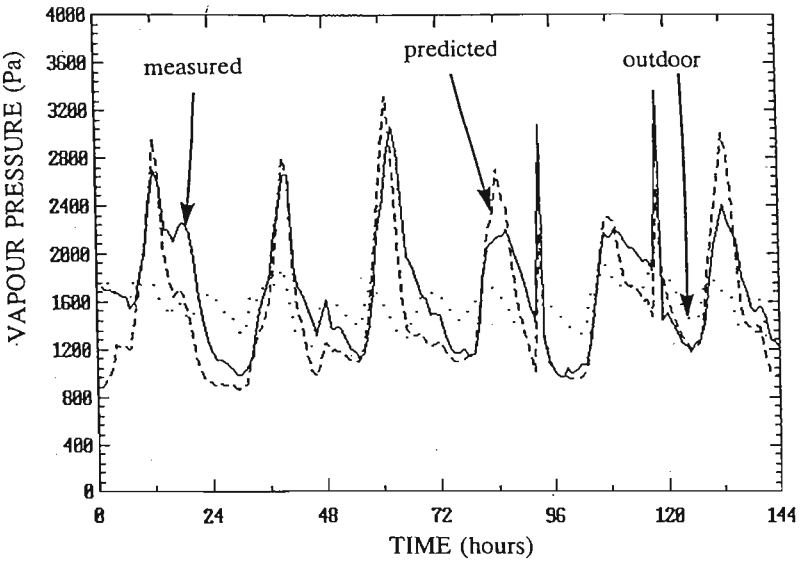

Figure 5-43a Measured (solid line) and predicted (dashed line) vapour pressure for attic 6 and outdoor vapour pressure (dotted line) over 6 day period from August 13 through 18, 1991.

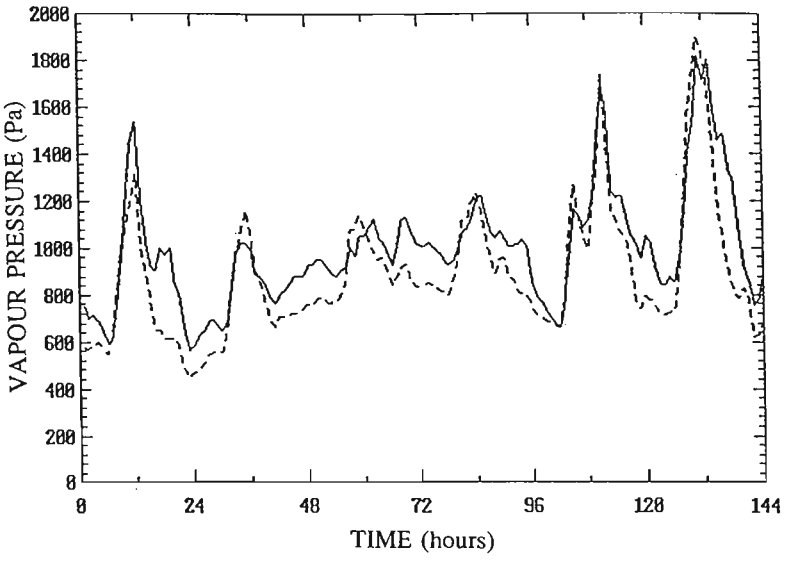

Figure 5-43b Measured (solid line) and predicted (dashed line) vapour pressure for attic 6 over 6 day period from May 15 through 20, 1991.

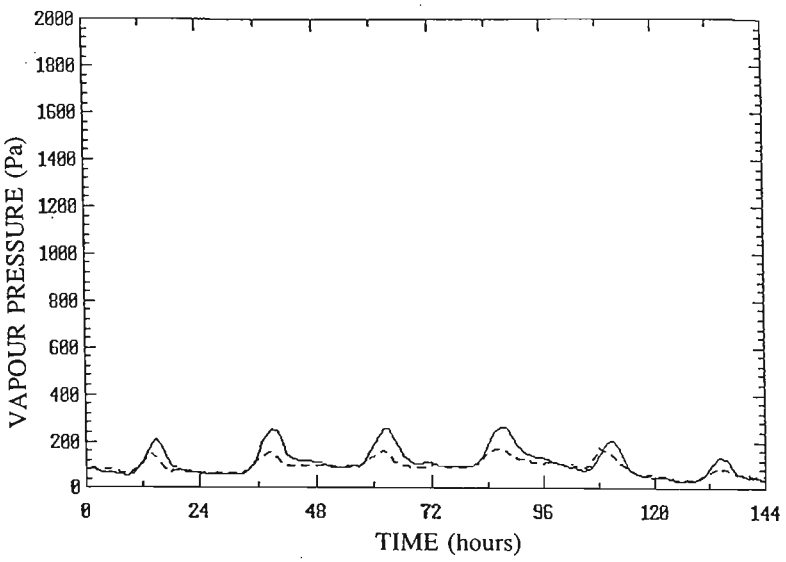

Figure 5-43c Measured (solid line) and predicted (dashed line) vapour pressure for attic 6 over 6 day period from January 1 through 6, 1991.

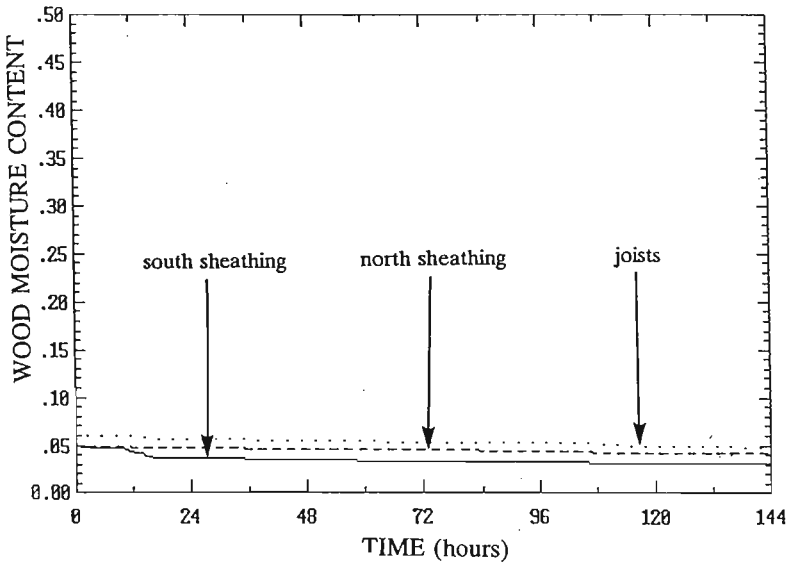

Figure 5-44 Predicted wood moisture content of the underlying wood for north and south sheathing and trusses in attic 5 for the period Jan.1 through 6, 1991.

SECTION SIX

ATTIC SIMULATIONS

In this section, the complete model will be used to carry out simulations of attics under a wide variety of configurations and climatic zones. The first set of simulations are carried out for given ambient conditions where temperature varies periodically, relative humidity is constant or varies periodically, wind speed is constant, and cloud cover is 0 or 1. These parametric simulations highlight the important climate and building characteristics which affect attic moisture. The simulations are performed by running the combined ventilation, thermal and moisture transport models for one week (168 hours) and examining the resulting predictions. The effect of the changing input parameters is examined by looking at the predicted wood moisture contents, condensed mass of water, attic air relative humidity, attic air temperature and ventilation rates. The second set of full-scale simulations are carried out using actual weather data for selected climatic zones in Canada over a complete heating season.

6.1 PARAMETRIC SIMULATIONS

The model was run with two extremes of outdoor winter weather, a dry prairie climate and a damp maritime climate. For the prairie climate, ambient temperature was assumed to vary sinusoidally over a 24 hour cycle from a minimum of -20°C at midnight to a maximum of 0°C at noon. Ambient vapour pressure also varied sinusoidally, from 100 Pa at midnight to 200 Pa at noon, corresponding to 97% and 33% RH, respectively. These values were chosen as typical prairie values from the data measured at AHHRF. For the maritime climate, ambient temperature was assumed to be constant throughout the day at -1°C while the ambient relative humidity was 100%. These values were chosen as a typical Canadian maritime climate from weather data presented by CMHC (1987, p.25) for Halifax, Nova Scotia in December, January and February.

The cloud cover was either 1 (complete) or 0 (clear sky) for the whole simulation period in order to examine the extremes of this effect. The cloud cover changed the short wave solar radiation to the roof and the long wave radiation from the roof to the to the ground and sky. The solar radiation for clear skies was assumed to be zero from 5 pm. to 9 am. Between 9 am. and 5 pm. the solar radiation varied sinusoidally from zero to a peak of 550 W/m^2 on the south sheathing and 60 W/m^2 on the north sheathing. Again, these values were based on measurements taken on January 1, 1991 at AHHRF. For a cloudy day both sheathing surfaces were assumed to have the same peak solar radiation of 120 W/m^2 based on measurements taken on the December 25, 26, and 27, 1990 at AHHRF. The roof ridge was assumed to be in an east-west direction so that there was a south and north sloped sheathing surface.

For these simulations, three wind speeds were chosen: light winds of 0.5 m/s, average winds of 2.5 m/s and strong winds of 6 m/s. These wind speeds were based on the range of measured data at AHHRF and produced a large range of ventilation rates. The house was assumed to be completely exposed to the wind and for calculating wind pressure coefficients, the wind direction was assumed to be perpendicular to the roof ridge of the attic for all simulations.

The house used in the simulations was the same for all simulations with dimensions and leakage distribution based on the test houses at AHHRF. The houses were assumed to have no furnace flue in order to have as large an indoor-attic exchange rate (and hence, moisture load) as possible. The indoor relative humidity and temperature were constant throughout the simulations at 50% RH and 20°C, respectively. The interior zone was assumed to have a 4 Pa leakage area of 100 cm^2 with exponent n = 0.66 resulting in C = 0.0108 $m^3/s(Pa)^n$. These are values that would be typical for a house this size in Canada (see Sulatisky (1984)). The leakage distribution is also assumed to be similar to the AHHRF houses with 20% of leakage in the ceiling, 20% at floor level and 60% in the walls and the wall and floor leakage evenly distributed to the four sides of the building.

Two different attic leakage configurations were tested; a standard attic that had soffit and roof vents and a sealed attic. The standard attic had the same dimensions as attic 6 at AHHRF, with background distributed leakage, soffit vents above the north and south walls (parallel to the roof ridge), and an additional vent on each pitched roof surface. The total leakage area was calculated based on the Canadian building code (NBCC, 1990) which recommends that the vent area of the attic be 1/300 of the floor area; this results in a total 4 Pa leakage area of 1900 cm^2. This leakage was separated into 50% for the leakage in the soffits, 45% in the two roof vents and

5% background leakage in the sloped roof surfaces. The flow coefficient for the standard attic was calculated to be 0.0798 m^3/sPa^n assuming a flow exponent, n of 0.7. Each of the two roof vents had a leakage area of 431 cm^2 corresponding to a flow coefficient of 0.086 m^3/sPa^n for an assumed flow exponent of 0.5. The standard attic was also assumed to be constructed in the normal way without the raised heel trusses (as used in the test attics, see Fig.5-2). Thus, the attic volume was reduced to 38 m^3. The sealed attic was included to simulate a common practice in parts of Canada where attics are sealed to prevent snow entry. The sealed attic was the same size as the standard attic but had no soffit or roof vents. The background leakage was assumed to be 10% of the standard attic; however, the ceiling leakage was kept the same as the standard attic to maintain a moisture load. The 4 Pa leakage area of the attic was 134 cm^2 for an assumed flow exponent of 0.7 resulting in a flow coefficient of 0.0096 m^3/sPa^n.

The effect of having exhaust, supply, or balanced fans was tested for a sealed attic to see if fans could be used to alleviate moisture problems by increasing ventilation rates in low leakage attics. The balanced fan system had one fan supplying air to the attic and one fan extracting air from the attic. Each of the balanced fans had a rated flow rate of 7 ac/h (75 l/s) for a total of 14 ac/h; the single fans both had rated flow rates of 14 ac/h. The sealed attic that the fans were used in for the simulations is described below. A simulation was also included of the current practise for attics which is an extraction fan on a timer so that it only operates during the day. A range of fans sizes were simulated to determine if there was an optimum fan size to balance the effects of reduction of attic temperatures, which tends to increase moisture problems, and bringing dryer outdoor air into the attic to remove moisture.

Finally, different initial wood moisture contents were examined to determine their effects on moisture accumulation and attic wood drying. The two wood moisture contents chosen for these simulations were 5% and 15% moisture content. These different initial conditions were chosen to reflect different moisture histories of the wood.

A summary of the parametric simulations are given in Table 6-1 indicating which parameter was varied for a particular simulation. For each simulation, the following calculated values are given; the ventilation and indoor-attic exchange rates (where positive flow is flow into the attic), attic air temperature and relative humidity, inner node (surface) sheathing wood moisture contents, as well as the amount of condensed mass. The simulations indicated that condensed mass either accumulated over time or was periodic with deposition at night and evaporation during the day. For periodic deposition, the peak value was calculated, and for accumulating

condensed mass, the average accumulation per day was calculated. It should be noted that the condensed mass includes moisture that condenses from the attic air together with the moisture that is driven out of the cell walls of the wood and appears as "unbound" water (see Section 4.2).

Table 6-1
List of parametric simulations

Simulation	Attic Configuration	Initial Wood moisture content, %	Wind Speed m/s	Climatic Zone	Cloud Cover
1	Standard	5	0.5	Prairie (P)	0
2	Standard	5	2.5	P	0
3	Standard	5	6	P	0
4	Standard	5	0.5	P	1
5	Standard	5	2.5	P	1
6	Standard	5	6	P	1
7	Sealed	5	0.5	P	1
8	Standard	15	0.5	Maritime (M)	0
9	Standard	15	2.5	M	0
10	Standard	15	6	M	0
11	Standard	15	6	M	1
12	Standard	15	2.5	M	1
13	Standard	15	0.5	M	1
14	Standard	19	0.5	M	1
15	Standard	19	6	M	1
16	Standard	19	6	M	0
17	Sealed with Balanced Fans	15	6	M	0
18	Sealed with Exhaust Fan	15	6	M	0
19	Sealed with Supply Fan	15	6	M	0
20	Sealed with Balanced Fans	5	6	P	0

21	Sealed	15	6	M	0
22	Sealed	5	6	P	0
23	Sealed with Balanced Fans	15	6	M	1
24	Sealed	15	6	M	1
25	Sealed with Exhaust Fan 9 a.m. to 4 p.m.	15	6	M	1
26	Sealed with Exhaust Fan 9 a.m. to 4 p.m.	15	6	M	0
27	Sealed with Supply Fan Tout = -5°C	15	6	M	0
28	Sealed with Supply Fan of 50 cfm	15	6	M	0
29	Sealed with Supply Fan of 100 cfm	15	6	M	0

6.1.1 Results of Parametric Simulations

The simulations shown in Table 6-1 were all run for one week (168 hours), which was found to be sufficient for the predicted quantities to reach stationary values. For the predicted values that have strong diurnal values, the high and low as well as the mean values were calculated. The mean, high and low values are taken over the last 48 hours to remove any initial transient effects. Table 6-2 summarises the results for the simulations given in Table 6-1 and the discussion of these results is separated into a discussion of the moisture dynamics that occurs in an attic and then a discussion of the effect of ambient conditions on moisture in attics.

Moisture Dynamics In all simulations, it was observed that only the inner surface nodes of the wood components were affected by the changing conditions in the attic air. The surface wood moisture contents underwent relatively large changes mainly, in response to the large temperature variations that occur in the attic. During the day, moisture was released

Table 6-2
Summary of Attic Simulation Results

Simulation	Ventilation Rate, ac/h Attic (Ceiling)	Attic Air Temp. °C Mean (Hi,Lo)	Attic RH % Mean (Hi,Lo)	W_{MC},% South Sheathing Mean (Hi,Lo)	W_{MC},% North Sheathing Mean (Hi,Lo)	Condensation
1	1.9 (0.3)	-8.9 (12,-20)	53 (90,25)	5 (7,4)	7 (8,7)	-
2	7.9 (0.3)	-8.9 (5,-20)	53 (78,35)	8 (9,7)	9 (9,8)	-
3	25 (0)	-9.4 (3,-20)	53 (76,32)	8 (10,7)	8 (10,7)	-
4	2.4 (0.3)	-5.3 (8,-15)	49 (70,36)	8 (9,7)	8 (9,7)	-
5	8 (0.3)	-7.5 (4,-16)	55 (72,37)	8 (9,7)	8 (9,7)	-
6	25 (0)	-8.8 (4,-18)	52 (72,32)	8 (9,7)	8 (9,7)	-
7	0.3 (0.3)	-4.5 (8,-14)	60 (75,45)	9 (10,9)	9 (10,9)	-
8	2 (0.25)	-0.8 (12,-5)	61 (75,47)	8 (11,6)	12 (13,11)	-
9	7.3 (0.2)	-0.4 (5,-2)	86 (93,79)	17 (22,13)	25 (26,24)	-
10	24 (-0.1)	-0.7 (2,-2)	94 (97,90)	25 (29,20)	29 (30,29)	0.1 kg South periodic 0.6 kg North Periodic
11	24 (-0.1)	-0.1 (1,-1)	91 (93,90)	26 (27,25)	26 (27,25)	-
12	7.4 (0.2)	0.9 (6,0)	86 (87,85)	21 (21,23)	21 (21,23)	-
13	1.9 (0.3)	2.8 (8,2)	71 (73,67)	14 (15,13)	14 (15,13)	-
14	1.9 (0.3)	2.8 (8,2)	71 (73,67)	14 (15,13)	14 (15,13)	-
15	24 (-0.1)	-0.1 (1,-1)	93 (94,92)	26 (27,25)	26 (27,25)	-
16	24 (-0.1)	-0.7 (2,-2)	95 (97,90)	25 (29,20)	25 (29,20)	0.1 kg South periodic 0.6 kg North Periodic

17	9 (0.8)	-0.2 (3,-2)	93 (97,91)	27 (30,23)	30 (32,28)	0.3 kg South periodic 0.3 kg North Periodic
18	17 (2.7)	0.3 (3,-5)	96 (97,95)	30 (32,27)	31 (33,30)	2.2 kg South Periodic 2.2 kg/Day North Accumulates
19	16.6 (-2.1)	-1.4 (2,-2.5)	97 (100,92)	27 (28,23)	29 (30,28)	2 kg South Periodic 2 kg North Periodic
20	9.4 (0.8)	-9 (4,-18)	72 (95,48)	11 (12,9)	11 (12,9)	-
21	0.7 (0.7)	0.6 (4,-0.5)	90 (92,88)	22 (25,19)	30 (32,29)	1 kg North Periodic
22	0.8 (0.8)	-7.6 (5,-17)	87 (100,70)	14 (16,12)	15 (17,13)	1.7 kg South Periodic 2.6 kg North Periodic
23	9 (0.8)	0.6 (2,0)	95 (96,94)	29 (29,29)	29 (29,29)	-
24	0.7 (0.7)	1.5 (3,1)	97 (97,97)	32 (32,32)	32 (32,32)	1 kg/Day Accumulates North and South
25	5.4 (1.3)	1.3 (3,1)	97 (99,96)	32 (33,32)	32 (33,32)	0.4 kg/Day Accumulates North and South
26	5 (1.3)	0.3 (3,-0.5)	92 (95,90)	25 (27,18)	29 (30,29)	0.4 kg North Periodic
27	17 (-2.1)	-5.4 (-2,-7)	98 (100,92)	21 (21,19)	22 (25,21)	1.3 kg South Periodic 3 kg North Periodic
28	3 (0.5)	-0.1 (3,-2)	90 (92,88)	23 (25,19)	27 (29,26)	-
29	5 (-0.1)	-0.5 (3,-2)	87 (91,85)	21 (23,18)	24 (26,23)	-

from the wood since raising the temperature of wood at a given moisture content increases the vapour pressure resulting in mass transfer from the wood surface. Conversely, at night, the wood (particularly the sheathing) is cooled which reduces the vapour pressure of the wood resulting in mass transfer to the surface; recall that the model for wood allows moisture to appear as "unbound" water if cooling is sufficiently large. Figure 6-1 shows the wood moisture contents of the three surface wood layers for simulation 10 (standard attic in a maritime climate). During

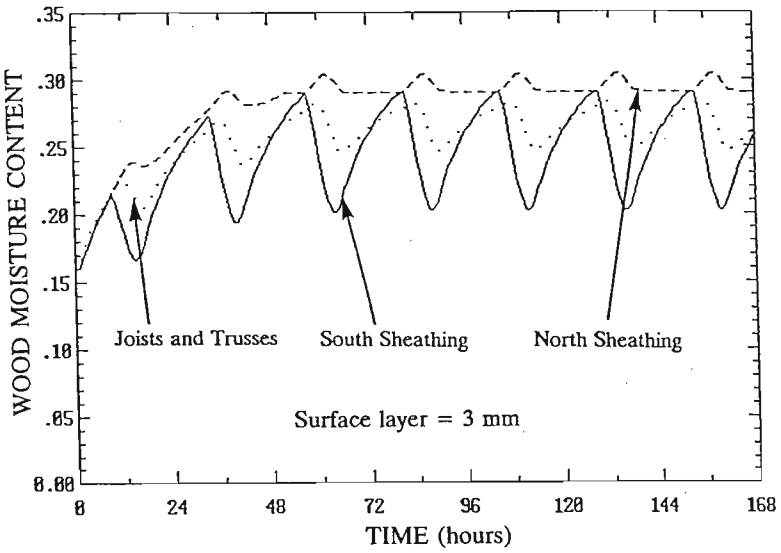

Figure 6-1 Diurnal variation of surface wood moisture content for simulation 10 (standard attic in maritime climate with 6 m/s wind speed and no cloud cover)

the night the wood moisture content of the south sheathing increases. When the sun comes up and heats this surface it rapidly loses this moisture, which is transferred to the attic air. This increases the vapour pressure in the air so that moisture is then transferred to the other two wood surfaces as shown by their increasing wood moisture content for the first couple of hours after the south sheathing starts to lose moisture. Later in the day, the north sheathing and the trusses have increased temperatures and so they too lose moisture. After the first 48 hours of the simulation, the north sheathing approaches saturation; the increase in wood moisture content during the first 48 hours represents the transient response of the wood to the initial moisture content of 15% and shows how rapidly the wood surface nodes respond. During the night, the south sheathing absorbs moisture from the attic air while the north sheathing (which is already at high moisture contents) is cooled resulting in "unbound" water condensing out of the wood. The dynamics of condensed mass appearing on the north and south sheathing surfaces is shown in Fig.6-2. As stated previously, this condensed mass is largely due to the decrease in temperature and results in "unbound" water appearing in the wood; the moisture model does not differentiate between visibly moisture or surface frost and this "unbound" water.

In some of the simulations, mass condenses on the sheathing at night and is later evaporated during the day. An example of periodic condensation is shown in Fig.6-3 for a sealed attic in a prairie climate with clear skies (simulation 22). The peak values are about 1.7 kg on the north sheathing and 2.6 kg on the south sheathing. The higher peak values for north sheathing are characteristic of clear sky simulations because the north sheathing does not receive as much solar radiation during the day and less moisture is removed during the day. In the worst cases, not all the condensed mass is removed by daytime solar gains. This results in mass accumulation as shown in Fig.6-4 for two consecutive weeks of a sealed attic with an extractor fan on a timer (simulation 25). The results in Fig.6-4 are for cloudy conditions where both sheathing surfaces experience the same radiation gains and losses and thus have the same temperatures and the same accumulating mass. The mass accumulates in a "ratcheting" fashion with more deposition at night than evaporation during the day. The mass accumulates at a net rate of about 0.4 kg/day on both sheathing surfaces. For clear skies, mass may accumulate on the north sheathing but appear periodically on the south sheathing due to its higher daytime temperature. This is illustrated in Fig.6-5 for simulation 18 which shows accumulation at night and evaporation during the day for both sheathing surfaces.

Climatic Zone A maritime climate with high ambient relative humidity produced much higher values of surface wood moisture content and attic air relative humidity. This can be

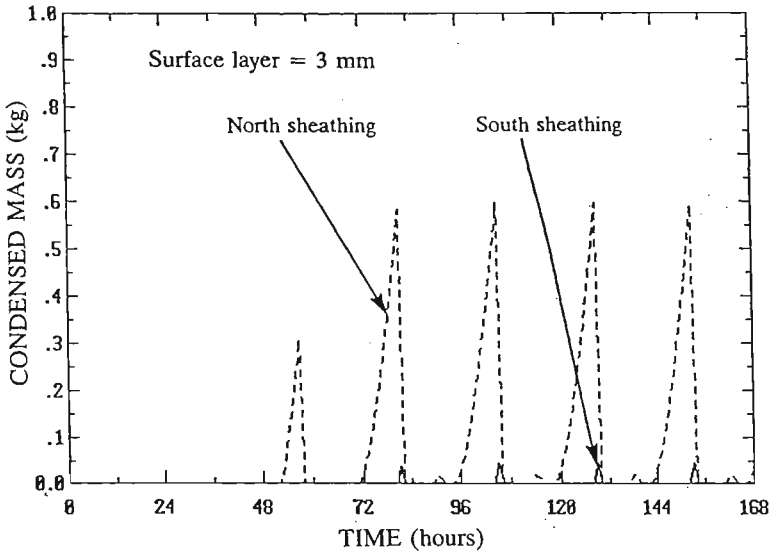

Figure 6-2 Diurnal variation of condensed mass on sheathing for simulation 10 (standard attic in maritime climate with 6 m/s wind speed and no cloud cover).

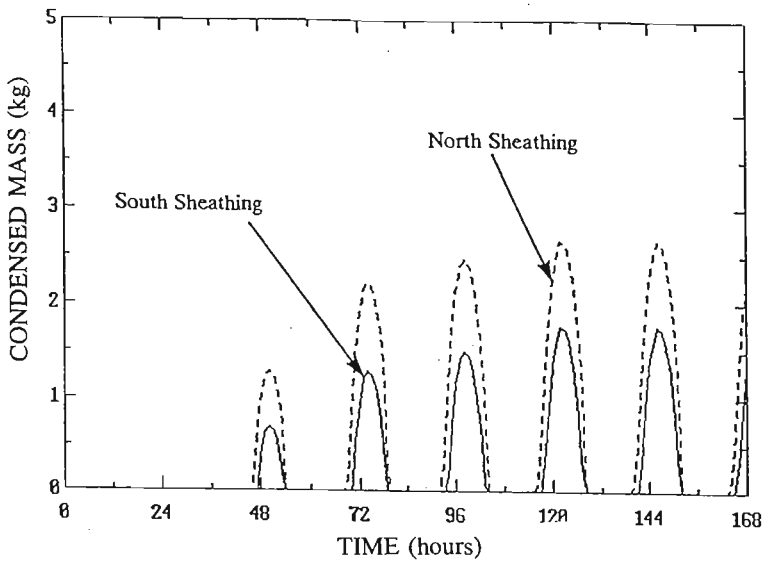

Figure 6-3 Diurnal variation of condensed mass for simulation 22 (sealed attic in a prairie climate with 6 m/s wind speed and no clouds).

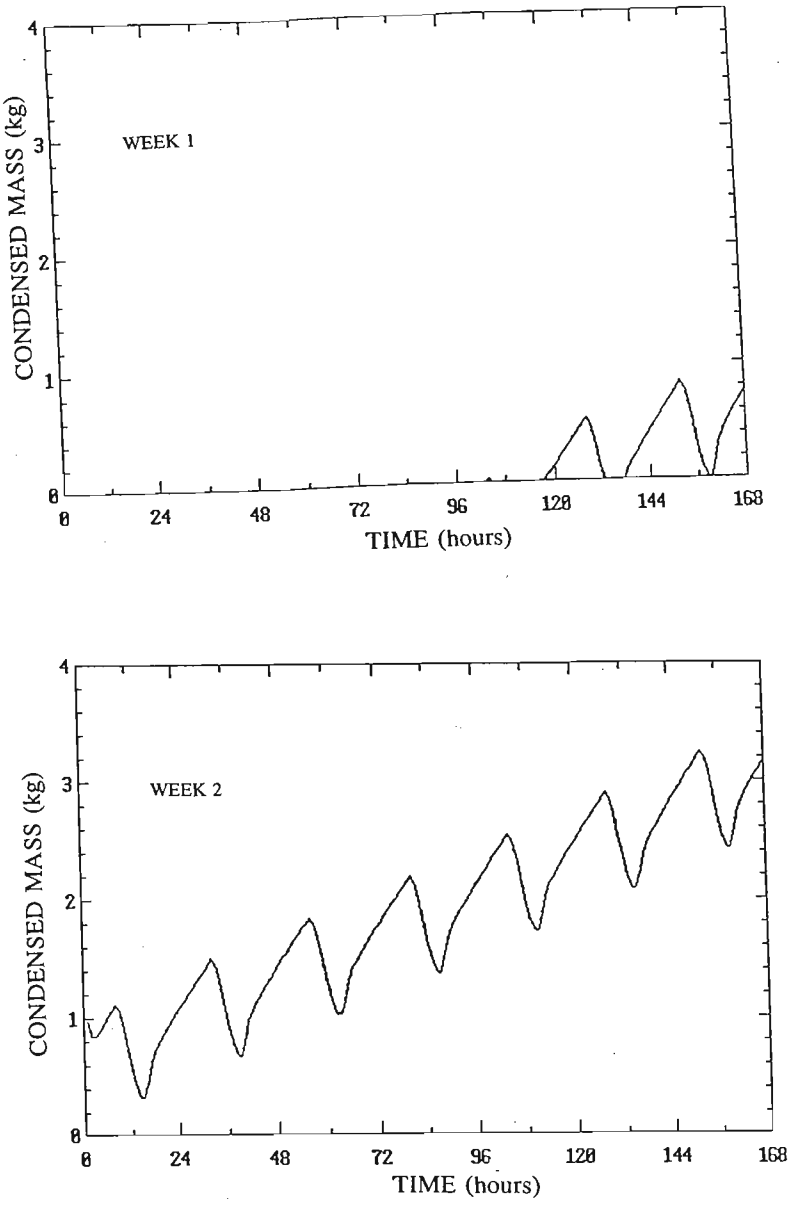

Figure 6-4 Accumulation of condensed mass on the north and south sheathing for simulation 25 (sealed attic with exhaust fan in a maritime climate with 6 m/s wind speed and complete cloud cover) over two week period.

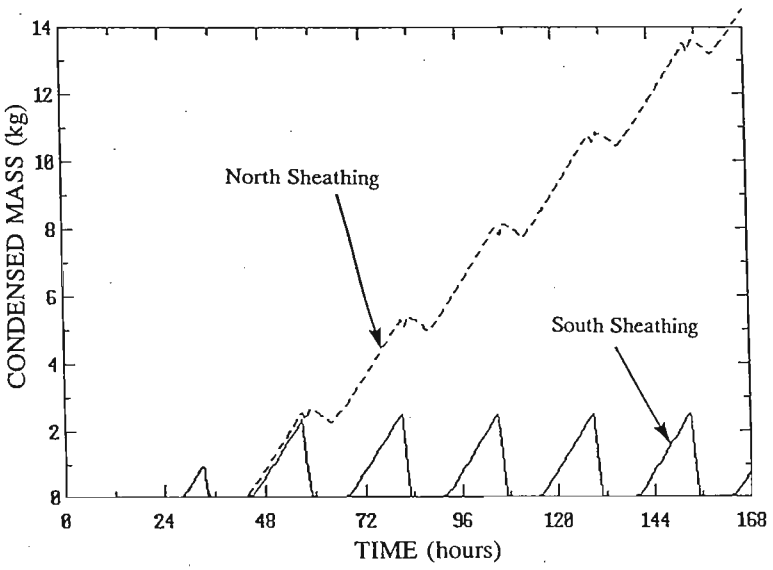

Figure 6-5 Variation of condensed mass with time on the north and south sheathing for simulation 18 (sealed attic with exhaust fan in a maritime climate with 6 m/s wind speed and no cloud cover).

seen by comparing the results of simulations 2 and 3 for the prairie climate to simulations 9 and 10 for the maritime climate. The maritime climate produced the worst situation for the standard attic (simulation 10) with the only case of condensation on the sheathing. Over all the simulations, in a prairie climate the wood was always drier (never above 10%). The maritime climate produced higher relative humidity values that were often close to saturation. The exception was for low wind speeds that produce low ventilation rates (simulations 8 and 12); the decreased ventilation rate resulted in increased attic air temperatures, increased saturation pressure, and therefore lower relative humidities.

Cloud Cover To best observe the results of changing cloud cover, simulations 1, 2 and, 3 for clear skies are compared to simulations 4, 5, and, 6 for cloudy skies. Clear skies produced larger extremes in all the predicted parameters due to the large change in temperatures from solar gains during the day and radiation to a clear sky at night. The most important reason for moisture deposition was cooling of the sheathing at night that was greatest for clear skies. Measurements on the test attics (see Fig.5-25) showed that the outer sheathing temperature was 3 to 4 C° below the ambient temperature and 4 to 5 C° below the attic air. The inner sheathing showed a smaller temperature depression of about 2 C° below the attic air, but was still the coldest attic surface. Simulation 10 and simulations 16 through 19 show that clear skies produced condensation on the interior of the attic sheathing due to sheathing undercooling.

Wind Speed The simulations showed that the effect of wind was very important principally because wind is the dominant driving force for attic ventilation. For the standard attic, ventilation rates ranged from about 2 to 25 ac/h for wind speeds of 0.5 m/s to 6 m/s. The effect of ventilation rate on the model predictions is shown by simulations 8, 9, and 10. The high ventilation rate in simulation 10 had the highest relative humidity (94% compared with 61%), the highest surface wood moisture content (29% compared with 12%) and condensing mass when the low ventilation rate simulation 8 had none. These simulations show that increased ventilation rates produced cold attics which ultimately resulted in mass condensing from the outdoor ventilation air. For example, in simulation 1 with a ventilation rate of 1.9 ac/h, the mean attic air temperature was -8.9 °C with peak temperature of 12 °C while in simulation 3 with a ventilation rate of 25 ac/h, the mean and peak temperatures were -9.4 and 3°C, respectively. This indicates that well-ventilated attics are cold. Despite the low humidity ratio of the outdoor air, the high ventilation rates still convect a large mass of vapour through the attic which can accumulate on the sheathing at night. A secondary effect

of increasing wind speed is the reduction in the ceiling flow (and hence, the moisture load on the attic). This reduction is illustrated by comparing groups of simulations where only the wind speed changed ie. simulations 1, 2, and 3, simulations 4, 5, and 6, simulations 8, 9, and 10 and simulations 11, 12 and 13. The maximum indoor-attic exchange rate of 0.3 ac/h represents a mass flow of 0.084 kg/hr at indoor conditions of 20°C and 50% relative humidity. However, the ceiling moisture flow is still small compared with the moisture flow due to attic ventilation; at the lowest ventilation rate of 2 ac/h (simulation 8) in a maritime climate of -1°C and 100% relative humidity, the ventilation flow supplies 0.263 kg/hr. This shows that even at low ventilation rates the flow of moisture from outside is more important than the flow through the ceiling for a standard attic; however, this is not true if the indoor-attic exchange rate is the dominant moisture source as in the case of sealed attics or attics with exhaust fans.

Sealed Attics The sealed attics had the same dimensions as the standard attic but only 10% of the background leakage and no other vents; however, these attics retained the same amount of ceiling leakage as the standard attics which meant that the ceiling leakage was a much greater proportion of the total attic leakage. Simulations 7, 21, 22, and 24 show that the majority of the attic ventilation was due to the ceiling flow which was directed into the attic. With all the incoming air at a high moisture content (humidity ratio of 0.00738 kg_{H2O}/kg_{air}), this produced high wood moisture contents and more condensation problems; the sealed attic was the only one that produced condensation in a prairie climate (simulation 22) although this is probably a temperature effect producing "unbound" water. The sealed attic simulations clearly showed that, although external moisture sources are eliminated, internally generated moisture becomes a major problem for these attics unless special attention is paid to sealing all indoor-attic leakage paths.

Exhaust and Supply Fans Fans were added to a sealed attic to find out if they would reduce moisture problems; the exhaust and supply fans both had rated flows of 14 ac/h (150 l/s) and operated continuously. The fans were only tested for the maritime climate because the prairie climate produced no appreciable moisture problems with the sealed attic in these simulations. Simulations 18 and 19 show how a supply fan reversed the direction of flow through the ceiling because it pressurizes the attic instead of depressurizing (as the exhaust fan does) while maintaining the same ventilation rate. For the exhaust fan (simulation 18), 2.7 ac/h flowed from the house into the attic and for the supply fan (simulations 19) 2.1 ac/h flowed from the attic to the house. This means that the moisture load on the attic from the

house interior is eliminated with the supply fan. However, the simulation results show that the supply fan produced relative humidities and wood moisture contents that were only about 2% to 3% less than with the exhaust fan and resulted in periodic condensed mass where the exhaust fan produced a net daily accumulation. The effect of fan direction on attic moisture is so similar because the supply fan tends to keep the attic colder (mean temperature of -1.4°C for the supply fan compared to 0.3°C for the exhaust fan). Cooling of the attic has an off-setting effect that reduces the influence of reversing the flow direction through the ceiling. It is interesting to note that both the supply and exhaust fans had worse results than the sealed attic with no fans shown in simulation 21. These results would suggest that the size of fan selected to provide ventilation was too large and that a smaller fan may be more effective (see discussion below on fan optimization).

Exhaust Fan on a Timer Attic ventilation fans are usually installed with a timer and simulations 25 and 26 were carried out for a sealed attic with an exhaust fan on a timer from 9 am. to 4 pm. The greatest potential for moisture removal occurs during the day when moisture is driven from the wood surfaces into the attic air. A fan on a timer produces high ventilation during the day whilst not over ventilating during the night. As shown above, for fans in continuous operation, over cooling of the attic at night can lead to moisture problems. Comparing simulations 26 to 18 shows that timed operation is an improvement over constant operation. The mean wood moisture contents were about 2% MC lower and there was five times less condensed mass on the north sheathing and no accumulation on the south sheathing. A comparison of simulations 26 and 19 shows that an exhaust fan on a timer was also an improvement over constant operation

Balanced Fans Simulation 17 was carried out for a sealed attic with balanced fans producing 7 ac/h based on the nominal rating of the fan. These results are compared to simulation 21 for the sealed attic in a maritime climate without fans. With the addition of a balanced fan system, the attic ventilation rate increased from 0.7 ac/h to 9 ac/h and the indoor-attic exchange rate only changed from 0.7 to 0.8 ac/h. This should have the effect of bringing more low moisture content air from outside into the attic, thus reducing moisture levels. The simulations show that using the balanced fan produced about 3% higher relative humidity, similar wood moisture contents, and similar condensed mass. The balanced fan operation produced no significant improvement for the sealed attic because the high ventilation rates produced colder attic temperatures than the unventilated sealed attic. As noted above the colder attic temperatures combined with high ventilation flows allowed

moisture to enter the attic and condense on the sheathing. Simulations 20 and 22 in the prairie climate are for a sealed attic with and without a balanced fan. These simulations show that the much drier prairie air has a drying effect on the attic. The attic relative humidity is reduced from 87% to 72%, the wood moisture contents are reduced by about 4% MC and condensed mass on the sheathing is eliminated.

Fan Size Optimization Simulations 19, 28 and 29 were performed to find if there was an optimum fan size that balanced the moisture removal potential of the fan with the cooling effects associated with the higher ventilation rates. The simulations were all performed for the maritime climate because the results of single fan simulations (discussed above) showed that the damp maritime climate requires fan size optimization. With too small a fan there is no flow reversal through the ceiling and warm, moist indoor air enters the attic producing moisture problems; with too large a fan the over-ventilated attic is too cold which again can lead to moisture problems. In the dry prairie climate it was shown that the extra moisture removal potential of the dry air compensated for the additional attic cooling by ventilation fans, and fan size optimization was not crucial. The fans were chosen to be supply fans as these gave the best results in continuous operation; supply fans of 50, 100 and 300 cfm (0.024, 0.048 and 0.150 m^3/s and with maximum rated pressure differences of 32, 65 and 175 Pa) were simulated in simulations 28, 29, and 19; these fans produced mean attic ventilation rates of 3, 5 and 17 ac/h, respectively. From simulation 28, the 50 cfm fan did not supply enough flow to completely pressurize the attic and reverse the flow into the attic. This resulted in slightly higher relative humidity and wood moisture content values than with the 100 cfm fan (simulation 29). Both smaller fans were better than the 300 cfm fan since they produced higher attic temperatures due to their lower ventilation rates. For these simulations, the 100 cfm fan provided the best control of moisture in the sealed attic with similar results to that of the standard attic (simulation 9). The advantage of a sealed attic with supply fan is that the fan driven ventilation rate is independent of the weather conditions and control of moisture is more readily assured.

6.2 SIMULATIONS USING ACTUAL WEATHER DATA

A limited set of simulations were carried out for a gable-end attic on a house located in a closely spaced east-west row. The simulations were carried out in two different Canadian climatic zones (maritime and arctic) over a complete heating season. For this purpose, the heating season was assumed to cover the period from October 10 to March 25 which corresponds to

approximately 4000 hours. Weather data for one complete year (8760 hours) at various locations in Canada were obtained from CMHC and the last 2000 hours and first 2000 hours of the file were read in this order for the winter simulations. The solar radiation gains in these data files are for north, south, east, and west vertical walls; in carrying out the simulations, these data were converted to radiation gains on the sloped roof sections. In every simulation, the interior of the house was assumed to be at a fixed temperature and relative humidity of 20°C and 50%, respectively.

In the first set of simulations, the standard attic (described in Section 6.1) was subjected to the winter climate of St. John's, Newfoundland. These results were compared with simulations of the attic in two different configurations which produced higher and lower ventilation rates:

- the standard attic with an additional 6 vents (1 on each gable end and 2 on each sloped roof section) where each vent had a gross area of 431 cm^2.
- a sealed attic with no vents and 10% of the background leakage of the standard attic.

In each of these simulations, the initial conditions were chosen to be 80% relative humidity in the attic air, 20% wood moisture content for the surface layer and 10% for the underlying layer, and no condensed mass present. Results for the standard attic are presented in Figs.6-6a through 6-6d for the time variation of attic relative humidity, inner wood node moisture contents for the north and south sheathing and the trusses, and condensed mass accumulation on the north and south sheathing. For the base case of the standard attic, it is apparent that there is no seasonal accumulation of moisture in the attic. Attic relative humidities are generally below 100% and surface wood moisture contents are also below the fibre saturation point for much of the heating season, although there are periods when the wood surfaces would be wet. In Fig.6-6b there was very little difference between the moisture contents of the north and south sheathing while the trusses, on the whole, were slightly drier than the sheathing. It should be noted that the underlying wood nodes showed a slight tendency to dry throughout the winter period. As a consequence of these relatively dry attic conditions, the sheathing only occasionally experienced small amounts of condensed mass which evaporated shortly thereafter. The north and south sheathing experienced essentially the same condensed mass since the difference in solar gains on the north and south roof surfaces was very small. This small difference between the north and south sheathing was generally observed in all simulations that were performed for St. John's. From these results, it is observed that moisture accumulation on the wood surfaces is not a serious problem for the standard attic in the maritime climate.

The seasonal response of the standard attic with 6 additional vents is shown in Figs.6-7a

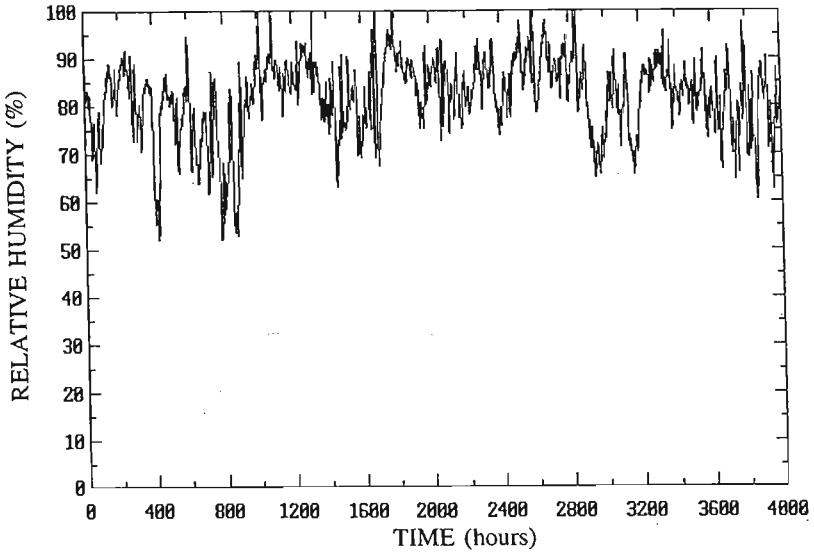

Figure 6-6a Relative humidity of attic air for simulation of the standard attic in St. John's, Nfdl from Oct. 10 (hour 0) to Mar. 25 (hour 4000).

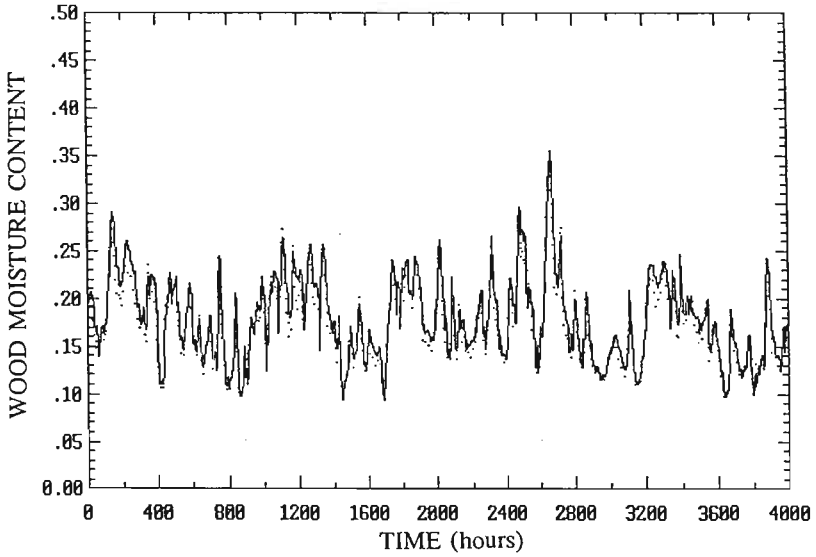

Figure 6-6b Surface wood moisture contents for north and south sheathing (same solid line) and trusses (dotted line) for standard attic simulation in St. John's, Nfld from Oct. 10 (hour 0) to Mar. 25 (hour 4000).

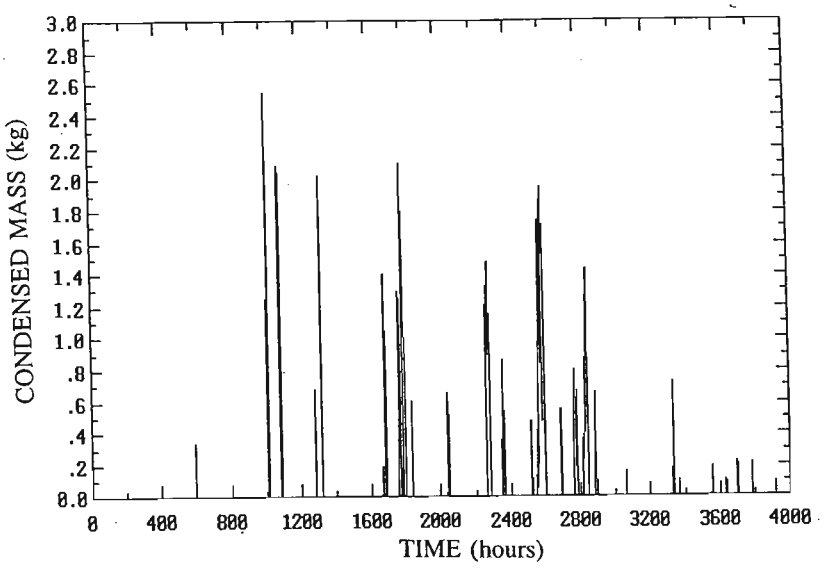

Figure 6-6c Condensed mass on the north sheathing for simulation of the standard attic in St. John's, Nfdl from Oct. 10 (hour 0) to Mar.25 (hour 4000).

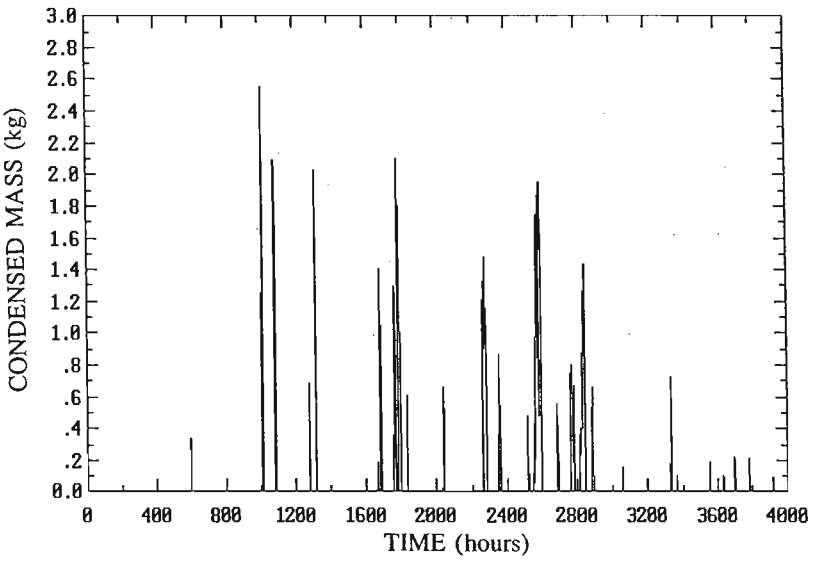

Figure 6-6d Condensed mass on the south sheathing for simulation of the standard attic in St. John's, Nfdl from Oct. 10 (hour 0) to Mar.25 (hour 4000).

through 6-7d where attic relative humidity, surface wood moisture contents, and condensed mass on the north and south sheathing are presented. As a general observation, the moisture contents in the air and on the sheathing surface is essentially the same, although the sheathing surfaces do experience a somewhat larger "swing" in moisture content. The higher ventilation rates produced by the additional vent area allow the attic wood to respond more rapidly to the changing ambient conditions. The amount of mass condensed is somewhat less than that of the standard attic; there are times when the added ventilation results in less condensed mass for example, at approximately hour 1300, there is a noticeable difference between the condensed masses. However, the important conclusion from this comparison is that the added ventilation did not entirely eliminate the condensed mass. This is essentially the same conclusion reached in the parametric simulations; **placing additional vents on a ventilated attic that has moisture problems may not result in any significant improvement.**

Going to the other extreme and sealing the attic (without blocking the ceiling leakage) can lead to much worse problems. This is illustrated in Figs.6-8a through 6-8d, where the sealed attic is exposed to the climate of St. John's. About 2 months into the simulation (approximately 1350 hours), the attic air and surface wood moisture contents reach saturation and remain close to those values through to March 25. These conditions are of course, accompanied by condensed mass appearing on the attic interior. Figure 6-8c shows accumulation of condensed mass on the north sheathing which is virtually identical to the south sheathing (not shown). There is a steady accumulation of condensed mass on the sheathing reaching a maximum of approximately 70 kg; this condensed mass is a direct result of interior moisture transported through the ceiling. Figure 6-8d shows that under these conditions, even the joists and trusses will begin to experience condensed mass accumulation, although the amounts are much less than for the sheathing. For this particular attic configuration, the simulation was extended for the next 4000 hours beyond March 25 to observe the drying process. The surface wood moisture contents and condensed mass on the north sheathing are shown in Figs.6-9a and 6-9b, respectively. Shortly after March 25, the drying process commenced resulting in rapid removal of the condensed mass at approximately hour 4600 in Fig.6-9b; the surface wood moisture content, however, remained saturated for a further 300 hours as shown in Fig.6-9a before the moisture contents began to decrease. The obvious question is "Does this pose a significant problem for wood components of the attic, particularly with regard to the growth of micro-organisms?" The answer to this question requires a micro-organism growth model for wood. Nonetheless, the simulations indicate that **sealed attics are prone to significant moisture accumulation unless the ceiling leakage can be effectively blocked**.

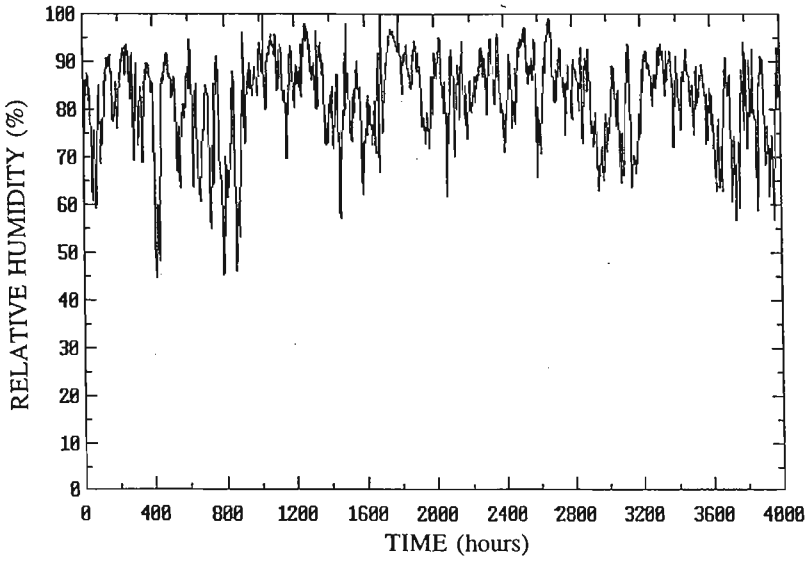

Figure 6-7a Relative humidity of attic air for simulation of the standard attic with 6 additional vents in St. John's, Nfdl from Oct. 10 to Mar.25.

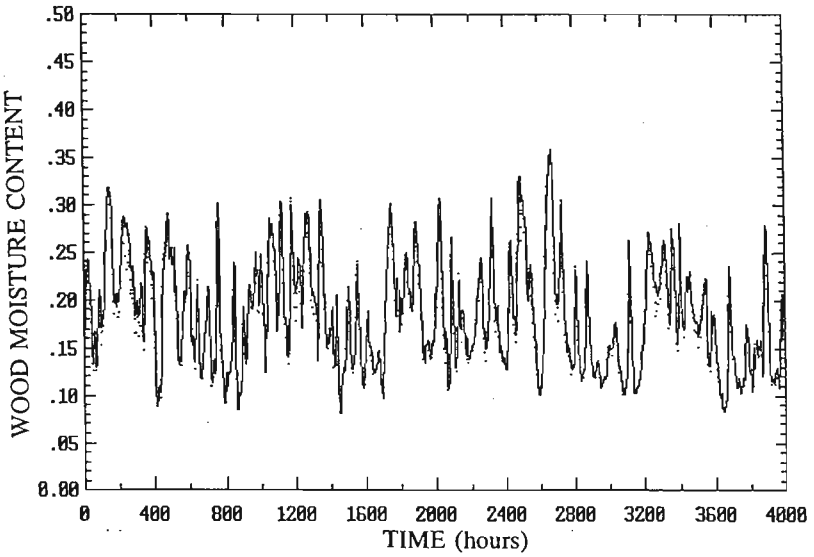

Figure 6-7b Surface wood moisture contents for north and south sheathing and trusses for simulation of the standard attic with 6 additional vents in St. John's, Nfdl from Oct. 10 to Mar.25.

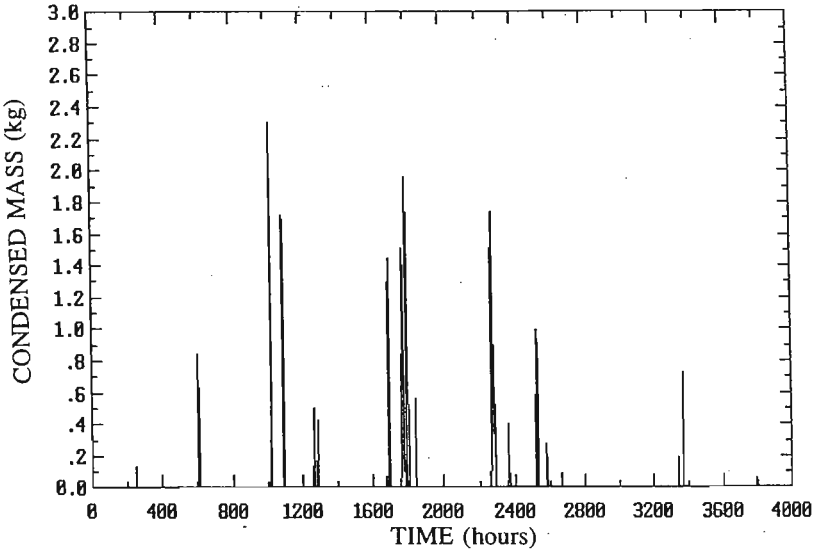

Figure 6-7c Condensed mass on the north sheathing for simulation of the standard attic with 6 additional vents in St. John's, Nfdl from Oct. 10 to Mar.25.

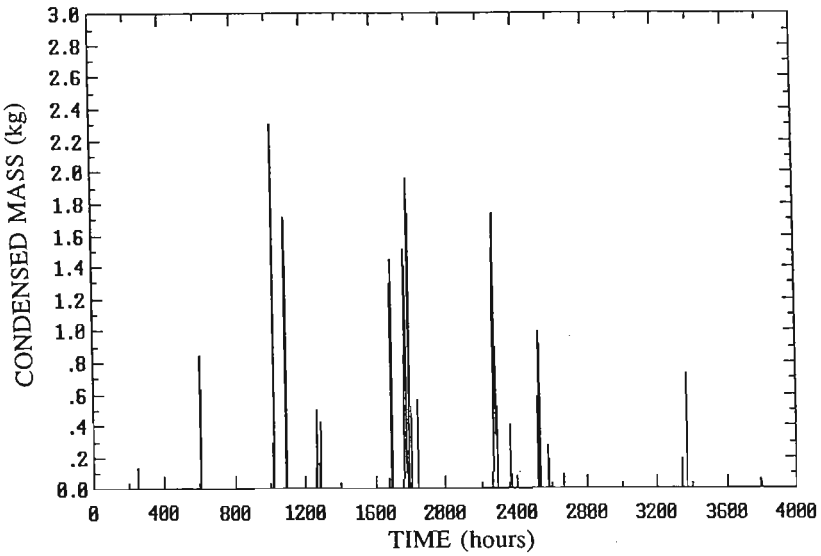

Figure 6-7d Condensed mass on the south sheathing for simulation of the standard attic with 6 additional vents in St. John's, Nfdl from Oct. 10 (hour 0) to Mar.25 (hour 4000).

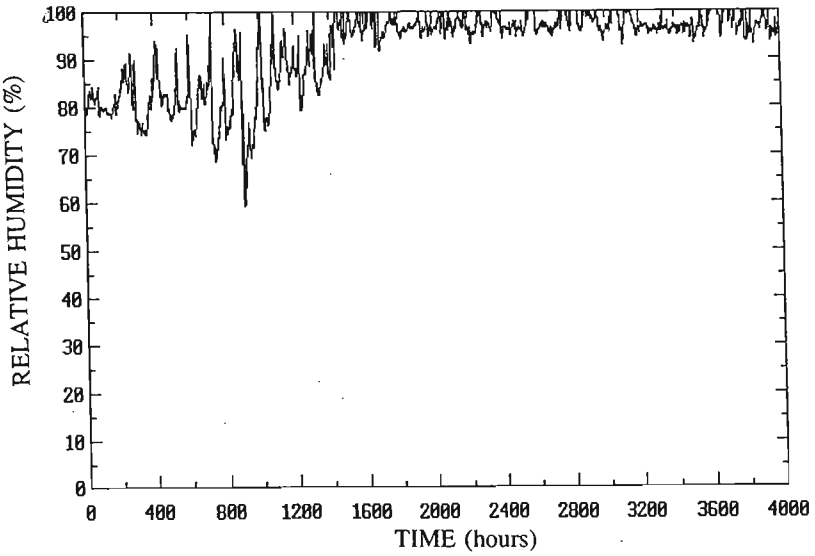

Figure 6-8a Relative humidity of attic air for simulation of the sealed attic in St. John's, Nfdl from Oct. 10 to Mar.25.

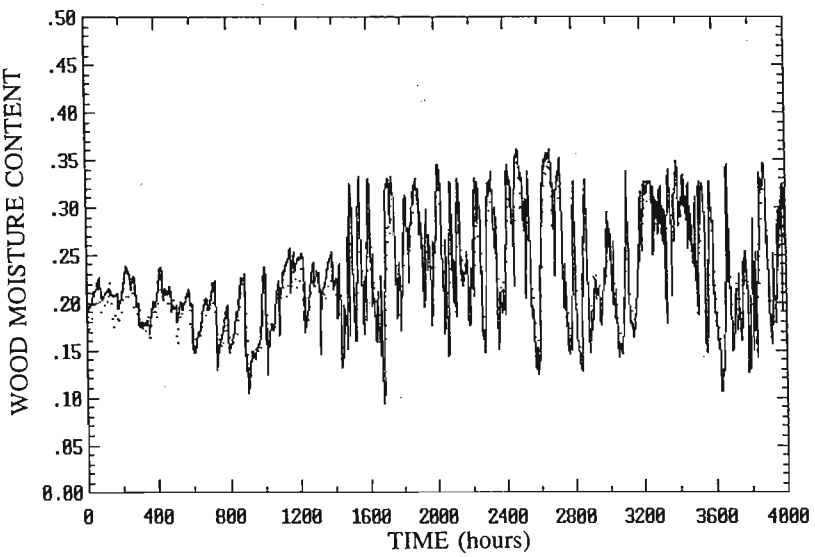

Figure 6-8b Surface wood moisture contents for north and south sheathing and trusses for simulation of the sealed attic in St. John's, Nfdl from Oct. 10 to Mar.25.

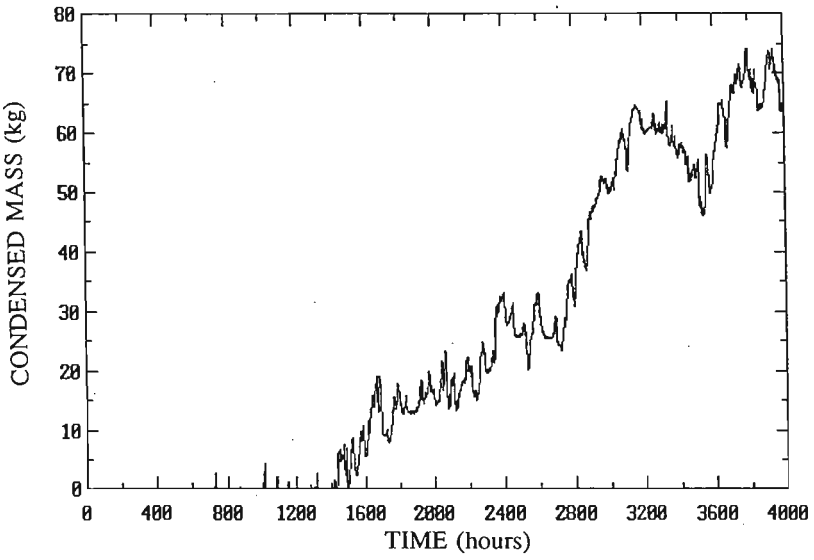

Figure 6-8c Condensed mass on the north sheathing for simulation of the sealed attic in St. John's, Nfdl from Oct. 10 to Mar.25.

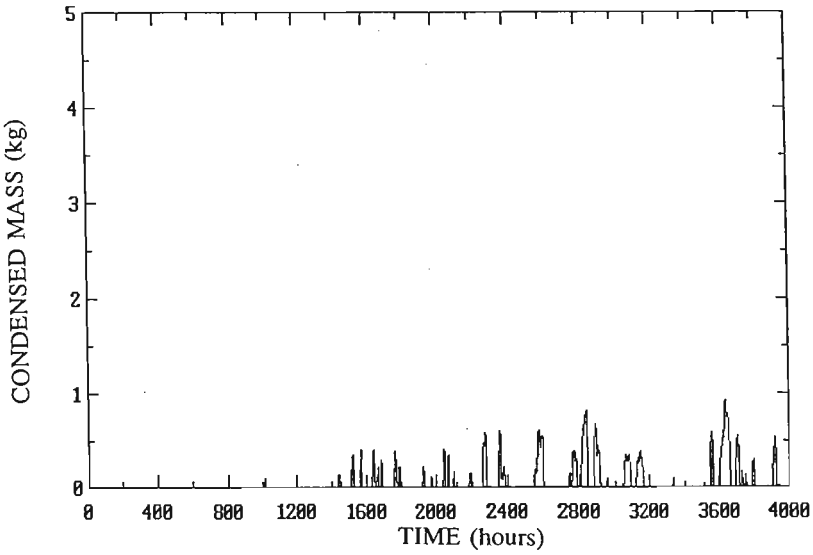

Figure 6-8d Condensed mass on joists and trusses for simulation of the sealed attic in St. John's, Nfdl from Oct. 10 to Mar.25.

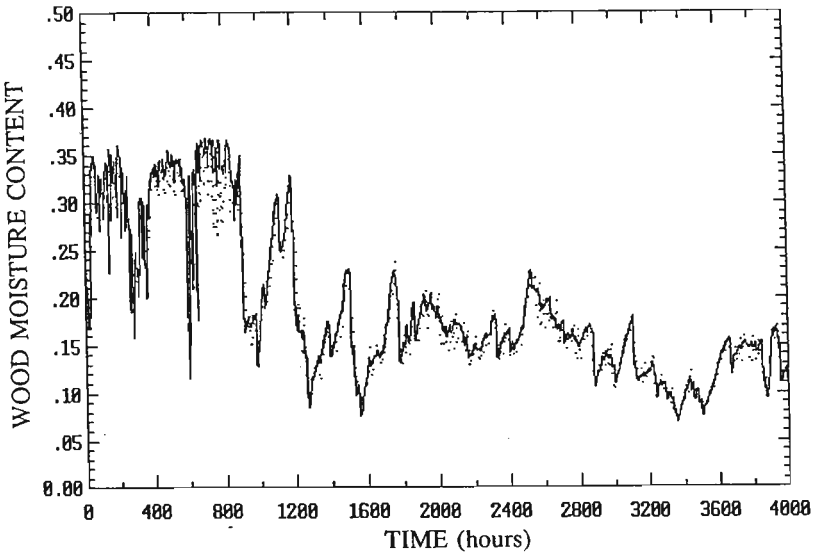

Figure 6-9a Surface wood moisture contents for north and south sheathing and trusses for simulation of the sealed attic in St. John's, Nfdl from Mar. 25 (hour 4000) to Sept 8 (hour 8000).

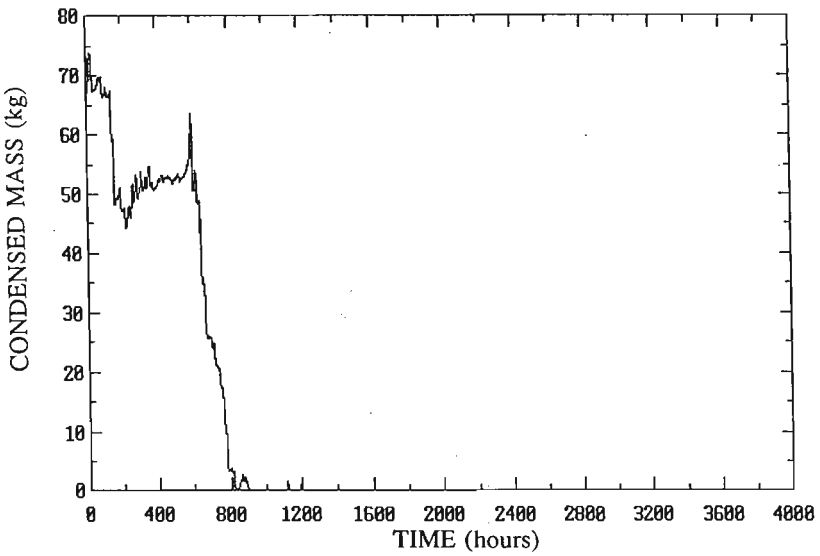

Figure 6-9b Condensed mass on north sheathing for simulation of the sealed attic in St. John's, Nfdl from Mar. 25 (hour 4000) to Sept 8 (hour 8000).

For the final simulation, the standard attic was exposed to the climate of Whitehorse, Yukon over the same heating season as for the St. John's simulations. However, the initial conditions in the attic were somewhat different: attic relative humidity was set at 50%, the sheathing and truss (both nodes) moisture contents were 10% and there was no condensed mass. The variations of attic relative humidity, moisture contents of the inner sheathing and trusses, condensed mass on the north sheathing, and condensed mass on the trusses are shown in Figs.6-10a through 6-10d. For much of the heating period, attic relative humidity is close to saturation, while the corresponding seasonally-averaged surface wood moisture content is only around 15%. This directly reflects the relationship between temperature, wood moisture content, and vapour pressure that was assumed in the moisture model. At low temperatures (which is characteristic of the arctic climate), the wood moisture content at which "unbound" water appears is significantly less than the fibre saturation point. Thus, at low moisture contents, condensed mass accumulates at the wood surface nodes. This condensed mass is shown in Fig.6-10c for the north sheathing; the amount condensed on the south sheathing is essentially identical to the north side since the amount of solar gain during the winter is relatively small for Whitehorse. A comparison of Figs.6-6c and 6-10c for the standard attic in two different climatic zones shows that the amount accumulated in the colder climate of Whitehorse is approximately 3 times as large as that in St. John's. Furthermore, for the colder climate, Fig.6-10d shows that condensed mass appeared on the trusses where none appeared in the maritime climate. From these simulations, it is clear that **in extreme climates, properly ventilated attics may still have excessive moisture accumulation.**

The results presented in this section are by no means an exhaustive survey of the full range of factors that affect moisture accumulation in attics. The factors that are important are climatic zone, attic leakage characteristics (both size and location of leaks), and mechanical ventilation. This study has been a first step towards understanding the complex relationship between these factors.

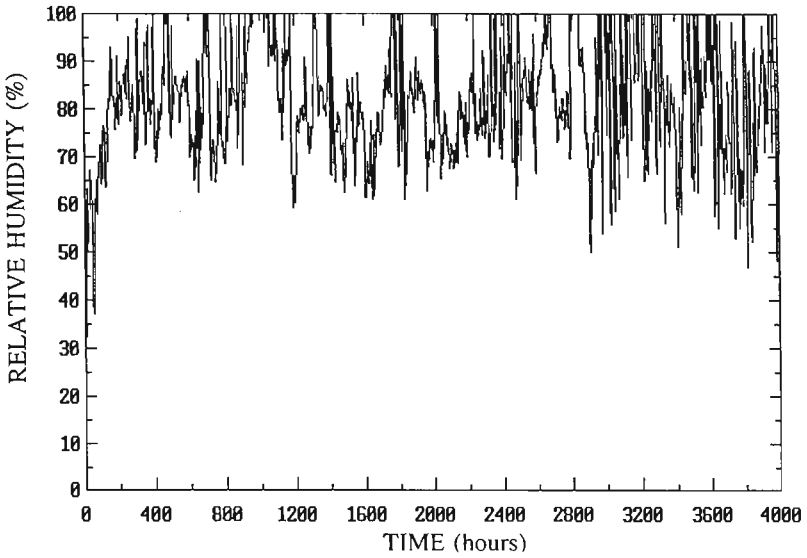

Figure 6-10a Relative humidity of attic air for simulation of the standard attic in Whitehorse, Yukon from Oct. 10 to Mar.25.

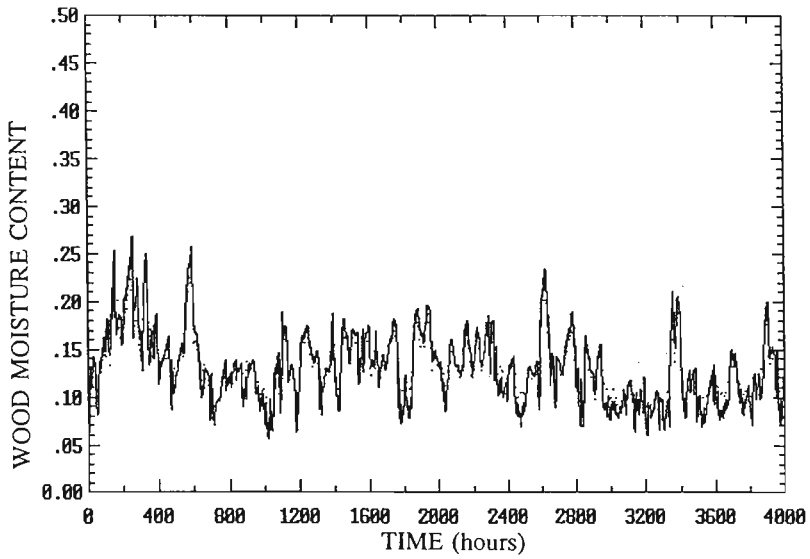

Figure 6-10b Surface wood moisture contents for north and south sheathing and trusses for simulation of the standard attic in Whitehorse, Yukon from Oct. 10 to Mar.25.

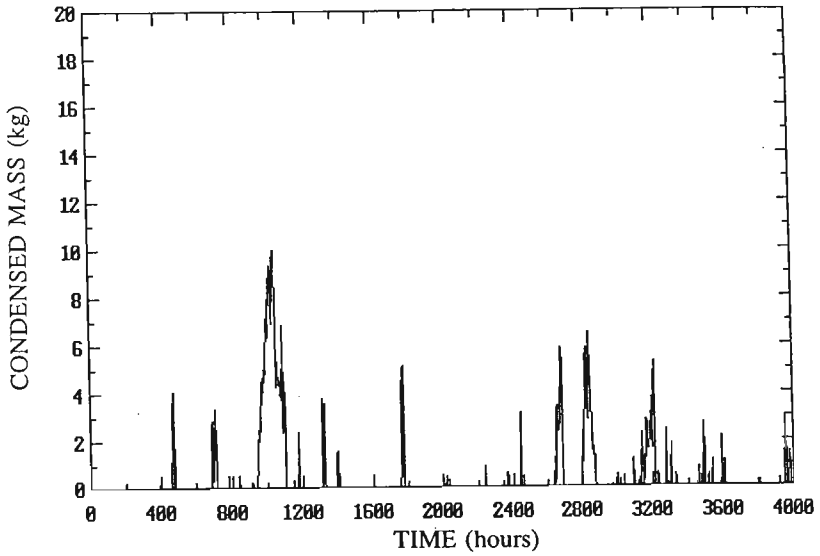

Figure 6-10c Condensed mass on the north sheathing for simulation of the standard attic in Whitehorse, Yukon from Oct. 10 to Mar.25.

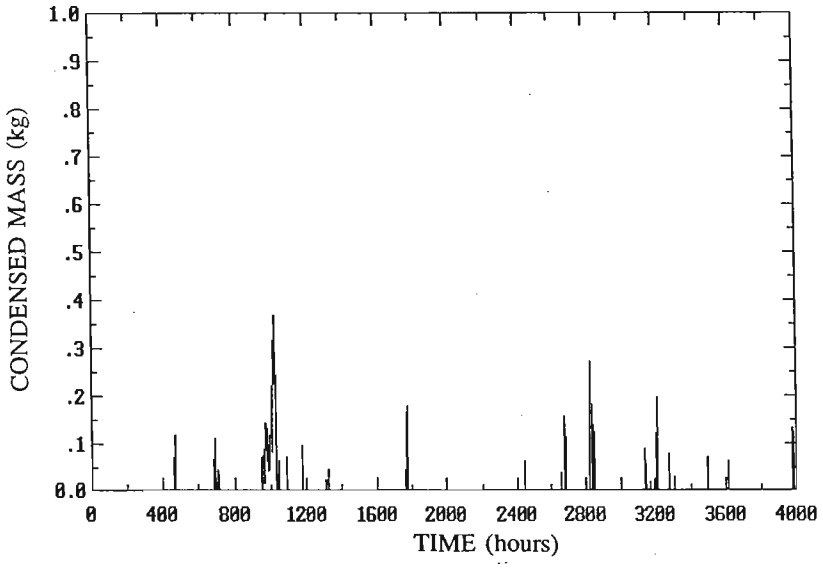

Figure 6-10d Condensed mass on joists and trusses for simulation of the standard attic in Whitehorse, Yukon from Oct. 10 to Mar.25.

SECTION SEVEN

CONCLUSIONS

A simulation model has been developed to investigate the dynamics of moisture accumulation in a conventional residential attic for given climatic zone and attic leakage configuration. The complete model integrates three separate models that predict the ventilation rates of an attic as a function of ambient conditions, the temperature distribution in an attic, and the distribution of moisture. Previous studies had modelled the thermal and moisture dynamics in attics but required that attic ventilation rates be specified a priori. The key to this simulation model has been the development and verification of a comprehensive model to predict ventilation rates in attics.

The ventilation model is a two zone model consisting of the interior and attic zones which are weakly coupled by interzonal leakage. The ventilation model performs an air mass balance on the two zones to calculate ventilation flows. These flows are calculated based on house and attic characteristics such as leakage area, distribution of leakage and wind shelter due to upwind obstacles. The key features of the two zone ventilation model are:

- wind pressure coefficients are calculated as a continuous function of wind angle and have different values depending on whether the house is isolated or is together with other houses in a row
- distributed leakage is combined with localised leakage to include the effects of flues and passive vents
- mechanical ventilation is incorporated using a fan performance curve that allows fan flow rates to vary with different ambient conditions
- indoor-attic exchange rates are calculated from the pressure difference between the two zones.

Ventilation model predictions were compared with field measurements of indoor and attic ventilation rates as well as, indoor-attic exchange rates taken in two separate test houses over a

wide range of ambient conditions encountered during the two year test period. In addition, predictions for attic ventilation rates produced by an attic fan operating in the exhaust and supply mode, were compared with measured data. On average, the two zone model was found to be able to reproduce the observed trends in measured flow rates for configurations, with reasonably good accuracy over a wide range of ambient conditions; the mean percentage error between the predicted and measured flow rates for the various configurations tested, are summarised in Table 7.1.

Table 7-1 Mean Error for Ventilation Model Predictions

House Zones	Configuration	Ambient conditions		Mean Error %
		Temperature	Wind speed	
House 5	Vents and flue closed	all	< 2 m/s	+6.4
House 5	Vents and flue closed	all	all	+3.0
Attic 5	No vents or soffits	all	all	-9.3
Attic 6	Soffits and roof vents	all	all	+4.3
Attic 6	Soffits and roof vents with attic fan in exhaust mode	all	all	-2.9
Attic 6	Soffits and roof vents with attic fan in supply mode	all	all	-4.3
Indoor-attic rates house 5	Through ceiling	all	< 2 m/s	+4.5
Indoor-attic rates house 6	Through ceiling	all	< 2 m/s	+14.3

The important conclusions that were obtained from the ventilation model and field measurements were the following:

- both attic and indoor ventilation rates increased significantly with wind speed
- attic ventilation rates were dominated by wind, producing rates that were approximately 4 to 5 times larger than those produced by attic-outdoor temperature differences
- attic ventilation rates were sensitive to wind direction, particularly when there is an

upwind obstacle that provided shelter

- the total attic vent area required by the Building Code produced unsheltered attic ventilation rates of approximately 3 ac/h (air changes per hour) per m/s of wind speed
- the stack effect produced by indoor-attic temperature differences was the main driving force for indoor-attic exchange rates
- the two zone model was able to correctly combine mechanical ventilation produced by fans with the natural ventilation.

The combined ventilation, thermal, and moisture model was verified by measurements taken in the two test houses over a two year period and showed that the combined model was able to reproduce the measured diurnal variations in attic vapour pressure. The combined model was then used in a number of parametric and full-scale simulations to identify certain trends and ventilation control strategies. A number of conclusions were reached based on this work:

- The two important sources of moisture for an attic are moisture convected from the interior to the attic by ceiling flow and moisture convected from outdoors by ventilation flow. Moisture due to ceiling flow is dominant when the attic is well sealed and ventilation rates are low. Moisture due to ventilation flow is dominant when ventilation rates are high and may pose a problem when the sheathing is cooled at night.
- Increased ventilation did not reduce attic air relative humidity, wood moisture content or condensation, and the worst case results always occurred at high wind speeds which produced high ventilation rates. The high ventilation rates reduce attic temperatures which exacerbates moisture accumulation.
- Sealed attics were warmer than ventilated attics but this was offset by indoor-attic air flow that convected large amounts of moisture into the attic. This results in high wood moisture contents and condensation problems in all climatic zones.
- A maritime climate always produced worse moisture problems than the dryer and colder prairie climate. The ability of moist maritime air to remove moisture from the attic is much less than with dry prairie air.
- For mechanical ventilation of attics, fan ventilation worked best when the fan was only on during the day when attic temperatures are relatively high and the potential for removing moisture is high.
- A single fan was found to provide good moisture control when installed as a supply fan that pressurizes the attic enough to reverse the direction of the air flow through the

ceiling. An optimum fan size was found which pressurized the attic enough to reverse the ceiling flow but did not over-ventilate the attic. For the attic considered in the simulations, a supply fan providing 5 ac/h was found to produce the best results.

- The simulations using balanced fans showed that the ambient conditions are an important consideration in fan installation. In a prairie climate it was found that the balanced fans resulted in reduced wood moisture contents but the damper maritime air resulted in increased wood moisture contents.

In the course of development and verification of the combined model, a number of limitations were identified with respect to model inputs and measurements and the following lists some improvements that are being considered:

- Since attic ventilation rates are predominantly wind-driven, the ventilation model could be improved with a more complete set of pressure coefficients over a range of building shapes, roof pitch angles, and wind direction. These measurements could be made with careful wind tunnel tests.
- One of the most important inputs to the moisture model was the moisture content/vapour pressure/temperature relationship for wood particularly, at temperatures below freezing. This relation determines not only wood vapour pressure from which mass fluxes are obtained, but also whether water condenses on the surface. This relation needs to be developed for different wood species and different wood components such as, plywood and waferboard.
- Verification of the thermal model could be improved with detailed measurements of night time radiation losses which are strongly dependent on cloud cover.
- In order to provide an in-depth verification of the moisture model, techniques need to be developed to remotely and accurately measure the amount of moisture accumulating on a surface such as, the roof sheathing.

With the attic simulation model in place, one of the remaining questions is "At what point does attic moisture accumulation become a serious problem?" There are many different aspects to this question but the two issues that seem most relevant are first, the growth of micro-organisms on wood surfaces that ultimately lead to structural deterioration and second, the direct effect of moisture absorption on the strength of roof sheathing. These questions need to be addressed and the present attic moisture simulation model will prove to be a useful tool for providing answers.

REFERENCES

Abrantes, V., (1985), "Thermal Exchanges Through Ventilated Attics", Proc. ASHRAE/DOE/BTECC Conf. on the Thermal Performance of the Exterior Envelopes of Buildings III, Clearwater Beach, Florida, pg.296.

Akins, R.E., Peterka, J.A., and Cermak, J.E., (1979), "Averaged Pressure Coefficients for Rectangular Buildings", Wind Engineering, Vol. 1, Proc. 5th Int. Conf. on Wind Engineering, pg.369.

ASHRAE, (1989), Handbook of Fundamentals, Atlanta, Georgia.

ASTM, (1982), "Measuring Air Leakage by the Fan Pressurization Method", Annual Book of ASTM Standards, part 18, pg.1484.

Alcoa Building Products, (undated), "Fundamentals of Residential Attic Ventilation", Sydney, Ohio.

Burch, D.M. and Luna, D.E., (1980), "A Mathematical Model for Predicting Attic Ventilation Rates Required For Prevention of Condensation on Roof Sheathing", ASHRAE Trans. Vol. 86, pg.201.

Burch, D.M., Lemay, M.R., Rian, B.J., and Parker, E.J., (1984), "Experimental Validation of an Attic Condensation Model", ASHRAE Trans., Vol. 90, Part 2A, pg.59.

Cleary, P.G., (1985), "Moisture Control by Attic Ventilation - An In Situ Study", ASHRAE Transactions, Vol.91, Part 1.

CGSB Standard 149.10-M86 (1986), "Determination of the Airtightness of Building Envelopes by the Fan Depressurization Method", Canadian General Standards Board.

CMHC (1983), "Moisture Induced Problems in NHA Housing", 3 Parts, Report prepared by Marshall Macklin Monaghan Ltd, Cat # NH20-1/2-1983-1E, Ottawa, Ontario.

CMHC, (1987), "Final Report on the Drying of Walls", Report prepared by Oboe Engineering Ltd, Ottawa, Ontario.

CMHC (1989a), "Attic Air Change Testing: Protocol Development", Report prepared by Buchan, Lawton, Parent Ltd, Ottawa, Ontario.

CMHC (1989b), "A Procedure for Determining Airtightness Characteristics of Attic Spaces", Report prepared by Sheltair Scientific Ltd., Ottawa, Ontario.

CMHC (1991), "Survey of Moisture Levels in Attics", Report prepared by Buchan, Lawton, Parent Ltd, Ottawa, Ontario.

Cunningham, M.J., (1990), "Modelling of Moisture Transfer in Structures -II. A Comparison of a Numerical Model, an Analytical Model and some Experimental Results", Building and Environment, Vol.25, No.2, pg.85.

Energy Design Update, (1993), "The Mysterious Origins of the "1:300: Rule", ed. J.D. Nisson, Vol.13, No.1, pg.7.

Ford, J.K., (1982), "Heat Flow and Moisture Dynamics in a Residential Attic", PU/CEES Report No.148, Princeton University.

Fuji, T., and Imura,, H., (1972), "Natural-Convection Heat Transfer from a Plate with Arbitrary Inclination", Int. J. Heat and Mass Transfer, Vol.15, pg.755.

Gorman, T.M., (1987), "Modelling Attic Humidity as a Function of Weather, Building Construction and Ventilation Rates", Ph.D. Dissertation, College of Environmental Science and Forestry, State University of New York.

Harrje, D.T., Gibson, R.G., Jacobson, D.I., Dutt, G.S., and Hans, G., (1985) "Field Measurements of Seasonal Wodd Moisture Variations in Residential Attics", PU/CEES Report No.188, Princeton University.

Hinrichs, H.S., (1962), "Comparative Study of the Effectiveness of Fixed Ventilating Louvers", ASHRAE Transactions, Vol. 68, pg.297.

Holman, J.P., (1981), Heat Transfer - 5th Ed., McGraw - Hill.

Hutcheon, N.B., (1963), "Humidified Buildings", Division of Building Research, National Research Counci of Canada, Canadian Building Digest No. 42.

Kollman, F.F.P. and Côté, W.A., (1968), Principles of Wood Science and Technology, Springer-Verlag, pg.190.

McAdams, W., (1954), Heat Transmission - 3rd Ed., McGraw-Hill, pg.249.

Modera, M., and Wilson, D.J., (1989), "The Effects of Wind on residential Building Leakage Measurements", Special Technical Publication of the ASTM Symposium on Air Change Rate and Air Tightness in Buildings, April 1989, Atlanta, GA.

National Building Code of Canada (NBCC), 1990, p.253.

Liddament, M.W., (1986), "Air Infiltration Calculation Techniques - An Applications Guide", Air Infiltration and Ventilation Centre.

Orr, H.W., (1974), "Condensation in Electrically Heated Homes", Division of Building Reasearch, National Research Council of Canada, Research Report No. 632.

Parmelee, G., and Aubele, W., (1952), "Radiant Energy Emission of Atmosphere and Ground", ASHVE Trans., Vol. 58, p.85.

Peavy, B.A., (1979), "A Model for Predicting the Thermal Performance of Ventilated Attics", Summer Attic and House Ventilation, NBS Special Publication 548, pg.119.

Pfaff, F., and Garrahan, P., (1986), "New Temperature Correction Factors for the Portable Resistance-type Moisture Meter", Forest Products Journal, Vol.36, pg.28.

Rose, W.B., (1992), "Measured Values of Temperature and Sheathing Moisture Content in Residential Attic Assemblies", Proc. of the ASHRAE/DOE/BTECC Thermal Performance of the Exterior Envelopes of Buildings V, Clearwater Beach, Florida, December, pg.379.

Saunders, C.H., (1982), "Air Movement in Houses: A New Approach", Building Research and Practice, Vol.10, No.3, May/June, pg.160.

Siau, J.F., (1984), Transport Processes in Wood, Springer Verlag.

Sulatisky, M., (1984), "Airtightness Tests on 200 New Houses Across Canada: Summary of Results", BETT publication No. 84.01, Energy, Mines and Resources Canada.

Walker, I.S., (1992), "Pressure Coefficients on Sheltered Buildings", Air Infiltration Review, Vol.13, No.4, Air Infiltration and Ventilation Centre, Coventry, U.K.

Wilkes, K.E., (1983), "Dynamic Thermal Performance of Walls and Ceilings/Attics", Proc. ASHRAE/DOE Conf. on the Thermal Performance of the Exterior Envelopes of Buildings II, pg.131.

Wilkes, K.E., (1989), "Model for the Thermal Performance of low-sloped Roofs", Proc. ASHRAE/DOE/BTECC/CIBSE Conf. on the Thermal Performance of the Exterior Envelopes of Buildings IV, Orlando, Florida, pg.184.

Wilson, D.J. and Walker, I.S., (1991), "Passive Ventilation to Maintain Indoor Air Quality", Department of Mechanical Engineering Report #81, University of Alberta, Edmonton, Canada.

Wiren, B.G., (1985), "Effects of Surrounding Buildings on Wind Pressure Distributions and Ventilation Losses for Single Family Houses : Parts 1 and 2", National Swedish Institute for Building Research Report M85:19.

Wood Engineering Handbook, (1982), U.S. Forest Products Laboratory, Prentice-Hall, pg.3-8.